

AD-A138 149

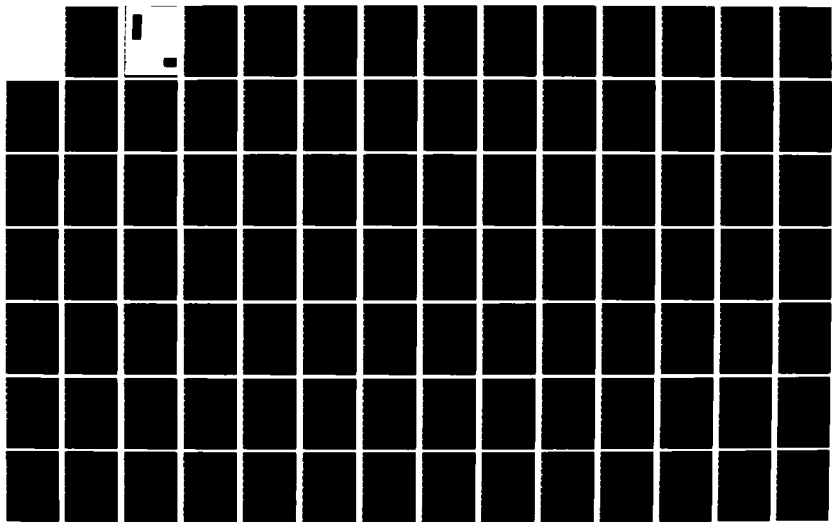
SUPERLATTICES AND SEMICONDUCTOR/SEMICONDUCTOR  
INTERFACES(U) CALIFORNIA INST OF TECH PASADENA  
T C MCGILL 17 JAN 84 ARO-17257. 6-EL DARG29-80-C-0103

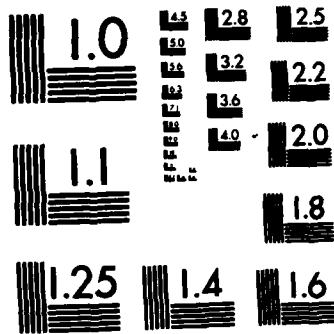
1/2

UNCLASSIFIED

F/G 20/12

NL





MICROCOPY RESOLUTION TEST CHART  
 NATIONAL BUREAU OF STANDARDS-1963-A

Unclassified

SECURITY CLASSIFICATION OF THIS PAGE (When Data Entered)

REPORT DOCUMENTATION PAGE		READ INSTRUCTIONS BEFORE COMPLETING FORM
1. REPORT NUMBER	2. GOVT ACCESSION NO. AD-A138149	3. RECIPIENT'S CATALOG NUMBER
4. TITLE (and Subtitle) SUPERLATTICES AND SEMICONDUCTOR/SEMICONDUCTOR INTERFACES	5. TYPE OF REPORT & PERIOD COVERED Final Report / Jan 30 - 31, 1983 <del>80 APR 1 - 83 JUL 31</del>	6. PERFORMING ORG. REPORT NUMBER
		7. AUTHOR(s) T. C. McGill
9. PERFORMING ORGANIZATION NAME AND ADDRESS CALIFORNIA INSTITUTE OF TECHNOLOGY 1201 East California Blvd. Pasadena, California 91125	10. PROGRAM ELEMENT, PROJECT, TASK AREA & WORK UNIT NUMBERS	
11. CONTROLLING OFFICE NAME AND ADDRESS U. S. Army Research Office Post Office Box 12211 Research Triangle Park, NC 27709	12. REPORT DATE January 17, 1984	13. NUMBER OF PAGES
	14. MONITORING AGENCY NAME & ADDRESS (if different from Controlling Office)	
15. SECURITY CLASS. (of this report)  Unclassified		15a. DECLASSIFICATION/DOWNGRADING SCHEDULE
		16. DISTRIBUTION STATEMENT (of this Report)  Approved for public release; distribution unlimited.
17. DISTRIBUTION STATEMENT (of the abstract entered in Block 20, if different from Report)		COLLECTE FEB 17 1984 A
18. SUPPLEMENTARY NOTES  The view, opinions, and/or findings contained in this report are those of the author(s) and should not be construed as an official Department of the Army position, policy, or decision, unless so designated by other documentation		
19. KEY WORDS (Continue on reverse side if necessary and identify by block number) Semiconductor devices, superlattices, and infrared detectors		
20. ABSTRACT (Continue on reverse side if necessary and identify by block number) We report on experimental and theoretical studies of the properties of superlattices and small structures. The major results include: the properties of HgTe-CdTe superlattices for IR detectors, transport over GaAlAs barriers, doping in small superlattices, new method of treating superlattices, and deep levels in CdTe.		



SECTION II  
SPECIFIC RESULTS

A. Superlattice Review Article

Under the support of this contract a major review article on the theory of superlattices was prepared for inclusion in a volume being edited by L. Chang (See Appendix A, Publication 1). The volume will be published by Academic Press sometime in the near future. This review article should stimulate continuing research into the properties of superlattices which are currently showing a great deal of promise for application in infrared detectors.

B. HgTe-CdTe Superlattices

Sometime ago under the sponsorship of the Army Research Office, J. N. Schulman and I proposed the use of HgCdTe superlattices as a new infrared material. During the period of sponsorship of this new program, we made substantial strides in our understanding of the HgTe-CdTe superlattice and indicated even more strongly its usefulness in the infrared materials area. In the original paper, it was pointed out that the HgTe-CdTe superlattice would allow one

to form materials with band gaps which were independent of the composition of Hg and Cd. In our more recent work, we have explored the implications of the superlattice for cutting down one of the major problems in narrow band gap materials, that is, the tunneling current in device structures. We find that the HgTe superlattice offers very substantial advantages over the corresponding alloy in the reduction of the tunneling current in narrow gap systems in various device applications. The results of this study are published in an Applied Physics Letter given as an appendix to this report. (Publication 2 and presented at the International Conference on Superlattices (see attached papers, Publications 3 and 4)).

### C. k . p Method for Treating Properties of Superlattices

Much of the early theoretical studies of superlattices was carried out in the tight-binding approximation. This theoretical approach has a major disadvantage in that it requires the input of parameters describing the electronic band structure of the bulk which are not directly measureable. Further, much of the interest in the HgTe-CdTe and other superlattices that might be used in infrared applications is in the electronic properties at near band gap. Hence, we have sought to develop a new theoretical

technique that lends itself to solving the problems of the near band gap properties and also will form the basis for describing devices formed from superlattices. The theoretical approach consists of defining an average material and then treating in perturbation theory the various perturbations due to the superlattice. This approximation can obtain very accurate properties for superlattices. This technique promises to form the basis for much of the treatment of both the physical properties and device properties of various superlattice structures.

#### D. Doping in Superlattices and Quantum Well Structures

One of the essential controlling aspects of semiconductors is doping. Doping is the basis under which we form many devices in homogeneous materials. Under this program, we made the first theoretical study of doping in small structures in superlattices. We have found that in the superlattice structure the binding energy of dopants can be changed very substantially. For example, in the GaAs-GaAlAs system, we have found that the binding energy of impurities can be increased by as much as a factor of four. The results are reported in the papers included in Appendix A, Publications 5, 6 and 7. Much of the theoretical work is now being investigated experimentally in a number of laboratories. Preliminary results indicate that our

predictions are in fact in agreement with what is being observed experimentally. The results of this study are reported in a number of publications which have been included in the attached appendices.

#### E. Tunneling and Transport Calculations for Barrier Structures

In recent years it has become widely accepted that in high speed devices the distribution of electrons at various critical parts of the device is very important in determining the actual speed of the device. We have carried out theoretical studies of the transport of electrons across GaAlAs structures imbedded in GaAs. We have found that for the conduction electrons it is possible to form thin layers of GaAlAs which will act as electron filters. For example, our theoretical work suggests that it should be possible to form thin layers of GaAlAs that will suppress the L point electrons and hence increase the speed performance of devices. The results are reported in the papers in Appendix A, see Publications 8 and 9). Experiments are currently in progress to attempt to verify these theoretical predictions.

#### F. Study of Deep Level Transient Spectroscopy for CdTe

Because of our interest in the properties of the

HgTe-CdTe interface, we have been making measurements at Caltech on the band offset for this structure. Early experiments by J. McCaldin and T. Kuech indicated that the band offset was substantial beyond that predicted by simple theoretical arguments. One possible cause of this deviation could have been deep levels imbedded in the CdTe. Hence, we embarked upon the first theoretical study of the deep level in CdTe, using deep level transient spectroscopy. Both n- and p-type samples were explored. The deep level spectra for these samples were reported in a series of papers which have been attached in Appendix A, Publications 10 and 11. This piece of work is forming the basis of much of our understanding of the deep levels in CdTe.

### SECTION III

#### STUDENTS AND VISITORS SUPPORTED UNDER THE ARO CONTRACT

Funds provided by the ARO have been used to support four graduate students and two visitors. Three of the graduate students were U.S. citizens and one was Canadian. Both of the visitors were citizens of the U.S. One graduate student that has been supported under this program who has completed his Ph.D. is currently working for the Xerox Corporation. The list of these various personnel, the position under which they were supported, their citizenship, and current position is given in the following table:

Person	Position at Time of Support	Citizenship	Current Position
Reuben Collins	grad student	USA	Finishing PhD
Christian Mailhiot	" "	Canadian	Xerox
D. L. Smith	visitor	USA	Los Alamos Scientific Labs
T. Jones	grad student	USA	Finishing PhD
R.Hauenstein	" "	USA	Finishing PhD
J.N.Schulman	visitor	USA	Professor of Physics University of Hawaii

**APPENDIX A**

**PUBLICATIONS SUPPORTED**

**BY**

**ARMY RESEARCH OFFICE CONTRACT**

**ASPECTS OF THE THEORY OF SUPERLATTICES**

**J. N. Schulman**

***Department of Physics and Astronomy***

***University of Hawaii***

***Honolulu, Hawaii 96822***

**and**

**T. C. McGill**

***T. J. Watson, Sr., Laboratory of Applied Physics***

***California Institute of Technology***

***Pasadena, California 91125***

**To Appear In**

**"Synthetic Modulated Structure Materials"**

**Edited by**

**L. L. Chang and B. C. Giessen**

**(Academic Press)**

## CONTENTS

<b>CHAPTER I: Introduction</b>	<b>4</b>
<b>CHAPTER II: General Concepts</b>	<b>5</b>
<b>A. Band Folding</b>	<b>6</b>
<b>B. Bulk Solutions with Complex Wave Vectors</b>	<b>7</b>
<b>CHAPTER III: Calculation of Electronic Properties</b>	<b>8</b>
<b>A. Band Offsets</b>	<b>9</b>
<b>B. Quantum Well Model</b>	<b>11</b>
<b>C. Two-Band Models</b>	<b>16</b>
<b>D. Full Tight-Binding Models</b>	<b>22</b>
<b>E. Pseudopotential Method</b>	<b>25</b>
<b>CHAPTER IV: Electronic Properties</b>	<b>27</b>
<b>A. Interface Electronic Structure</b>	<b>27</b>
<b>B. Band Gaps</b>	<b>29</b>
<b>C. Superlattice Wave Functions</b>	<b>32</b>
<b>CHAPTER V: Phonons</b>	<b>35</b>
<b>CHAPTER VI: Other Properties</b>	<b>39</b>

<b>CHAPTER VII: Conclusions</b>	<b>42</b>
<b>ACKNOWLEDGEMENT</b>	<b>44</b>
<b>REFERENCES</b>	<b>45</b>
<b>TABLES</b>	<b>51</b>
<b>FIGURE CAPTIONS</b>	<b>57</b>

## **I. INTRODUCTION**

Superlattices present the theorist with an opportunity to apply some of the basic principles of solid state physics. The basic question of the role of periodicity in determining the properties of solids is put to new test in the artificially created world of the superlattice. These new man-made materials offer possibilities for providing solids with new electronic spectra, lattice vibrations, collective excitations, transport properties and dielectric properties.

Much of the theory of the superlattice depends on adequately applying our understanding of the bulk properties of the constituent materials in the new periodic structure. In this approach to the problem, the superlattice is made up of layers of bulk materials with a nasty, hopefully unimportant, interface between adjacent layers. A full understanding of the superlattice requires that the interface region also be understood. The relationship between bulk and superlattice properties is discussed in Section II. Given the assumption that the interface does not cause undue disruption, there are several theoretical techniques which are useful in calculating superlattice electronic properties. The methods, which are generalizations to the superlattice of techniques that have previously been used to examine bulk semiconductors, are discussed in Section III. Section IV concentrates on some of the results of the calculations, illustrating typical characteristics of superlattice electronic structure. Section V surveys the physics of phonons in superlattices. Phenomena similar to that exhibited by the electronic spectra occur also for phonons. Section VI surveys a variety of physical phenomena in superlat-

tices, especially those which are just starting to be explored both theoretically and experimentally. These include optical properties, impurities, transport properties and collective excitations. Conclusions are presented in Section VII.

## **II. GENERAL CONCEPTS**

On the most fundamental level, any particular superlattice consisting of alternating layers of a specified pair of semiconductors with specified layer thicknesses can be viewed as a completely new material. A more useful approach recognizes that each alternating layer is made up of a bulk semiconductor, such as GaAs or AlAs, whose bulk properties may be well known. Although the following point of view may prove inaccurate when the alternating layers are very thin, it is often useful in obtaining a qualitative understanding of superlattice properties to consider it as consisting of alternating layers of semiconductors whose bulk properties are left somewhat intact. This does not imply, however, that the superlattice properties are necessarily a simple superposition of the properties of its two constituents. Although the bulk properties, such as the electrostatic potential or ionic positions, are envisioned as remaining unchanged, the boundary conditions satisfied by the electron or phonon wave functions are influenced by the thickness of the layers in the superlattice. This section discusses two concepts which follow from this point of view: band folding and mixing of bulk solutions with complex wave vectors.

## A. Band Folding

The band folding concept is a simple method for obtaining an approximate understanding of electron or phonon dispersion curves in a superlattice. Defining the  $z$  direction to be perpendicular to the alternating layers, the electron or phonon energy,  $E$ , versus wave vector in the  $z$  direction,  $k_z$ , can be roughly predicted from the known  $E$  versus  $k_z$  dispersion curves for the bulk materials. This can be done by displaying the bulk dispersion curves while assuming an extended bulk unit cell in the  $z$  direction. For a superlattice with a total of  $L$  atomic layers of its constituent semiconductors per superlattice unit cell, the bulk unit cell should also consist of  $L$  layers. In the extended zone scheme, the superlattice potential would open up gaps in the bulk dispersion curves at intervals of  $2\pi/La$  (where  $a$  is the spacing between atomic layers) in  $k_z$ . Folding these curves back into a single Brillouin zone of width  $2\pi/La$  would give the superlattice dispersion curves. Thus, folding back the bulk dispersion curves in the same manner as if there were an extended unit cell gives an approximation to the superlattice dispersion curves.

Although this approximation seems crude, it is useful in sorting out the multiplicity of superlattice bands produced due to the large superlattice unit cell as compared to the bulk unit cell and can lead to qualitative results for the dispersion curves. Figure 1 shows a clear example. The GaAs-AlAs (100) superlattice band structure in the [100] direction is plotted for three GaAs layer thicknesses (Ivanov and Pollmann, 1979). The folded bulk GaAs band structures (dotted lines) provide good approximations to the superlattice curves (solid line).

The main differences are shifts in energy and a splitting of bulk degeneracies at zone edges.

### B. Bulk Solutions with Complex Wave Vectors

Another useful concept which relates the superlattice properties to those of its constituent bulk materials is that of describing the superlattice electron or phonon wave function in terms of bulk states with complex wave vectors. By these are meant solutions to the bulk Schrödinger equation with complex values of  $k_x$ :

$$H_i \psi_n^{(i)}(\vec{k}_t, k_x^{(n)}, \vec{r}) = E \psi_n^{(i)}(\vec{k}_t, k_x^{(n)}, \vec{r}), \quad (1)$$

with  $i = 1, 2$  labelling the two bulk semiconductors,  $\vec{k}_t$ , the wave vector parallel to the superlattice planes, and  $n$  labelling the allowed  $k_x$  values for fixed  $\vec{k}_t$ ,  $i$ , and  $E$ . Recently, a simple and efficient method for finding the complex  $k_x$  solutions to this equation has been developed within the tight-binding,  $k \cdot p$ , and pseudopotential schemes (Chang and Schulman, 1982).

The usefulness of the complex wave vector states is that the superlattice Hamiltonian away from any disruption near the interfaces is equal to the bulk Hamiltonians of one or the other of the constituent materials. The superlattice wave function in these regions, therefore, can be written as a linear combination of bulk complex solutions with the same energy and  $\vec{k}_t$  (Schulman and McGill (1981), Schulman and Chang (1981a)).

$$\psi(\vec{r}) = \sum_n C_n^{(i)} \psi_n^{(i)}(\vec{r}), \quad (2)$$

within material  $i$ . The solutions with complex values of  $k_x$  represent evanescent

states with decay lengths equal to  $(\text{Im}(k_x))^{-1}$ .

In general, a full calculation is needed to determine the exact linear combinations in Eq. (2). There are energy ranges of interest, however, in which symmetry or other considerations limit the number of complex  $k_x$  bulk states which contribute substantially to the superlattice wave function. In these cases much can be learned about the superlattice wave function from an analysis of the complex wave vector bulk states alone. In the more general case, the coefficients  $C_n^{(j)}$  in Eq. (2) give the mixing of the complex wave vector bulk states by the superlattice potential. This will be discussed in more detail in section IV C.

### III. CALCULATION OF ELECTRONIC PROPERTIES

This section will discuss the methods which have been used to calculate the electronic properties of semiconductor superlattices. In order of increasing computational complexity, these are the quantum well model, the two-band approximation, the full tight-binding method, and the pseudopotential method. The different methods rely to varying degree on empirical parameters which are related to the bulk or atomic properties of the two constituent semiconductors. The effects of this and of the other assumptions in the various models on the calculated electronic properties will be discussed here.

## A. Band Offsets

The first three methods share a common empirical parameter whose value must be found — the band offset. In all three methods the bulk band structure of each constituent material, or at least that part of it which is of interest, is independently determined with an arbitrary energy zero. The parameters which produce the bulk band structures are then to be used in the superlattice calculation, but first the relative energy lineup, the band offset, must be determined.

Attempts to calculate the offsets theoretically have not been conclusive. Several approaches have been taken. The simplest guide to the offset value is the electron affinity rule (Milnes and Feucht, 1972). This method locates the conduction band edge of each material relative to the vacuum using the experimentally determined bulk electron affinity. Inaccuracies arise from experimental uncertainties (typically tenths of eV's), and the omission of surface and interface effects. Harrison (1980) used a unified tight-binding model to predict electron affinities, and thus offsets, theoretically for several materials. Trends seem to be qualitatively described, but the accuracy is limited by the omission of interface effects and self-consistency. Two more detailed, theoretical attempts to determine the offsets were the electrostatic potential matching scheme of Frensley and Kroemer (1977) and the application of the self-consistent pseudopotential method (Pickett et al., 1978, Ihm et al., 1979) to the problem. As will be shown, these methods also had limited success. It is possible that a more detailed structural and chemical knowledge of the atomic layers very close to the interface is needed to produce more accurate values.

Tables 1, 2, and 3 demonstrate the variation in the values of the offsets as calculated by several methods. Also listed are experimentally determined values, which for the GaAs-Ga<sub>(1-x)</sub>Al<sub>x</sub>As and InAs-GaSb superlattices are relatively well determined. For example, Table 1 lists values for the GaAs-AlAs valence band maxima discontinuity as a fraction of the total difference in direct band gaps between the two semiconductors (see Fig. 2). The generally accepted value is that of Dingle, Gossard, and Wiegmann (1975),  $\Delta E_v/\Delta E_g = 0.15$ . This value was originally determined by using a simple well model to fit features in the optical absorption spectra of the GaAs-Ga<sub>(1-x)</sub>Al<sub>x</sub>As superlattice. It has since then been used successfully in analyzing optical spectra from superlattices, quantum wells, and two-dimensional electron gases at the GaAs-Ga<sub>(1-x)</sub>Al<sub>x</sub>As interface. Only the theoretical calculation of Pickett et al., using a self-consistent pseudopotential method, is close to that of Dingle et al. The electrostatic potential matching scheme of Frensley and Kroemer (1977) and the unified tight-binding model of Harrison (1980) both produce discontinuities which are substantially different from Dingle's value.

The situation is similar for the InAs-GaSb heterojunction (Table 2). The critical parameter here is  $E_g$ , the GaSb valence band maximum energy minus the InAs conduction band minimum energy (see Fig. 3). Several experiments have been successfully analyzed using values of  $E_g$  between 0.06 and 0.15 eV. Using electron affinities to locate the conduction band edges relative to the vacuum level seems to be accurate in this case (Sai-Halasz et al., 1977). It produces a value for  $E_g$  of 0.14 eV which compares well with the 0.15 eV value deduced from

analyzing experimental superlattice energy gaps with a simple two-band model (Sai-Halass et al., 1978a). Madhukar et al. (1979) fit the same data with a tight-binding model and found a value of 0.06 eV for  $E_g$ . In this case Harrison's method agrees roughly with the experimental findings, while Frensley and Kroemer's does not. The self-consistent pseudopotential method which seemed successful in the GaAs-AlAs case is less accurate for InAs-GaSb, perhaps due to the neglect of the spin-orbit interaction (Ihm et al., 1979).

The band offsets which have been most extensively studied experimentally are those of the Ge-GaAs system (Table 3). The consensus of the more recent experiments (Kraut et al., 1980, Mönch et al., 1980, Bauer, 1981) is that the valence band discontinuity lies between 0.36 eV and 0.53 eV. The electron affinity rule (Shay et al., 1976) fails here, while the theoretical approaches give a large range of values (Frensley and Kroemer, 1977, Pickett et al., 1978, Harrison, 1980, Baraff et al., 1977, Kunc and Martin, 1980).

The CdTe-HgTe heterojunction and superlattice are at an early stage of experimental investigation. Measurements by Kuech and McCaldin (1982) imply a valence band offset in this system that is not as small as that predicted by electron affinity arguments. They speculate, however that this may be caused by inversion at the interface and that the true offset may be small.

## B. Quantum Well Model

The electronic structure of superlattices of certain compositions and in certain energy ranges can be obtained from a simple quantum well model. For ex-

ample, the band offsets for the GaAs-Ga<sub>(1-x)</sub>Al<sub>x</sub>As superlattice are such that the bulk conduction band minima and valence band maxima line up as shown in Fig. 2. The band gap of the Ga<sub>(1-x)</sub>Al<sub>x</sub>As forms a barrier to the electrons in the GaAs conduction well and the holes in the GaAs valence well. The simplest calculation based on this model uses the effective mass approximation and writes the electronic wave function as a plane wave, just as in the Kronig-Penney problem (Esaki and Tsu, 1970). The energy solutions form a series of minibands within the conduction and valence wells.

It is clear that for values of  $x$  such that the Ga<sub>(1-x)</sub>Al<sub>x</sub>As alloy has a direct band gap, the band edges indicated in Fig. 2 should be the direct edges. For  $x$  greater than 0.4, however, Ga<sub>(1-x)</sub>Al<sub>x</sub>As has an indirect conduction band minimum at the X-point. The quantum well model gives no guidance as to which minimum to use. In general, a more detailed calculation which includes more of the band structure is needed.

This model has been widely used to analyze experimental data, especially optical experiments. As long as the widths of the alternating layers are large,  $> 50 \text{ \AA}$ , the quantum well model should give an adequate description of the electronic structure of the lowest conduction bands and highest valence bands. This has indeed been the case for most of the superlattices on which experiments have been performed.

Several steps can be taken within this framework to improve agreement with experiment over the simple Kronig-Penney calculation and to extend the validity of the model over a larger energy range. A major defect in the model is the as-

sumed parabolic bulk energy dispersion curves at all energies resulting from the effective mass approximation. Since the accuracy in the determination of the superlattice energy levels can be no better than that for the bulk semiconductors, it is important to use bulk dispersion curves which are as accurate as possible. Fig. 4 illustrates the deviation from parabolicity of the bulk GaAs and AlAs energy bands in the fundamental band gap region. It shows parabolic dispersion curves superimposed on dispersion curves determined from a tight-binding calculation with the same effective masses at the valence and conduction band edges (Schulman and Chang, 1981a). In order for a superlattice state energy to be correctly computed from a Kronig-Penney model calculation, it is necessary that the energy lie within the parabolic regions of the GaAs and AlAs bulk bands.

It can be seen that the GaAs conduction band parabolic curve begins to depart significantly from the results of the tight-binding calculation for energies greater than roughly 0.5 eV above the conduction band minimum. Fortunately, most recent experiments on GaAs-Ga<sub>(1-x)</sub>Al<sub>x</sub>As superlattices have investigated electronic states which fall within this range of energy. For example a GaAs-AlAs superlattice made from alternating layers with widths of 50Å each has a lowest conduction band energy of only about 0.1 eV above the GaAs edge (Mendez et al., (1981)). Thus, the departure from parabolicity in superlattices with thicker GaAs layers, or for superlattices with Ga<sub>(1-x)</sub>Al<sub>x</sub>As layers replacing the AlAs (which can also have small lowest conduction band energies) is moderate.

Also important is the effect of non-parabolicity in the Ga<sub>(1-x)</sub>Al<sub>x</sub>As layers. The lowest superlattice conduction band energy, while quite close to the GaAs

conduction band edge, is, because of the band offsets, far from the  $\text{Ga}_{(1-x)}\text{Al}_x\text{As}$  conduction band edge at the zone center, except for small values of  $x$ . Thus, the deviation from parabolicity in the  $\text{Ga}_{(1-x)}\text{Al}_x\text{As}$  can be substantial. The extreme case, shown in Fig. 4 for  $x = 1$ , results in a large difference in bulk  $k_x$  between the tight-binding and parabolic dispersion curves for energies close to the GaAs conduction band edge. Again, many of the experimental results reported in the literature which were analyzed using the Kronig-Penney model pertained to GaAs- $\text{Ga}_{(1-x)}\text{Al}_x\text{As}$  superlattices with small values of  $x$ , so that large errors would not be expected in those cases. Also, since the superlattice state in this energy range is highly localized in the GaAs layers, the  $\text{Ga}_{(1-x)}\text{Al}_x\text{As}$  dispersion is less important in influencing the superlattice state energy.

An illustration of the error resulting from the use of a Kronig-Penney calculation for the quantum well model is shown in Fig. 5 (Schulman and Chang, 1981a). Superlattice conduction minimum dispersion curves in the  $z$  direction calculated using the Kronig-Penney and tight-binding methods are shown for superlattices with two layers of AlAs alternating with a varying number of GaAs layers. Agreement between the two methods decreases for superlattices with smaller numbers of GaAs layers because the resulting energies are further from the GaAs conduction band minimum and the effects of non-parabolicity become more important. The two methods have also been compared for higher lying superlattice conduction states. These correspond to higher states in the quantum wells. The discrepancies between the two methods follow the same pattern — higher energies have greater discrepancies.

Figure 5 also shows that for energies above  $\approx 0.52$  eV the predictions of the two methods diverge. The tight-binding curves flatten out at this energy, whereas the Kronig-Penney curve continues to increase with increasing perpendicular wave vector. Its significance is that it is the indirect conduction band minimum energy at the X-point in both GaAs and AlAs (with the specified band offsets). Near it, the superlattice state is more closely related to the bulk X-point states than it is to the zone center states. The Kronig-Penney model ignores these states and thus it fails completely here. Note that this energy is far below the AlAs direct conduction band minimum.

There have been several attempts to improve the Kronig-Penney model while keeping within the same basic framework. Mukherji and Nag (1975, 1978) modified the very simplest model by using different effective masses for the two-constituent semiconductors. They also artificially imposed a modification of the parabolic dispersion curve using Kane's relationship for an energy dependent effective mass. GaAs-Ga $_{(1-x)}$ Al $_x$ As superlattice conduction band energies were calculated for superlattices with  $x$  values of 0.2, 0.5, and 0.7. The GaAs layer width used was 50Å, while the Ga $_{(1-x)}$ Al $_x$ As width varied from 10Å to 100Å. They found that including non-parabolicity decreased the superlattice conduction state energies (measured relative to the GaAs conduction band minimum) by as much as 15% for  $x = 0.2$  and 25% for  $x = 0.5$  and 0.7.

In addition, Mukherji and Nag made the first attempt to evaluate the effect of the indirect Ga $_{(1-x)}$ Al $_x$ As X-point conduction band minimum on the superlattice conduction band states. They found that the lowest energy states were not related

to the X-point minimum, even for  $x$  values such that  $\text{Ga}_{(1-x)}\text{Al}_x\text{As}$  is indirect. They predicted additional narrow bands above the conduction band minimum which would be derived from the X-point states. This result is supported by the tight-binding calculation, as shown in Fig. 5.

In general the simple Kronig-Penney model must be applied with special care when analyzing experiments in which optical transitions between superlattice states composed of bulk states away from the zone center are important. This was attempted by Mendez et al. (1981) in their analyses of electroreflectance spectra of  $\text{In}_{(1-x)}\text{Ga}_x\text{As} - \text{GaSb}_{(1-y)}\text{As}_y$  and  $\text{GaAs} - \text{Ga}_{(1-x)}\text{Al}_x\text{As}$  superlattices. Not surprisingly, they showed that the variation of the optical transition energies for transitions away from the zone center as a function of layer thickness in the  $\text{In}_{(1-x)}\text{Ga}_x\text{As} - \text{GaSb}_{(1-y)}\text{As}_y$  system did not follow Kronig-Penney behavior. The more complicated behavior they did observe must be analyzed using Mukherji and Nag's method or the more detailed tight-binding or pseudopotential methods which can describe bulk band structures away from the zone center.

### C. Two-Band Models

The two-band model is the simplest model which realistically incorporates some elements of the band structure of the constituent semiconductors. The two bands of interest are the lowest conduction band and the light hole band. It provides two major improvements over a Kronig-Penney type calculation. First, the bulk dispersion curves resulting from the model are parabolic near the zone center, but contain the corrections to parabolicity for larger values of the wave

vector. In fact, an excellent estimate of the departure from parabolicity of the bulk bands, and thus of the accuracy of a superlattice energy calculated using the Kronig-Penney model, can be estimated using simple formulas derivable from a Kane type two-band model (Kane, 1957). The bulk conduction and valence band dispersion curves in this model can be written as (Schulman and McGill, 1981)

$$E = E_v + \frac{\hbar^2 \gamma^2}{m_-} \pm \frac{\hbar^2 \gamma \sqrt{k^2 + \gamma^2}}{m_{\pm}}, \quad (3)$$

where

$$\gamma = \sqrt{\frac{E_g}{\hbar^2 \left( \frac{1}{m_+} + \frac{1}{m_-} \right)}}.$$

Here,  $E_v$  is the energy of the valence band edge,  $m_-$  is the valence band effective mass,  $m_+$  is the conduction band effective mass, and  $E_g$  is the band gap. Other two band models would produce slightly different forms for the dispersion relation as compared to Eq. (3), depending on the basis set used (Sai-Hyatt et al., 1978b).

The second improvement over the Kronig-Penney model is that the two-band model recognizes that Bloch states are matched at the interfaces. In the Kronig-Penney model the states are plane waves with different normal components of the wave vectors in the two alternating layers. No account is taken of the differences in the periodic part of the bulk Bloch functions, which are ignored. The two-band model allows the Bloch functions in each material to differ from each other. This makes the boundary conditions at the interfaces more realistic, although more complicated.

Also, the use of Bloch functions in the two-band model includes the possible mixing of bulk states from different bands in forming the superlattice state. This

is an especially important effect in the InAs-GaSb superlattice in which the band offsets are such that the InAs lowest conduction band is near in energy to the GaSb valence band maximum. Superlattice states which mix the InAs conduction band state and the GaSb light hole state would be expected (Sai-Halasz et al., 1977). A similar effect occurs in the GaAs-Ga<sub>(1-x)</sub>Al<sub>x</sub>As superlattice valence bands where the light hole and spin-orbit split-off bands can interact. Section IV will give examples of this mixing.

There have been two types of two-band model calculations carried out for superlattices: those based on a Kane type analysis (Sai-Halasz et al., 1977, White and Sham, 1981, Bastard, 1981, 1982b) and those based on the tight-binding method (Sai-Halasz et al., 1978b, Ivanov and Pollmann, 1979). Sai-Halasz et al. (1977) used Bloch functions obtained from Kane's two-band Hamiltonian to replace the plane waves of the Kronig-Penney model. The superlattice dispersion relation was then obtained by matching the wave function and its derivative at the interfaces. The resulting superlattice dispersion relation is

$$\cos(kd_0) = \cos(k_1 d_1) \cos(k_2 d_2) - f \sin(k_1 d_1) \sin(k_2 d_2), \quad (4)$$

with

$$f = \frac{1}{2} \left( w + \frac{1}{w} \right),$$

and

$$w = \frac{ik_1 + \frac{u_1'}{u_1}}{ik_2 + \frac{u_2'}{u_2}}.$$

Here,  $k$  is the superlattice wave vector in the direction perpendicular to the interface,  $d_0$  is the superlattice period,  $d_1$  and  $d_2$  are the thicknesses of the alternating slabs,  $k_1$  and  $k_2$  are the wave vectors of the Bloch states in the alternating layers, and  $u_1$ ,  $u_2$ ,  $u_1'$  and  $u_2'$  are the values of the periodic parts of the Bloch states and their first derivatives in the alternating slabs at the interfaces. The Kronig-Penney formula is recovered if the logarithmic derivatives are set equal to zero.

The effect of including two bands in their calculation is clearly demonstrated in Fig. 6. The superlattice dispersion curves for three  $\text{In}_{(1-x)}\text{Ga}_x\text{As}-\text{GaSb}_{(1-y)}\text{As}_y$  superlattices with three sets of  $x$ ,  $y$  values: (a)  $x=0$ ,  $y=0$ , (b)  $x=0.75$ ,  $y=0.15$ , (c)  $x=0.67$ ,  $y=0.70$  are shown. The bulk conduction and valence band edges and the band offsets are also indicated. In case (c), the dispersion curves calculated using the Kronig-Penney and two-band models are almost identical. This follows from the large energy separation between the bulk  $\text{In}_{(1-x)}\text{Ga}_x\text{As}$  conduction band and the bulk valence band of the  $\text{GaSb}_{(1-y)}\text{As}_y$ . Substantial deviation from the Kronig-Penney model is found for alloy superlattices (a) and (b) in which the conduction and valence bands of the different materials are close in energy.

G. Bastard (1981,1982b) made use of the same Kane formalism and also obtained Eq. (4). Investigating the boundary conditions in more detail, he expressed the correction to the Kronig-Penney boundary conditions for the quantum well model in a simple way. First, the effective mass envelope function is assumed continuous across the interface. Then, the derivative of the envelope function divided

by a simple function of the band energy is matched. This reduces to matching the derivative divided by the effective mass at interfaces in which band mixing is small, such as in the GaAs-Ga<sub>(1-x)</sub>Al<sub>x</sub>As superlattice. For the interacting band case, the InAs-GaSb superlattice, the full expression is used.

The other two-band calculation based on the Kane model is that of White and Sham (1981). White and Sham derived boundary conditions which matched light hole band and conduction band wave functions across the interfaces, but not their derivatives. Bastard(1982b) has demonstrated the equivalence of these boundary conditions with his own. Since both Bastard's and White and Sham's methods produce reasonable agreement with experimental data, it is probable that the inaccuracies in their boundary conditions are not significant within the range in which the two-band model is applicable. As shown in section IV C, more than two bands can contribute significantly to the superlattice wave functions close to the interface, so that their boundary conditions would not be expected to be particularly accurate in general. In a recent development(Altarelli, 1982), Altarelli has devised a new, very efficient method for calculating superlattice electronic properties within a similar two-band kane model framework.

There have been two two-band model calculations on superlattices based on the tight-binding method, one for the InAs-GaSb superlattice (Sai-Halasz et al., 1978b) and one for the GaAs-Ga<sub>(1-x)</sub>Al<sub>x</sub>As superlattice (Ivanov and Pollmann, 1979). Both use a basis set consisting of one s orbital on the cation and one p orbital on the anion. The empirical parameters were chosen to reproduce the experimental bulk data on band gaps, effective masses and band offsets. Thus,

these models could be expected to describe the lowest conduction band and light hole valence band well. In addition, Sai-Halasz et al. included the dispersion in the heavy hole band by allowing p orbitals on the cation to interact with the p orbitals on the anion. Both calculations produced superlattice dispersion curves and thickness dependent energy levels. Also, Sai-Halasz et al., used a self-consistent Thomas-Fermi approximation to investigate band bending in the InAs-GaSb superlattice.

A notable feature of both of these calculations is that unlike the conventional tight-binding model the complexity of these calculations does not increase with the thickness of the alternating superlattice layers. Sai-Halasz et al. replaced the Hamiltonian method with a transfer matrix approach. The superlattice bands are found by examining the trace of the transfer matrix. Ivanov and Pollmann used an equivalent approach based on a resolvent technique within a Green's function formulation of scattering theory.

The limitation of the two-band model is that it is valid only within a limited energy range. A major improvement of the two-band model over the quantum well model is in its ability to describe the bulk dispersion curve for imaginary values of the wave vector,  $k_z$ . As shown in Fig. 4, a GaAs-AlAs superlattice state with an energy slightly above the GaAs conduction band minimum has an energy which lies well within the AlAs band gap. The two-band model produces an excellent approximation to the full tight-binding dispersion curve which connects the conduction band minimum and valence band maximum across the AlAs gap. The two curves fall almost on top of each other in Fig.4. The superlattice

dispersion curve which results is in closer agreement with that of the full tight-binding calculations than that of the quantum well calculation (Fig. 5) in both energy location and in shape of the curve. The two-band model also fails, however, when the superlattice energy approaches the X-point energy and for the same reason: the bulk band structure away from  $Re(k_x) = 0$  is ignored.

The two-band model is obviously inadequate in describing superlattice states in which more than two bulk states may be expected to contribute significantly. For example, the band offsets in the InAs-GaSb superlattice are such that certain superlattice valence band state energies are near the InAs conduction band minimum, the GaSb light hole band maximum, and the GaSb spin-orbit split-off band maximum. A more detailed model is thus necessary to include all three bulk states.

#### D. Full Tight-binding Models

The simplest model which incorporates a realistic description of the bulk band structures is the tight-binding model. First introduced for the GaAs-AlAs superlattice (Schulman and McGill, 1977, 1979c), it has also been applied to the InAs-GaSb (Nucho and Madhukar, 1978, Madhukar et al., 1979, Madhukar and Nucho, 1979), CdTe-HgTe (Schulman and McGill, 1979a, 1979b, 1981), Si-GaP (Madhukar and Delgado, 1981), and GaAs-GaAsP (Osborn, 1982) superlattices. As most commonly employed, the tight-binding method makes use of one s-orbital and three p-orbitals per anion and cation. Thus, a total of eight bands, four valence and four conduction, can be described. As in the two-band model, the

empirical parameters in the theory are chosen to reproduce features in the bulk band structures such as optical transition energies and effective masses. The valence bands are quite accurately fit in this way (Chadi and Cohen, 1975). The conduction bands are more troublesome, but can also be adequately described for the purposes of a superlattice calculation by including second neighbor overlap parameters (Schulman and McGill, 1977) or more orbitals (Schulman and Chang, 1981a).

The overlap parameters between orbitals on opposite sides of the interface between the two alternating semiconductors must be considered separately. In superlattices with a common anion, such as GaAs-AlAs, the As-cation overlaps have been taken to be the same as for the bulk materials. The second neighbor cation matrix elements and the on-site As matrix elements were taken to be the average of those for the two bulk materials (Schulman and McGill, 1977). The InAs-GaSb calculations made use of bulk InSb and GaAs parameters at the interfaces (Nucho and Madhukar, 1978).

These assumptions point out the main limitation of the tight-binding method: the approximate description of the interface electronic structure. This model, like the quantum well and two-band models, assumes a bulk-like potential right up to the interface. No self-consistency in the electronic density or atomic rearrangement, which would modify the potential near the interface, is included. Fortunately, as will be discussed subsequently, calculations which include a self-consistent redistribution of electronic charge show that its effect is small and of short range. Also, for lattice matched semiconductors with similar valence

electronic structure little atomic rearrangement is expected.

As mentioned previously, the original formulation of the tight-binding method for superlattices made use of a Hamiltonian matrix whose dimension grows linearly with the superlattice unit cell length in the  $z$ -direction. This was a serious limitation on the usefulness of the method, as superlattices of only about forty atoms per unit cell in the  $z$ -direction could be handled. Recently, an equivalent reformulation of the method has been developed (Schulman and Chang, 1981a, 1983) which employs a Hamiltonian of constant dimension. In addition, this method allows a clear analysis of the superlattice electronic state in terms of the bulk Bloch states of which it is composed.

In this method the superlattice state of energy  $E$  and specified  $\vec{k}_\perp$  is written as in eqs. (1) and (2) as a sum of bulk Bloch states with complex values of  $k_z$ . The number of Bloch states needed is, for instance, sixteen for each material for a (100) superlattice when four orbitals per atom and up to second neighbor interactions are included (Osbourn and Smith, 1979). They can be found using the method of Chang and Schulman (1982) or Schulman and Chang (1983). The thirty-two Bloch states thus form a basis in which the Hamiltonian matrix is written. Diagonalizing this Hamiltonian gives the superlattice state energy and the correct linear combination of Bloch states needed to describe it. Since the Bloch states which form the basis are energy dependent, however, it is necessary to iterate this method so that the energy resulting from diagonalizing the Hamiltonian is the same as that used in finding the Bloch states. In practice, very few (two to five) iterations are needed and the computer time involved is insignificant.

## E. Pseudopotential Method

The pseudopotential method is the most sophisticated of the methods so far described. Its principle advantage is that it incorporates detailed, albeit pseudo-wave functions. With the pseudo-wave functions, the valence charge density and the resulting electrostatic potentials can be estimated.

The pseudopotential model, as it has been applied to superlattices, also has empirical parameters that must be determined. The parameters in this case determine the form and intensity of the atomic pseudopotentials. They have been fit by attempting to reproduce features of the atomic or the bulk electronic structures or both. The empirical pseudopotential method (Caruthers and Lin-Chung, 1977, 1978, Andreoni et al., 1978) uses these parameters to create the superlattice potential by superimposing the atomic pseudopotentials. A basis set (usually plane wave) is chosen and the electronic properties are calculated by diagonalizing the Hamiltonian. The self-consistent pseudopotential method continues and calculates a new electrostatic potential based on the charge distribution given by the wave functions.

The self-consistent pseudopotential method allows a direct determination of the band offsets between the two semiconductors. The most common method for achieving this (Pickett et al., 1978, Ihm et al., 1979, Kunc and Martin, 1980) is to determine the average electrostatic potentials in the separate bulk materials and then to determine them again on either side of, and away from, an interface formed by joining them. The shift in the difference between the potentials of the two materials determines the offsets.

The main disadvantage of the pseudopotential method is the computational difficulties involved for superlattices with large alternating layer thicknesses. For example, Caruthers and Lin-Chung in their non-self-consistent calculation found that for a general wave vector the largest GaAs-AlAs superlattice for which it was practical to carry out their calculation consisted of just three layers of GaAs alternating with three layers of AlAs (Caruthers and Lin-Chung, 1978). At the zone center, they could treat a total of eighteen layers of GaAs and AlAs per superlattice unit cell. It is possible that this limitation could be eliminated by expanding the superlattice state in terms of bulk states with complex values of  $k_x$ , as was done within the tight-binding formalism. A method which finds the complex  $k_x$  states within the pseudopotential and k-p formalisms has been developed (Chang and Schulman, 1982), but it has not yet been applied to the superlattice problem.

Another difficulty of the pseudopotential method is one it shares with the tight-binding method. Similar calculations carried through based on somewhat different empirical pseudopotential parameters give conflicting results. This will be discussed in more detail in Section IV.

The non-self-consistent pseudopotential method has an additional difficulty when applied to the superlattice problem. As it has been applied so far, the band offsets between the bulk semiconductors are a product, not an input, of the calculation (Caruthers and Lin-Chung, 1978). However, Pickett et al. (1978) have shown for the (110) Ge-GaAs and GaAs-AlAs interfaces that the offsets can change substantially when self-consistency is included. It is unclear whether

the offsets produced by the nonself-consistent calculations agree with accepted values.

#### **IV. ELECTRONIC PROPERTIES**

In this section we will discuss a few of the electronic properties of semiconductor superlattices which have been investigated theoretically using the methods of Section III. Of special interest is the electronic structure in the energy range of the band gap, for example, band gap dependences on superlattice parameters and the character of the electronic states. Also to be discussed are the related problems of the confinement of electronic states and the mixing of bulk states by the superlattice potential.

The focus in this section will be on the two superlattice systems which have been the most thoroughly investigated theoretically. These are the GaAs-AlAs and InAs-GaSb superlattices. Also to be mentioned is the CdTe-HgTe superlattice. This system has only recently been fabricated in the laboratory (Faurie, 1981). Prior theoretical calculations (Schulman and McGill, 1979a, 1979b) predict unique properties for this superlattice.

##### **A. Interface Electronic Structure**

The electronic properties of semiconductor interfaces have been studied extensively and reviewed elsewhere (Pollmann, 1980). There are two important

results from these calculations which are most relevant to superlattices. The first is the values of the band offsets. This has been discussed in Section II. The second and related result is the effect of the interface on the electrostatic potential and thus the superlattice Hamiltonian. If the presence of the interface disrupts the potential at large distances away from the interface the approximation employed by the quantum well, two band, and tight-binding models, consisting of using parameters characteristic of the bulk materials close to the interface, is inadequate.

Fortunately, detailed studies of the interface potential show that the interfacial disruption can be slight and highly localized within two or three atomic planes from the interface. For example, Fig. 7 shows the potential averaged over planes parallel to the interface near the GaAs-AlAs and Ge-GaAs interfaces (Pickett et al., 1978). It can be seen that the potential is indistinguishable from bulk-like within two layers. The main effect of the joining of the two materials is the shift in average bulk potentials brought about by the self-consistent iteration. The effect is incorporated in the value of the band offset and thus can be included empirically in the less sophisticated models.

The short range of the disruption near the interface is not surprising for two lattice matched semiconductors with similar chemical character such as GaAs-AlAs, InAs-GaSb, and CdTe-HgTe. Other pairs of materials may not be so simple and could exhibit as yet unknown reconstruction and charge transfer.

## B. Band Gaps

Since the alternating materials out of which a superlattice is constructed are semiconductors, it is not surprising that the superlattice itself is also usually a semiconductor. Of practical significance is the fact that the superlattice band gap is adjustable by varying the thicknesses of its alternating layers.

There have been several calculations of the superlattice band gap dependence on layer thickness for the GaAs-ALAs, for the InAs-GaSb, and for the CdTe-HgTe systems. The GaAs-ALAs superlattice will be discussed first.

For large GaAs and ALAs alternating layer thicknesses, the band gap dependence is smooth and monotonically decreasing with GaAs layer thickness, just as would be the case for a series of square wells separated by finite barriers. Both the conduction electrons and the valence holes in the GaAs layers near the band edges are in these effective wells, as seen in Fig. 2. The Kronig-Penney, two-band and tight-binding models all show this simple behavior down to very thin GaAs and ALAs layer thicknesses — about  $10\text{\AA}$ . So do two of the three pseudopotential calculations performed on this system (Andreoni et al., 1978, Pickett et al., 1978). The exception is the pseudopotential calculation of Caruthers and Lin-Chung (1978). They find an almost flat variation of band gap with layer thickness for up to nine atomic layers each of GaAs and ALAs (as compared with Kronig-Penney behavior). Consistent with this result is that the lowest conduction band state in their calculation does not resemble the state for a particle in a well. Instead, it has a large charge density very close (within two atomic layers) to the GaAs-ALAs interfaces. They conclude that this is caused by an abruptly changing potential

at the interface. Andreoni et al.(1978), and implicitly all others who have calculated the band gap variation claim that Caruthers and Lin-Chung overestimated the cationic potential difference and thus the abruptness of the change in the interface potential.

For very thin layers, the quantum well model does break down. Andreoni et al. find that the thin layer superlattices have band structures very close to that of the alloy with the same composition. The tight-binding study of Schulman and McGill (1979c) is in qualitative agreement, but predicts a faster decrease in band gap with increasing thickness. This may be due to the inaccuracies in the effective masses produced by the particular choice of parameters in the tight-binding model. Indeed, subsequent studies using the tight-binding model have been careful to ensure that experimental effective masses were obtained. This has resulted in the more successful reproduction of experimental band gaps.

The InAs-GaSb superlattice band gap variation cannot be analyzed in quite so simple a manner, but the well model still leads to a qualitative understanding. Fig. 3 shows that the bottommost conduction states should be localized in the InAs layers while the topmost valence states would be mostly in the GaSb layers. What is not obvious is the relative energy positioning of the lowest InAs and highest GaSb like state. For large layer thicknesses, in fact, the states cross: the InAs state has a lower energy than the GaSb state. When this occurs, the superlattice becomes a semi-metal (Chang et al., 1979, Guldner et al., 1980). Rough agreement for the thickness at cross-over exists among theoretical calculations (Sai-Halasz et al., 1978b, Madhukar et al., 1979, Chang, 1980) and experiment

(Chang et al., 1979) - about 100Å each of InAs and GaSb.

The problem with the quantum well model as applied to the InAs-GaSb superlattice is that the well limits are not well defined. For example, the bottom-most conduction state, which is mostly localized in the InAs layers, will decay into the GaSb layers. However, the effective well edge which governs the decay is not simply the GaSb conduction band edge, because the InAs state can join onto the GaSb light hole state as well as the GaSb conduction minimum state.

A similar situation exists for the CdTe-HgTe superlattice. Due to their common anions, band offsets for this superlattice have been conjectured to be such that the valence band maxima of bulk CdTe and HgTe are very close in energy (Schulman and McGill, 1979a), Fig. 8. The zero band gap of HgTe and the small value of the valence band discontinuity lead to unique band gap behavior. The state at the conduction band minimum in the superlattice is made up of conduction band states in the HgTe layers, as the simple quantum well model would lead one to expect. However, the large (1.6 eV) conduction band discontinuity does not confine the electron. The close proximity of the CdTe valence band maximum to the HgTe conduction band minimum allows the electrons to tunnel through the CdTe layers with relative ease (Schulman and McGill, 1981). This superlattice also exhibits an interesting transition from an alloy-like conduction minimum electronic structure for small layer thicknesses to quantum well behavior as the layer thickness increases (Schulman and McGill, 1979b). This is manifested by a transition in symmetry of the conduction band minimum state as the layer thickness increases. The overall dependence of band

gap on layer thickness follows the trend explained by the well model (Schulman and McGill, 1979a; Bastard, 1982b). The gap goes to zero for large HgTe layer thicknesses, and increases with decreasing HgTe layer thickness or increasing CdTe ("barrier") thickness.

### C. Superlattice Wave Functions

As discussed previously, the short range of the interfacial disruption of the otherwise bulk-like potential allows the superlattice state to be accurately described as a linear combination of bulk states in each material with complex wave vector values. In this section the decomposition of the superlattice state into its bulk state components will be illustrated. As a particular example, several valence band superlattice states at the Brillouin zone center of the (100) GaAs-AlAs superlattice consisting of 50Å (seventeen atomic double layers) of GaAs alternating with the same amount of AlAs will be examined in detail. The theoretical framework used is that of the empirical tight-binding method (Schulman and Chang, 1981b).

Typical types of superlattice states are the following. The simplest of the states are similar in form to Kronig-Penney well type states. These are states in which just one bulk state from near the bulk zone center dominates in each material. Spatial plots of these states have distinctive single or multiple peaked structures which are basically discrete lattice versions of sine waves. Other superlattice states have more than one bulk state contributing significantly. Their spatial plots are correspondingly more complicated. Bulk states with non-zero

real and imaginary parts play an important role in many superlattice states. Even when they decay rapidly away from the interface (large  $Im(k_x)$ ) they can represent a significant contribution close to the interface itself and, therefore, are important in determining the matching of bulk states across the interface. This implies that models that omit these states, such as the Kronig-Penney and two-band models, may not describe the boundary conditions at the interface realistically.

The complex wave vectors of the bulk states which make up the superlattice state are shown in Fig. 9. The complex band structures of GaAs and AlAs are displayed in the same manner as in Fig. 4. The spin-orbit interaction is included here. The complex wave vectors for a superlattice state with a given energy can be seen by finding the bulk complex states with the same energy. For example, the state in Table 4 with energy  $-0.06$  eV is composed of bulk complex states at that energy in Fig. 9. It shows that there are four distinct bands at energy  $-0.06$  eV in GaAs and four in AlAs. There are actually a total of twenty bands for each material, but they are related to the four shown by negating or complex conjugating the wave vector, or by other symmetries peculiar to the (100) direction in zincblende materials (Chang, 1982). Two of the four GaAs wave vectors are purely real - those in the light and heavy hole bands. The spin-orbit split-off band wave vector is purely imaginary, and the state emanating down from the conduction band minimum near the X point is complex. The light and heavy hole AlAs wave vectors are purely imaginary.

Table 4 lists all of the superlattice state energies at the zone center between  $-0.41$  eV and  $1.56$  eV (the energy zero is the bulk GaAs valence band maximum).

Also indicated are the bulk GaAs and AlAs states which give the dominant contribution to each superlattice state. They are labelled by the bulk complex bands to which they belong: conduction, heavy hole, light hole, or spin-orbit split-off bands. There is some ambiguity in assigning these labels to the complex bands, because there are no band gaps in complex wave vector space. For example, a band originating from the conduction band minimum connects with the light hole band maximum. Points on this curve with energies closer to the conduction band minimum are labelled as being conduction band states in Table 4.

An example of a superlattice state in which one bulk state is dominant is the state with energy  $-0.06$  eV. Bulk GaAs and AlAs light hole states contribute substantially more than the others in this case. A spatial plot of the wave function shows that the state resembles closely a bottommost light hole quantum well state. The same state plotted with the coefficients of the bulk GaAs states other than the light hole state set equal to zero is only slightly different. This demonstrates that the one band quantum well model would be a reasonable approximation in describing the state. Similarly, the state with energy  $-0.02$  eV is found to be the bottommost heavy hole quantum well state. The states with energies between  $-0.02$  and  $-0.22$  eV all resemble heavy or light hole quantum well states, including excited states.

The next state, with energy  $-0.27$  eV, is low enough in energy so that it is below the AlAs valence band edge. It has a dominant heavy hole band contribution in the AlAs layers with a purely real AlAs wave vector. The wave function thus has a substantial amplitude in the AlAs as well as the GaAs layers.

This is true of all the states with energies between  $-0.27$  eV and  $-0.39$  eV. In addition, the states with energies of  $-0.29$  eV,  $-0.35$  eV, and  $-0.39$  eV have more than one bulk state with substantial coefficients, as indicated. The state with energy  $-0.40$  eV, as shown in Fig. 10 is interesting because it corresponds to the ground state spin-orbit split-off band quantum well state, although this is not obvious from examining its spatial plot. Only when the coefficients of the bulk states other than for the split-off state are set equal to zero does the characteristic well state appear. Thus, the one band, quantum well model would not be expected to describe this state accurately. The state with energy  $-0.41$  eV is an excited light hole band well state.

## V. PHONONS

Lattice vibrations in superlattices exhibit many of the same phenomena associated with the new superlattice periodicity as electrons do. The additional periodicity shows up as a folding of the phonon dispersion curves onto a Brillouin zone decreased in size along the superlattice repeat direction. This folding process results in additional modes at the zone center.

This phenomenon has been explored theoretically by Tsu and Jha (1972), Barker et al. (1978), and in a continuum model for the acoustic modes by Colvard et al. (1980). The effects of phonon folding can be illustrated by considering the results of Barker et al.(1978). They considered a one-dimensional model of a

(100) GaAs-ALAs superlattice as illustrated in Fig. 11.

The force constants for ALAs and GaAs were taken to be the same, only the masses were assumed to be different. The force constants were chosen to give a "good" fit to the phonon dispersion curves of GaAs. The resulting phonon dispersion curves for the monolayer and bilayer GaAs-ALAs superlattice are presented in Fig. 12. The additional dispersion curves— those over the four expected for bulk GaAs or ALAs—are due to the phonon folding. Of course, some small shifts in the frequencies also occur.

An important quantity determining infrared optical spectra is the infrared absorption strength  $S$ . It is given by

$$S = \frac{2}{\pi} \int \frac{\epsilon_2(\omega)}{\omega} d\omega,$$

where  $\epsilon_2(\omega)$  is the imaginary part of the dielectric constant, and the integral is taken over the absorption from a given transition. Using their one-dimensional model for the lattice vibrations and an appropriate value of the effective charge, Barker et al.(1978) calculated  $S$  for all the  $q = 0$  phonon modes. The results of this calculation are given in Table 5. Some important points should be noted from the results in this table. First, the intensities of the modes which are analogous to the bulk modes are rather large. Second, modes which are produced by the folding are very weak, where they are allowed.

Further, these authors estimated the relative Raman intensities for modes which can produce scattering with the incident light incoming along the (100) direction, the  $z$ -direction, and polarized along the  $x$ -direction. The detected photons are outgoing in the  $z$ -direction with polarisation in either the  $x$  ( $R_{zz}$ ) or

y direction ( $R_{xy}$ ). The results of these are presented in Table 6. In contrast to the case of the infrared absorption some of the additional modes are predicted to be rather strongly Raman active. This difference is due simply to the rather large difference in the bond polarizabilities for AlAs and GaAs which appear in the Raman scattering intensities in contrast to the rather small difference between the effective charges in GaAs and AlAs.

As noted by Merlin et al. (1980), the simple theory of Barker et al. (1978) did not take into account the long range forces acting on the superlattice polar phonons. They note that one should observe additional phonon modes which result not just from the decrease in zone size, but also from the differences in the polar phonons propagating normal and parallel to the superlattice layers. They examined the problem using a simple theory for the dielectric function of a layered medium (Rytov, 1956a). If  $\epsilon_1$  and  $\epsilon_2$  are the dielectric constants for layers with thickness  $d_1$  and  $d_2$ , respectively, then

$$\epsilon_{\perp} = \frac{d_1 \epsilon_1 + d_2 \epsilon_2}{(d_1 + d_2)} \quad (5)$$

$$\epsilon_{\parallel} = \frac{\epsilon_1 \epsilon_2 (d_1 + d_2)}{d_1 \epsilon_2 + d_2 \epsilon_1} \quad (6)$$

For superlattices with the symmetry  $D_{2d}$ , there are two modes: a singly degenerate  $B_2$  mode and a doubly degenerate  $E$  mode. The LO and TO phonons of both  $B_2$  and  $E$  types are given by the zeros and poles of the appropriate dielectric functions:  $B_2(\text{LO})$  is the zero of  $\epsilon_{\perp}$ ;  $B_2(\text{TO})$  is the pole of  $\epsilon_{\parallel}$ ;  $E(\text{LO})$  is the zero of  $\epsilon_{\perp}$ , and  $E(\text{TO})$  is the pole of  $\epsilon_{\parallel}$ . This long range effect alone can produce two phonons of each type, whereas in the case of the bulk III-V semiconductor, we would find only one mode of each type. The physics associated with

these additional modes is different from that producing the dispersion curve folding. The first is due to the dielectric anisotropy, while the second is due to the changes in the local periodicity.

A model similar to the Kronig-Penney model has been applied to the long wavelength acoustic phonon modes (Colvard et al., 1980). In this calculation one considers a layered elastic medium characterized by densities and sound velocities appropriate to the direction under consideration. Using the results from Rytov (1956b), they find that the dispersion curve,  $\Omega$  vs  $q$ , for LA phonons in the (100) direction is given by

$$\cos(qd) = \cos \frac{\Omega d_1}{C_1} \cos \frac{\Omega d_2}{C_2} - \frac{1+k^2}{2k} \sin \frac{\Omega d_1}{C_1} \sin \frac{\Omega d_2}{C_2},$$

where  $k = (C_1 \rho_1)/(C_2 \rho_2)$ , with  $C_1$  and  $C_2$ , and  $\rho_1$  and  $\rho_2$  being the sound velocities and densities appropriate for the two layers, respectively. The widths of the individual layers are  $d_1$  and  $d_2$ , and  $d$  is the total thickness. This formula for the dispersion curve results in a number of branches. They correspond to the LA acoustic branch of the bulk material folded into the smaller Brillouin zone of the superlattice.

Recently Ren and Dow(1982) have treated the effect of the dispersion curve folding on umklapp processes that influence thermal conductivity. They find that the additional umklapp scattering processes can produce rather substantial decreases in the thermal conductivity.

While most of the fundamental physics has been mapped out in these simple model calculations, detailed calculations of comparable sophistication to the tight-binding and pseudopotential calculations for the electronic spectra have not been

carried out. These could provide the kind of detailed insight provided by similar calculations of the electronic spectra.

## VL OTHER PROPERTIES

The elementary excitations discussed above result in a number of observable properties of semiconductor superlattices. In this section, we address some of the properties that have not been discussed earlier.

Many of the useful properties of semiconductors are due to the properties of impurities in the semiconductors. In superlattices the properties of the standard shallow dopants as well as deep levels are modified substantially from their properties in the corresponding bulk materials. Bastard (1982a), and Mailhiot and coworkers (1982a,b) have considered the case of a Coulombic center in a quantum well. Bastard assumed that the carrier was confined in an infinite well. He finds substantial modifications in the binding energy in that the binding is found to increase as the well thickness is decreased. Mailhiot et al. (1982a,b) have treated the case of a donor in a GaAs layer sandwiched between two layers of  $\text{Ga}_{(1-x)}\text{Al}_x\text{As}$ . The properties of the  $\text{Ga}_{(1-x)}\text{Al}_x\text{As}$  layers are included explicitly by taking account the finite band offset and the differences in effective masses and dielectric constants. The results of their calculation for an impurity at the center of the GaAs well are given in Fig. 13. They find that, while the binding energy at first increases due to the confinement of the donor wave function in the layer,

for thin layers the properties of the  $\text{Ga}_{(1-x)}\text{Al}_x\text{As}$  layers dominate leading to binding energies that are the same as those for the  $\text{Ga}_{(1-x)}\text{Al}_x\text{As}$  alloy. Both Bastard, and Mailhot and co-workers studied the variation of the binding energy due to position in the layer. Both find that there is substantial variations in the binding energy due to moving the impurity about in the well.

The current theories make use of the effective mass approximation which is valid for the case of donors in  $\text{GaAs-Ga}_{(1-x)}\text{Al}_x\text{As}$  as long as  $x$  is such that the  $\text{Ga}_{(1-x)}\text{Al}_x\text{As}$  is direct(Ando, 1982). However, for acceptors or donors in other systems, it will be necessary to include explicitly the bandstructure of the quantum well structure instead of simply applying the effective mass approximation.

Excitons in superlattices can be quite different from those in normal bulk semiconductors. For the case of  $\text{GaAs-Ga}_{(1-x)}\text{Al}_x\text{As}$  where the electron near the conduction band edge and hole near the valence band edge are confined in the same layers, the behavior of the binding energy is very similar to that found in the case of impurities. In the limit of very thin layers and total confinement the binding energy should approach that of a two-dimensional exciton which binds four times as strongly as a three dimensional exciton (Bassani and Parravicini, 1975). Calculations on the the infinite well model by Bastard et al.(1982a) give the expected results. In superlattices, other cases are also possible. For example in the case of  $\text{InAs-GaSb}$  (Bastard et al., 1982), the electron and hole are in different layers and the binding energy of the exciton is reduced over the three dimensional value.

One theoretical study suggests that nonlinear optical properties of superlattices could be quite large (Tsu, 1971). The additional dispersion due to the shortened Brillouin zone can produce a substantial nonlinear optical response. While this phenomenon has been studied theoretically it has not been explored in detail. In particular the role of scattering which will tend to suppress this phenomenon has not been included.

Much of the transport theory for heterostructures has dealt with the transport along the interface between the GaAs and  $\text{Ga}_{(1-x)}\text{Al}_x\text{As}$  and hence do not involve true superlattice effects. The original suggestion by Esaki and Tsu(1970) of negative resistance for currents perpendicular to the superlattice layers due to the curvature in the mini-bands has not been explored extensively. The mean free path of the carriers are sufficiently small that they reduce this effect substantially.

Ktitorov and coworkers(1971) have suggested that one might observe Stark ladders(Wannier, 1960) in superlattices. However, the scattering of the carriers and the large inter-subband matrix elements due to the applied electric field are likely to make it difficult to observe such a phenomenon.

Chin and coworkers(1980) have proposed that a superlattice structure would have widely different electron and hole impact ionization rates. This proposal has led to other suggestions for ways to control the impact ionization phenomenon(Blauvelt, et al., 1981; Tanoue and Sakai, 1982).

The collective excitations of the carriers in semiconductor superlattices have been explored by Das Sarma and Madhukar(1981) and Das Sarma and Quinn(1982). Das Sarma and Quinn have explored the optical plasmons, acoustic plasmons,

magnetoplasmons, helicon, and Alfvén waves as the superlattice parameters are changed in such a way as to go from the two-dimensional to the three-dimensional limit.

## VII. CONCLUSIONS

Techniques have been developed for treating the electronic spectra of ideal superlattices using both first principles and empirical techniques. The empirical techniques (two-band model, tight-binding model) are very successful in treating the properties of superlattices since they allow the extrapolation of our knowledge of the band structure of the bulk semiconductor to the properties of superlattices. Calculations based on these techniques have provided results for the electronic band structure of abrupt superlattices. Perhaps more importantly these techniques provide a method for treating some of the questions about transport, impurity states, excitonic states, deviations from an ideal abrupt interface (i. e., grading), alloys, etc. Self-consistent calculations allow the examination of the charge densities at the interface and hence give some information about the interface region.

The lattice vibrations of superlattices have not been treated in as much detail as the electronic properties. The techniques for treating these problems at the same level as the electronic properties are available but have not been applied.

The properties that are of real interest are those that can lead to novel

applications. A partial list of these novel applications would include linear and nonlinear optical properties, and transport properties. As discussed in this chapter some of the interesting transport properties include widely different impact ionization rates and negative resistance phenomena. Here a great deal remains to be done. The theorist can hope to make precise calculations based on experience with bulk semiconductors. Theoretical investigations of these properties should indicate which superlattice systems should be studied.

In this chapter, we have not addressed the very important question presented by realistic interfaces and their preparation. These include: the character and stability of the interface in the superlattice and the mechanisms of growth. For these problems, theoretical work is difficult but essential in guiding the experimental studies in the field.

## **ACKNOWLEDGMENT**

The authors wish to gratefully acknowledge the Army Research Office for supporting the preparation of this manuscript under Contract No. DAAG29-80-C-0103. One of us(JNS) would like to acknowledge the support provided by the Office of Naval Research under Contract No. N00014-82-K-0458.

## REFERENCES

- Altarelli, M. (1982). Proc. 16th Int. Conf. Physics of Semiconductors, Montpellier, 1982 edited by M. Averous (North Holland, Amsterdam, 1983) p. 747.
- Ando, T. and Mori, S.(1982). *Surface Science* 113,124.
- Andreoni, W., Baldereschi, A., and Car, R. (1978). *Solid State Commun.* 27, 821.
- Baraff, G. A., Appelbaum, J. A., and Hamann, D. R. (1977). *Phys. Rev. Lett.* 38, 237.
- Barker, A. S., Merz, J. L., and Gossard, A. C. (1978). *Phys. Rev.* B17, 3181.
- Bassani, F. and Parravicini, G. Pastori(1975). *Electronic States and Optical Transitions in Solids* (Pergamon Press, Oxford)pp. 188-190.
- Bastard, G. (1981). *Phys. Rev.* B24, 5693.
- Bastard, G. (1982a). *Surface Science* 113,165.
- Bastard, G. (1982b). *Phys. Rev.* B25, 7584.
- Bastard, G., Mendez, E. E., Chang, L. L. and Esaki, L. (1982). *Phys. Rev.* B26, 1974.
- Bauer, R. S. (1981). Private communication.
- Blauvelt, H., Margalit, S. and Yariv, A.(1981). *Electron. Lett.* 18,375.
- Caruthers, E. and Lin-Chung, P. J. (1977). *Phys. Rev. Lett.* 38, 1543.

- Caruthers, E. and Lin-Chung, P. J. (1978). *J. Vac. Sci. Technol.* 15, 1459.
- Chadi, D. J. and Cohen, M. L. (1975). *Phys. Status Solidi (b)* 68, 405.
- Chang, L. L., Kawai, N. J., Sai-Halasz, G. A., Ludeke, R. and Esaki, L. (1979). *Appl. Phys. Lett.* 35, 939.
- Chang, L. L. (1980). Proc. 15th Int. Conf. Physics of Semiconductors, Kyoto, 1980 *J. Phys. Soc. Japan* 49, suppl. A., p. 997.
- Chang, Y. C. (1982). *Phys. Rev.* B25, 605.
- Chang, Y. C., and Schulman, J. N. (1982). *Phys. Rev.* B25, 3975.
- Chin, R., Holonyak, Jr., N., Stillman, G. E., Tang, J. Y. and Hess, K. (1980). *Electron. Lett.* 33, 467.
- Colvard, C., Merlin, R., Klein, M. V., and Gossard, A. C. (1980). *Phys. Rev. Lett.* 45, 298.
- Das Sarma, S. and Madhukar, A. (1981). *Phys. Rev.* B23, 805.
- Das Sarma, S. and Quinn, J. J. (1982). *Phys. Rev.* B25, 7603.
- Dingle, R., Gossard, A. C., and Wiegmann, W. (1975). *Phys. Rev. Lett.* 34, 1327.
- Dubrovskii, G. B., and Belyarskii, V. I. (1981). *Phys. Stat. Sol. (b)* 103, 131.
- Esaki, L. and Tsu, R. (1970). *IBM J. Res. Develop.* 14, 61.

Faurie, J. P. (1981). *J. Cryst. Growth* 54, 577.

Frenaley, W. R., and Kroemer, H. (1977). *Phys. Rev.* B16, 2642.

Harrison, W. A. (1980). *Electronic Structure and the Properties of Solids*, (Freeman, San Francisco).

Ihm, J., Lam, P. K., and Cohen, M. L. (1979) *Phys. Rev.* B20, 4120.

Ivanov, I., and Pollmann, J. (1979). *Solid State Commun.* 32, 869.

Kane, E. O. (1957). *J. Phys. Chem. Solids* 1, 249.

Ktitorov, S. A., Simin, G. S. and Sindalovskii, V. Ya. (1971). *Fiz. Tverd. Tela* 13, 2230(*Sov. Phys.-Solid State* 13, 1872 (1972)).

Kraut, E. A., Grant, R. W., Waldrop, J. R. and Kowalczyk, S. P. (1980). *Phys. Rev. Lett.* 44, 1620.

Kuech, T., and McCaldin, J. (1982). *J. Appl. Phys.* 53, 3121.

Kunc, K., and Martin, R. M. (1980). Proc. 15th Int. Conf. Physics of Semiconductors, Kyoto, 1980, *J. Phys. Soc. Japan* 49, suppl. A. p.1117.

Madhukar, A., Dandekar, N. V., and Nucho, R. N. (1979). *J. Vac. Sci. and Technol.* 16, 1507.

Madhukar, A., and Delgado, J. (1981) *Solid State Commun.* 37, 199.

Madhukar, A., and Nucho, R. N. (1979) *Solid State Commun.* 32, 331.

- Mailhot, C., Chang, Y. C., and McGill, T. C. (1982a). *Surface Science* 113, 161.
- Mailhot, C., Chang, Y. C., and McGill, T. C. (1982b). *Phys. Rev.* B26, 4449.
- Mendez, E. E., Chang, L. L., Landgren, G., Ludeke, R., Esaki, L., and Pollak, F. H. (1981). *Phys. Rev. Lett.* 46, 1230.
- Merlin, R., Colvard, C., Klein, M. V., Morkoç, H., Cho, A. Y., and Gossard, A. C. (1980). *Appl. Phys. Lett.* 36, 43.
- Milnes, A. G. and Feucht, D. L. (1972). *Heterojunctions and Metal-Semiconductor Junctions*, (Academic Press, New York) pp. 34ff.
- Mönch, W., and Gant, H. (1980). *J. Vac. Sci. and Technol.* 17, 1094.
- Mukherji, D., and Nag, B. R. (1975). *Phys. Rev.* B12, 4338.
- Mukherji, D., and Nag, B. R. (1978). *Solid State Electronics* 21, 555.
- Nucho, R. N., and Madhukar, A. (1978). *J. Vac. Sci. and Technol.* 15, 1530.
- Osbourn, G. C. (1982). *J. of Appl. Phys.* 53, 1586.
- Osbourn, G. C., and Smith, D. L. (1979). *Phys. Rev.* B19, 2124.
- Perfetti, P., Denley, D., Mills, K. A., and Shirley, D. A. (1978). *Appl. Phys. Lett.* 33, 667.
- Pickett, W. E., Louie, S. G., and Cohen, M. L. (1978). *Phys. Rev.* B17, 815.

Pollmann, J. (1980). *Festkörperprobleme (Advances in Solid State Physics) 20*, J. Treusch (ed.), Vieweg, Braunschweig, p.117.

Ren, S. Y. and Dow, J. D. (1982). *Phys. Rev. B* **25**, 3750.

Rytov, S. M. (1956a). *Sov. Phys. JETP* **2**, 466.

Rytov, S. M. (1956b). *Akust. Zh.* **2**, 71 (*Sov. Phys. Acoust.* **2**, 68 (1956)).

Sai-Halasz, G. A., Tsu, R., and Esaki, L. (1977). *Appl. Phys. Lett.* **30**, 651.

Sai-Halasz, G. A., Chang, L. L., Welter, J.-M., Chang, C.-A., and Esaki, L. (1978a). *Solid State Commun.* **27**, 935.

Sai-Halasz, G. A., Esaki, L., and Harrison, W. A. (1978b). *Phys. Rev.* **B18**, 2812.

Schulman, J. N., and Chang, Y. C. (1981a). *Phys. Rev.* **B24**, 4445.

Schulman, J. N., and Chang, Y. C. (1981b). Unpublished. Parameters used were similar to those used in Schulman and Chang, 1981a with the addition of the spin-orbit interaction.

Schulman, J. N., and Chang, Y. C. (1983). *Phys. Rev. B* to be published.

Schulman, J. N., and McGill, T. C., (1977). *Phys. Rev. Lett.* **39**, 1680.

Schulman, J. N., and McGill, T. C., (1979a). *Appl. Phys. Lett.* **34**, 663.

Schulman, J. N., and McGill, T. C., (1979b). *J. Vac. Sci. and Technol.* **16**, 1513.

Schulman, J. N., and McGill, T. C., (1979c). *Phys. Rev.* **B19**, 6341.

Schulman, J. N., and McGill, T. C., (1981). *Phys. Rev.* **B23**, 4149.

Shay, J. L., Wagner, S., and Phillips, J. C. (1976) *Appl. Phys. Lett.* **28**, 31.

Tanoue, T. and Sakaki, H. (1982). *Appl. Phys. Lett.* **41**, 67.

Tsu, R. and Esaki, L.(1971). *Appl. Phys. Lett.* **19**, 246.

Tsu, R., and Jha, S. S. (1972). *Appl. Phys. Lett.* **20**, 16.

Wannier, G. H. (1960). *Elements of Solid State Theory* (Cambridge University Press, London)pp. 190-193.

White, S. R., and Sham, L. J. (1981). *Phys. Rev. Lett.* **47**, 879.

**TABLE 1.** GaAs-AlAs heterojunction band offsets expressed as  $\Delta E_v/\Delta E_g$ , where  $\Delta E_v$  is the GaAs valence maximum energy minus the AlAs valence band maximum energy and  $\Delta E_g$  is the AlAs direct band gap minus the GaAs direct band gap. Specific orientations are indicated.

Source	$\Delta E_v/\Delta E_g$
Frensley (1977)	0.56
Pickett (1978) (110)	0.17
Harrison (1980)	0.03
Dingle (1975) (100)	0.15

**TABLE 2.** InAs-GaSb heterojunction band offsets expressed as  $E_0$ , the GaSb valence band maximum energy minus the InAs conduction band minimum energy. Specific orientations are indicated.

Source	$E_0$
Frensley (1977)	-0.14
Ihm (1979) (100)	-0.21
Harrison (1980)	0.10
Madhukar (1979) (100)	0.06
Sai-Halasz (1978a) (100)	0.15
Sai-Halasz (1977)	0.14

**TABLE 3.** Ge-GaAs heterojunction band offsets.  $\Delta E_v$  is the Ge valence band maximum minus the GaAs valence band maximum energy.  $\Delta E_c$  is the GaAs conduction band minimum minus the Ge conduction band minimum energy. Specific orientations are indicated. Values in parentheses assume  $\Delta E_v + \Delta E_c = .75$  eV.

Source	$\Delta E_v$	$\Delta E_c$
Frensley (1977)	0.71	0.07
Pickett (1978) (110)	0.35	0.40
Harrison (1980)	0.41	0.35
Baraff (1977) (100)	(0.75)	0
Kunc (1980) (100)	-0.03	0.78
Perfetti (1978) (100)	0.25	0.50
Kraut (1980) (110)	0.53	(0.22)
Mönch (1980) (110)	(0.36)	0.39
Bauer (1981) (110)	0.4	(0.35)
Shay (1976)	0.69	0.06

**TABLE 4.** GaAs-AlAs (100) superlattice states at the Brillouin zone center for 50Å of GaAs alternating with 50Å of AlAs between -0.42 eV and 1.56 eV. The complex wave vectors of the dominant bulk states are given in units of  $a^{-1}$ , where  $a$  is the conventional lattice spacing. The GaAs valence band maximum is the zero of energy. The symbols c, hh, lh, and so stand for the bulk conduction, heavy hole, light hole, and split-off valence bands.

Energy	GaAs	AlAs
1.56 eV	c-(0.29,0)	c-(0,0.93)
-0.02	hh-(0.28,0)	hh-(0,1.12)
-0.06	lh-(0.19,0)	lh-(0,0.44)
-0.08	hh-(0.57,0)	hh-(0,0.96)
-0.17	hh-(0.82,0)	hh-(0,0.64)
-0.22	lh-(0.48,0)	lh-(0,0.15)
-0.27	hh-(1.05,0)	hh-(0.45,0)
-0.29	so-(0,.28),lh-(0.64,0)	hh-(0.87,0),so-(0,0.79)
-0.35	hh-(1.22),lh-(0.79,0)	hh-(0.87,0),so-(0,0.79)
-0.38	hh-(1.28,0)	hh-(1.00,0)
-0.39	hh-(1.29,0),lh-(0.88,0)	lh-(0.51,0)
-0.40	so-(0.24,0)	so-(0,0.63)
-0.41	lh-(0.94,0)	so-(0,0.57)

**TABLE 5.** The transverse phonon frequencies  $\nu_j$  and infrared strengths  $S_j$  for modes in the model bulk GaAs and AlAs; the one-on-one superlattice; and the two-on-two superlattice. The results are from Barker et al.(1978).

GaAs		AlAs	
$\nu_j(\text{cm}^{-1})$	$S_j$	$\nu_j(\text{cm}^{-1})$	$S_j$
269.0	1.93	363.0	2.0
<b>Monolayer (1,1)</b>		<b>Bilayer (2,2)</b>	
85.2	0.0087	57.5	0.0
262.8	0.82	59.0	0.0039
357.8	1.13	86.2	0.0
		260.4	0.0
		266.2	0.90
		354.6	0.0
		360.5	1.06

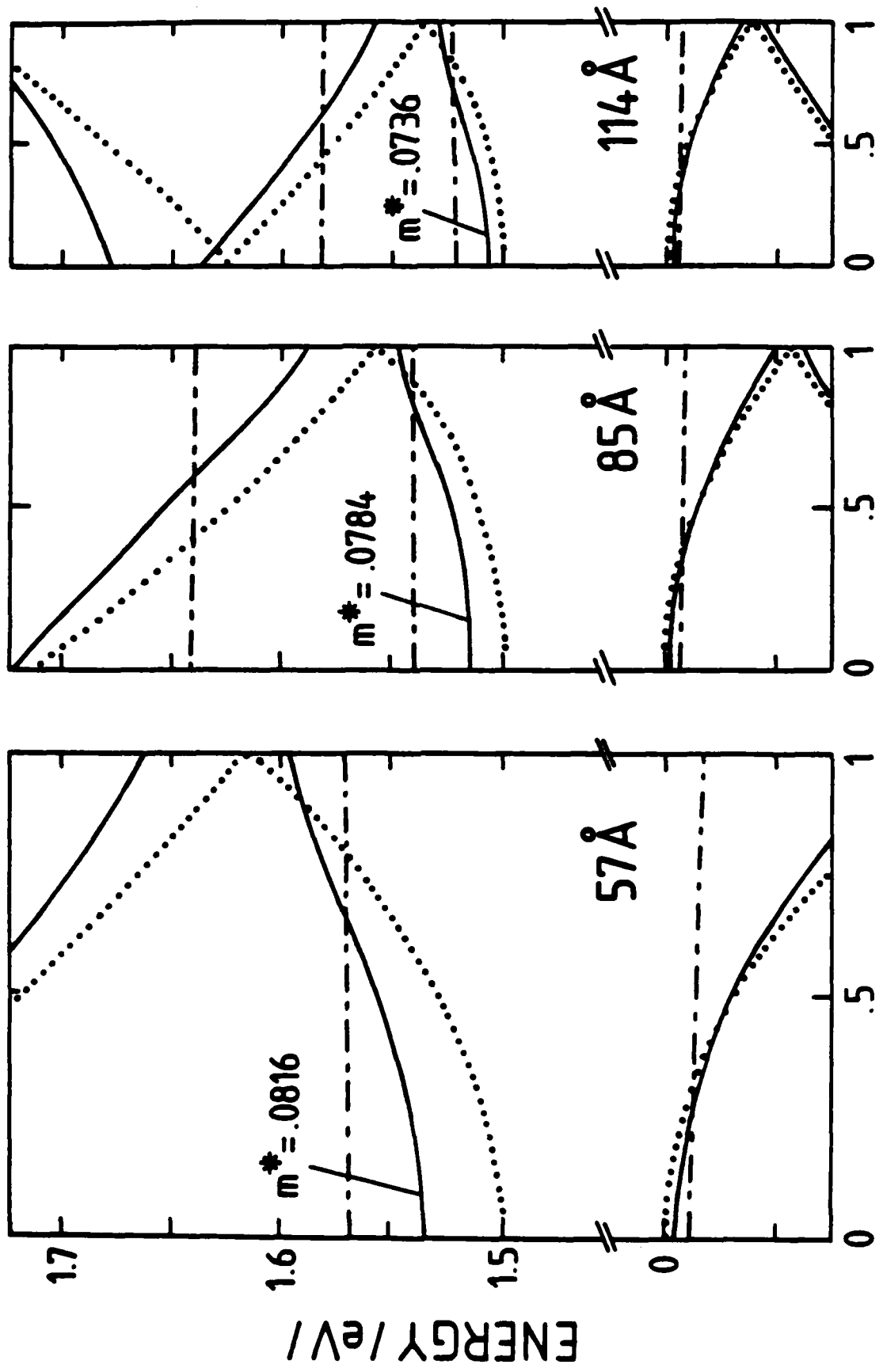
**TABLE 6.** The longitudinal phonon frequencies  $\nu_j$  and Raman strengths for bulk GaAs and AlAs; the one-on-one superlattice; and the two-on-two superlattice. The results are from Barker et al.(1978).

GaAs			AlAs		
$\nu_j(\text{cm}^{-1})$	$R_{zz}$	$R_{zy}$	$\nu_j(\text{cm}^{-1})$	$R_{zz}$	$R_{zy}$
289.0	0.0	6.7	391.4	0.0	0.72
<b>Monolayer (1,1)</b>			<b>Bilayer (2,2)</b>		
201.4	32.7	0.0	118.4	24.5	0.0
241.3	0.0	2.41	120.8	0.0	0.11
372.1	0.0	1.18	201.4	0.0	0.0
			236.4	3.02	0.0
			277.3	0.0	2.86
			356.1	1.03	0.0
			381.8	0.0	0.68

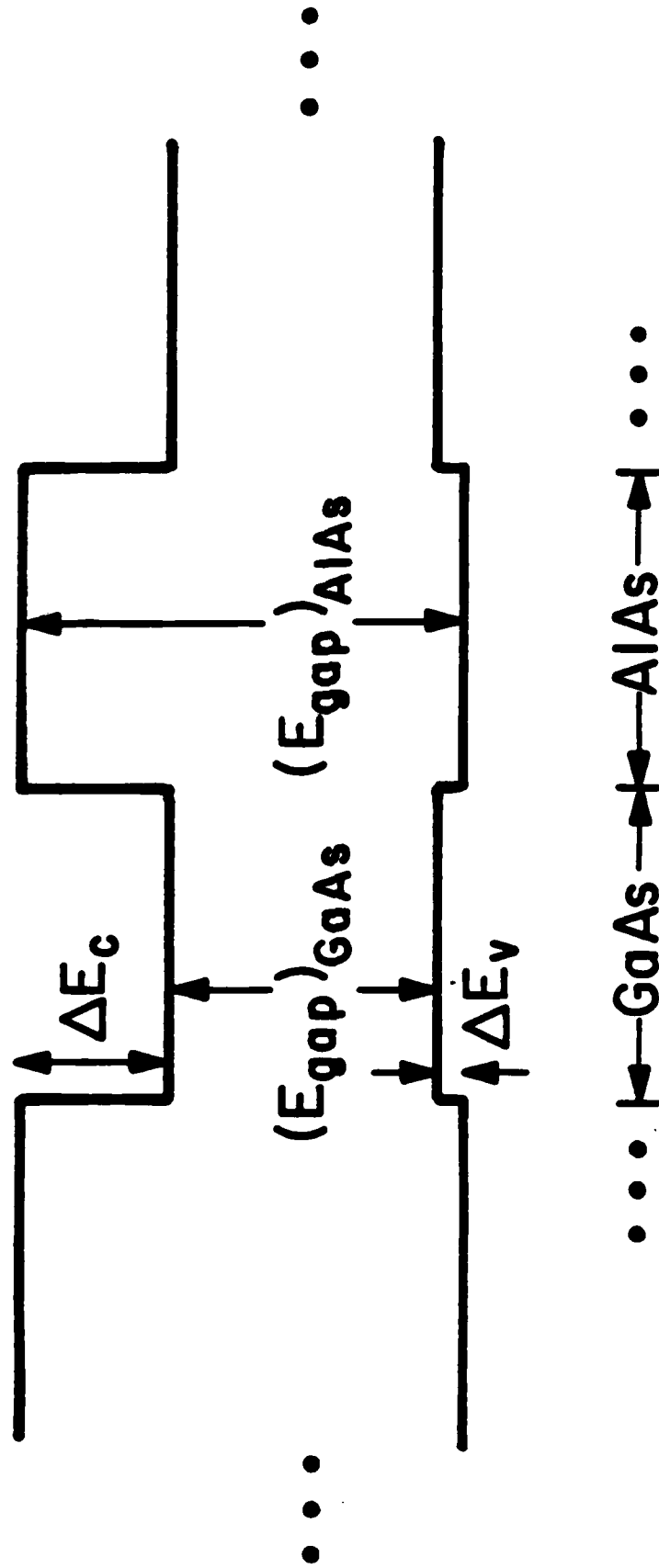
## FIGURE CAPTIONS

- FIGURE 1.** GaAs-ALAs superlattice bands in the [100] direction for GaAs slab thicknesses of 57, 85, and 114Å. Solid lines: 11Å ALAs slab thickness. Dash-dotted lines: 85Å ALAs slab thickness. Dotted lines: folded bulk GaAs band structure.
- FIGURE 2.** Line-up of the GaAs and ALAs conduction and valence band edges in the GaAs-ALAs superlattice.  $\Delta E_v$  and  $\Delta E_c$  are the valence and conduction band edge discontinuities.
- FIGURE 3.** Line-up of the InAs and GaSb conduction and valence band edges in the InAs-GaSb superlattice.  $E_g$  is the energy separation between the GaSb valence band maximum and the InAs conduction band minimum.
- FIGURE 4.** Complex band structure of GaAs and ALAs near zone center along [100] direction.  $Re(k_x)$  is plotted to the right of each figure,  $Im(k_x)$  is to the left. Solid lines: tight-binding model. Dashed lines: two-band model. Dash-dotted lines: Kronig-Penney model. The GaAs conduction band minimum is the energy zero. The ALAs valence band maximum is close to  $-1.7$  eV. From Schulman and Chang (1981a).
- FIGURE 5.** Superlattice conduction band minimum dispersion curves in the  $z$  direction for superlattices with two layers of ALAs alternating with  $N$  layers of GaAs, for  $N = 3, 4, 5, 8, 10, 15, 20$  as indicated. Solid curve: tight-binding model. Dashed curve: Kronig-Penney model. Dash-dotted curve: two-band model. Energy is relative to the GaAs conduction band minimum.  $L$  is the total number of alternating GaAs and ALAs layers. From Schulman and Chang (1981a).
- FIGURE 6.** Upper part:  $E$  vs.  $k_x$  relationships for three  $In_{(1-x)}Ga_xAs - GaSb_{(1-y)}As_y$  superlattices consisting of four layers each of  $In_{(1-x)}Ga_xAs$  and  $GaSb_{(1-y)}As_y$  together with their potential profiles. The  $x$  and  $y$  values are given in the text.  $k_{d_0} = \pi/d_0$  where  $d_0$  is the bulk lattice constant. Solid curves: two-band model. Dashed curve: Kronig-Penney model. Lower part: energy gaps vs. layer thickness. From Sai-Halasz et al. (1977).
- FIGURE 7.** Empirical and self-consistent potentials, averaged parallel to the interface, for the (110) interfaces of (a) Ge-GaAs and (b) ALAs-GaAs. The large arrow denotes the geometric interface, while the smaller arrows show the positions of atomic planes. From Pickett et al. (1978).

- FIGURE 8.** Proposed line-up of the CdTe–HgTe conduction and valence band edges in the CdTe–HgTe superlattice. HgTe is a zero band gap semiconductor.
- FIGURE 9.** Complex band structures of GaAs and AlAs along the [100] direction. Both the real bands ( $Im(k_x) = 0$ ) and the purely imaginary bands ( $Re(k_x) = 0$ ) are denoted by solid lines. The complex bands ( $Re(k_x) \neq 0$  and  $Im(k_x) \neq 0$ ) are denoted by pairs of dashed lines. The lines associated with  $Re(k_x)$  and  $Im(k_x)$  are plotted in the right and left portions of each figure, respectively. Energy is relative to the GaAs valence band maximum.
- FIGURE 10.** Zone center electronic state with energy  $-0.40$  eV relative to the GaAs conduction band minimum in a GaAs–AlAs superlattice with  $50\text{\AA}$  GaAs and AlAs layer thicknesses. Filled circles: anion. Open circles: cation. Solid line: total state. Dashed line: light hole bulk state contribution only. The left half is in the GaAs layers and the right half is in the AlAs layers. From Schulman and Chang (1981b).
- FIGURE 11.** The linear chain model for the GaAs–AlAs superlattice. The springs and appropriate spring constants are indicated. The values of these parameters are given in Barker et al.(1978).
- FIGURE 12.** The phonon dispersion curves for the one-on-one and two-on-two GaAs–AlAs superlattices obtained in the linear chain approximation (after Barker et al. 1978).
- FIGURE 13.** The binding energy of a donor in the center of a GaAs well surrounded by two layers of  $Ga_{(1-x)}Al_xAs$ . The ordinate is the number of GaAs layers. The alloy concentration  $x$  is varied from 0.1 to 0.4(from Mailhiot et al. (1982b))



$k_{\perp}$  in units  $4\pi/a(N_a + N_b)$



$\dots \leftarrow GaAs \rightarrow AlAs \rightarrow \dots$

Fig.

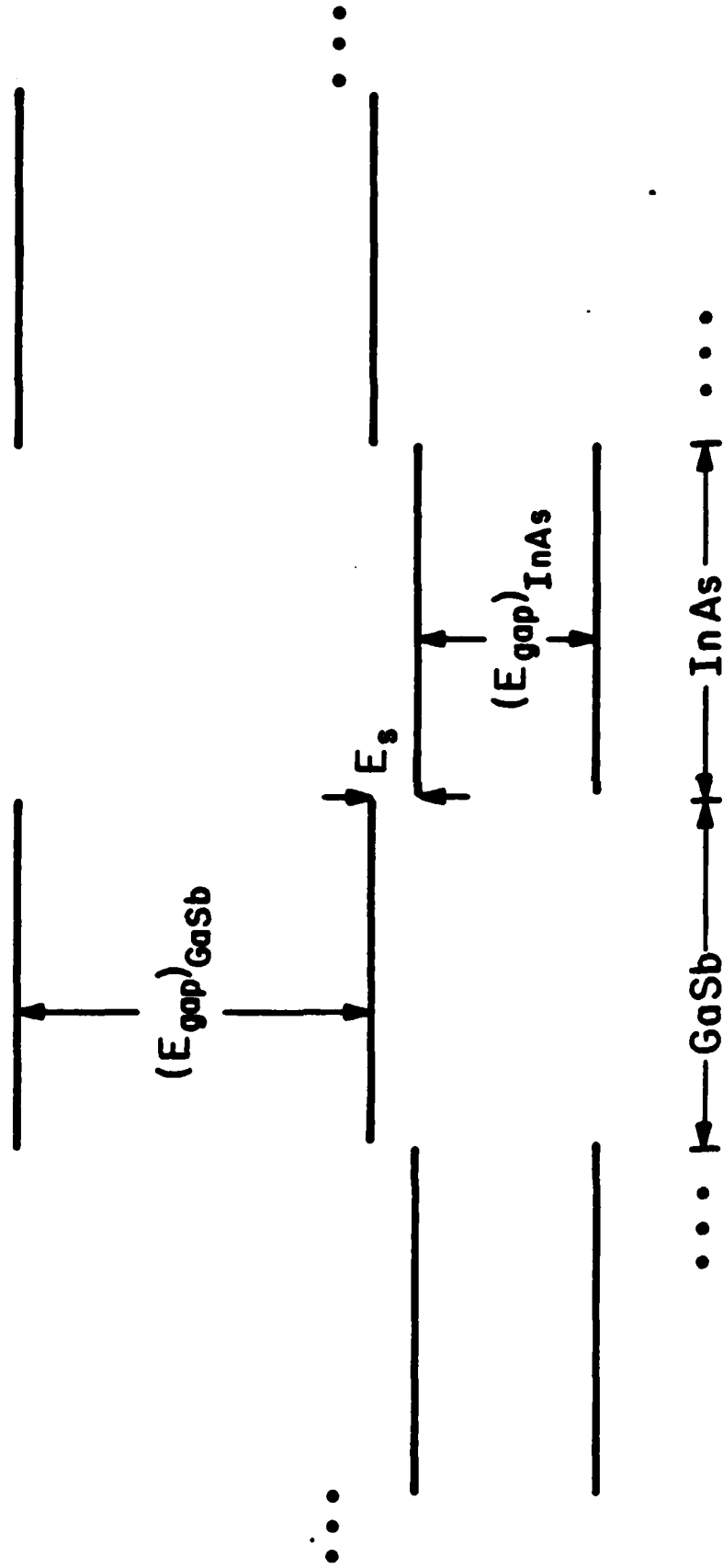


Fig. 3

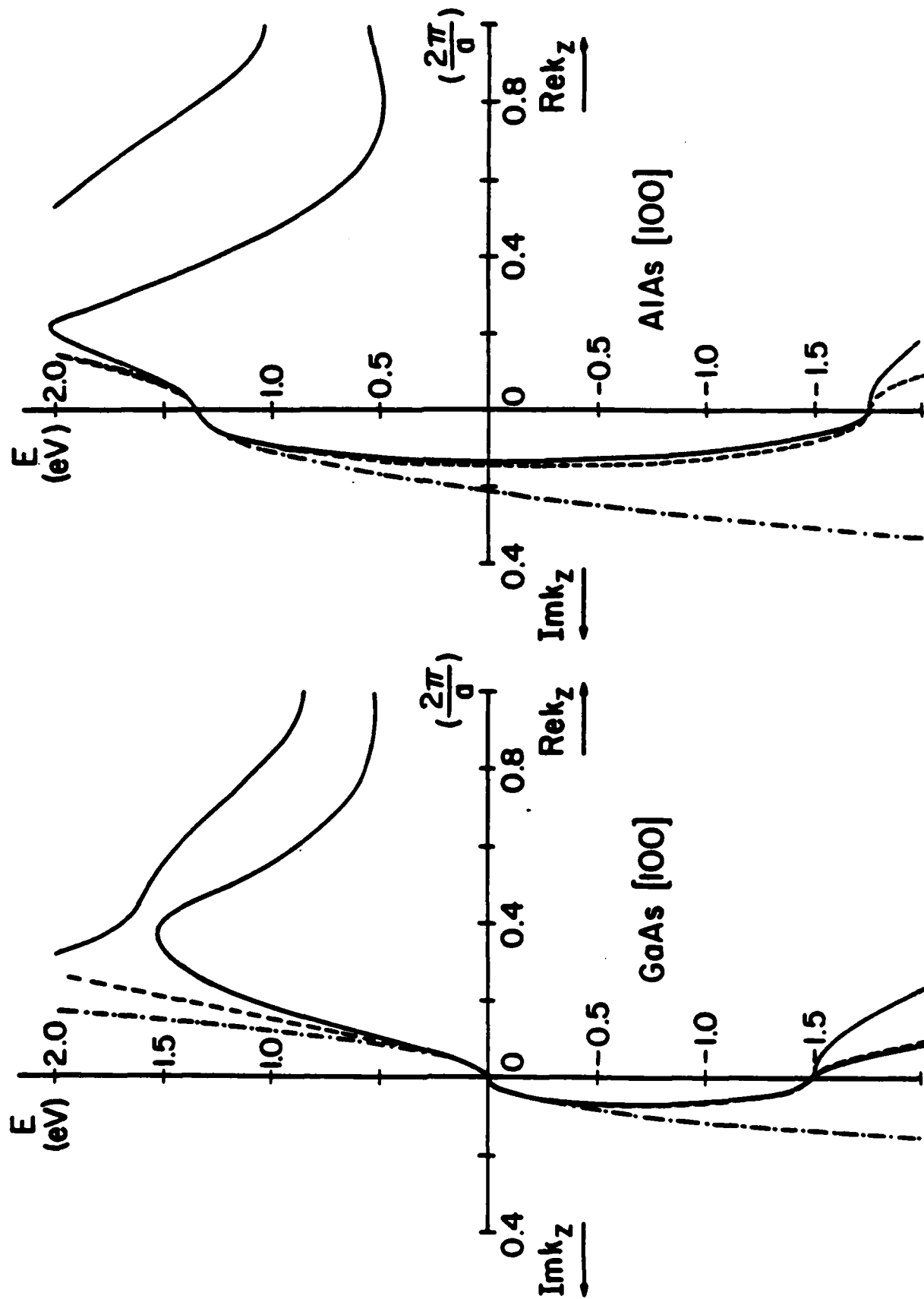


Fig. 4

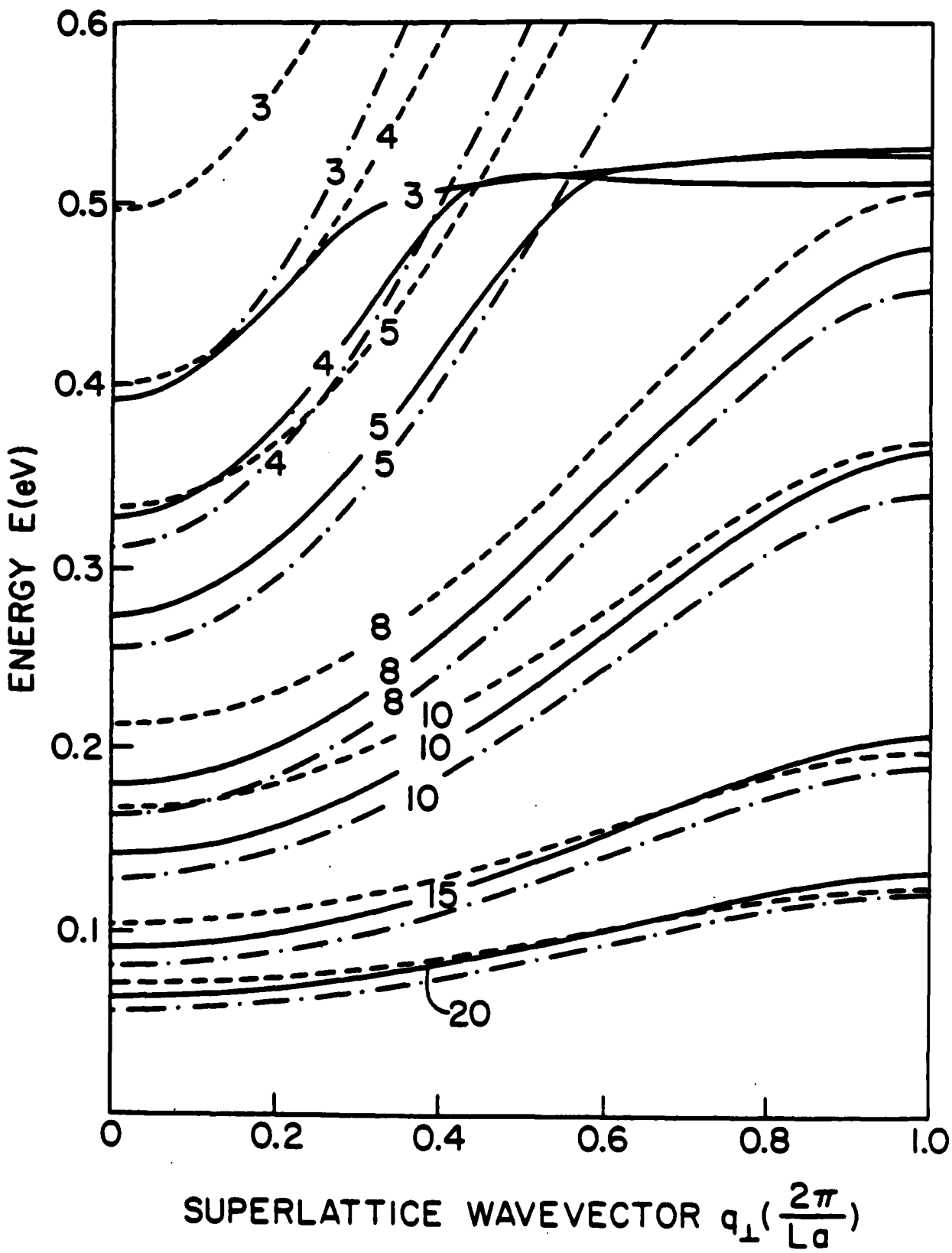


Fig. 5

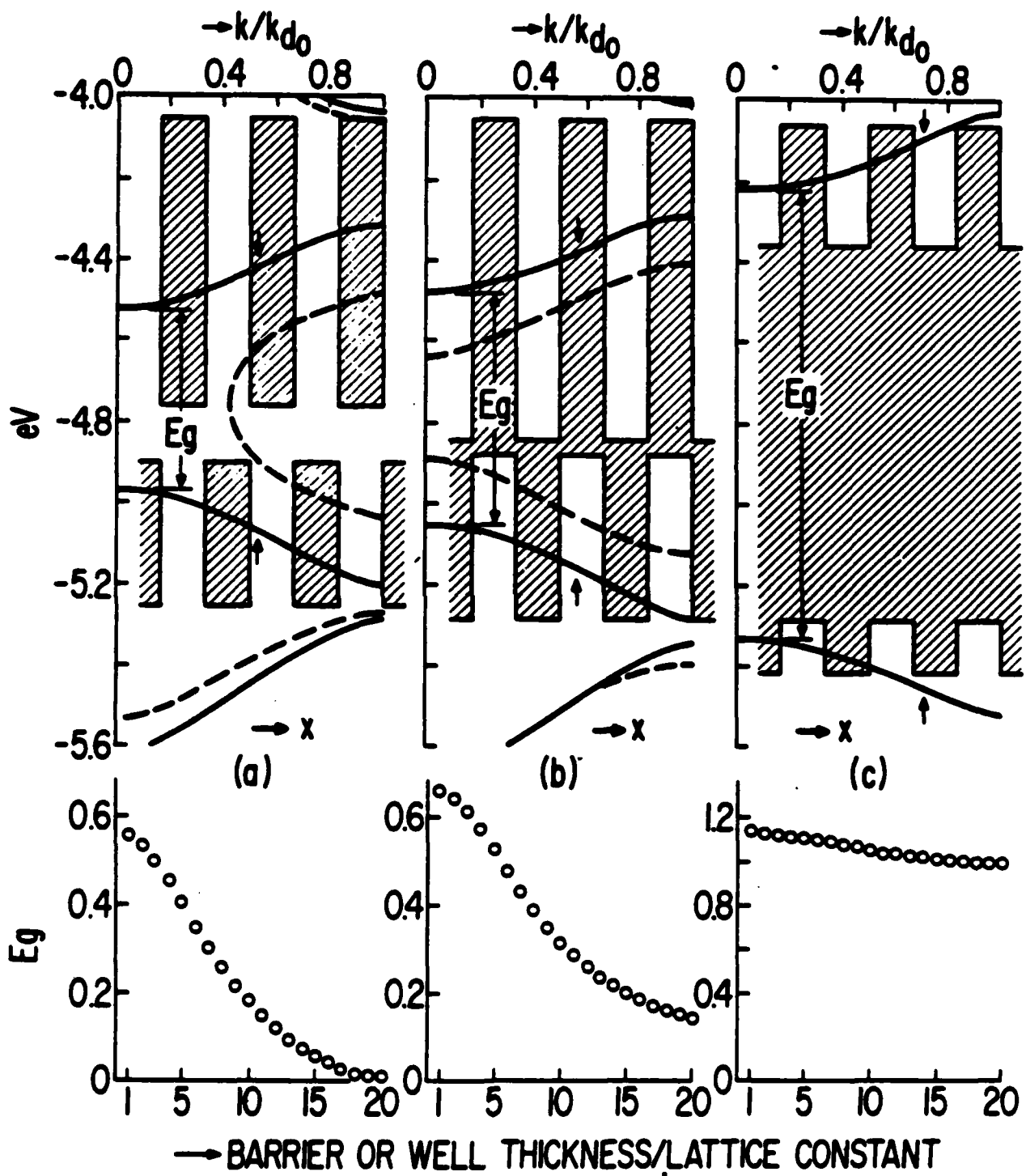


Fig. 6

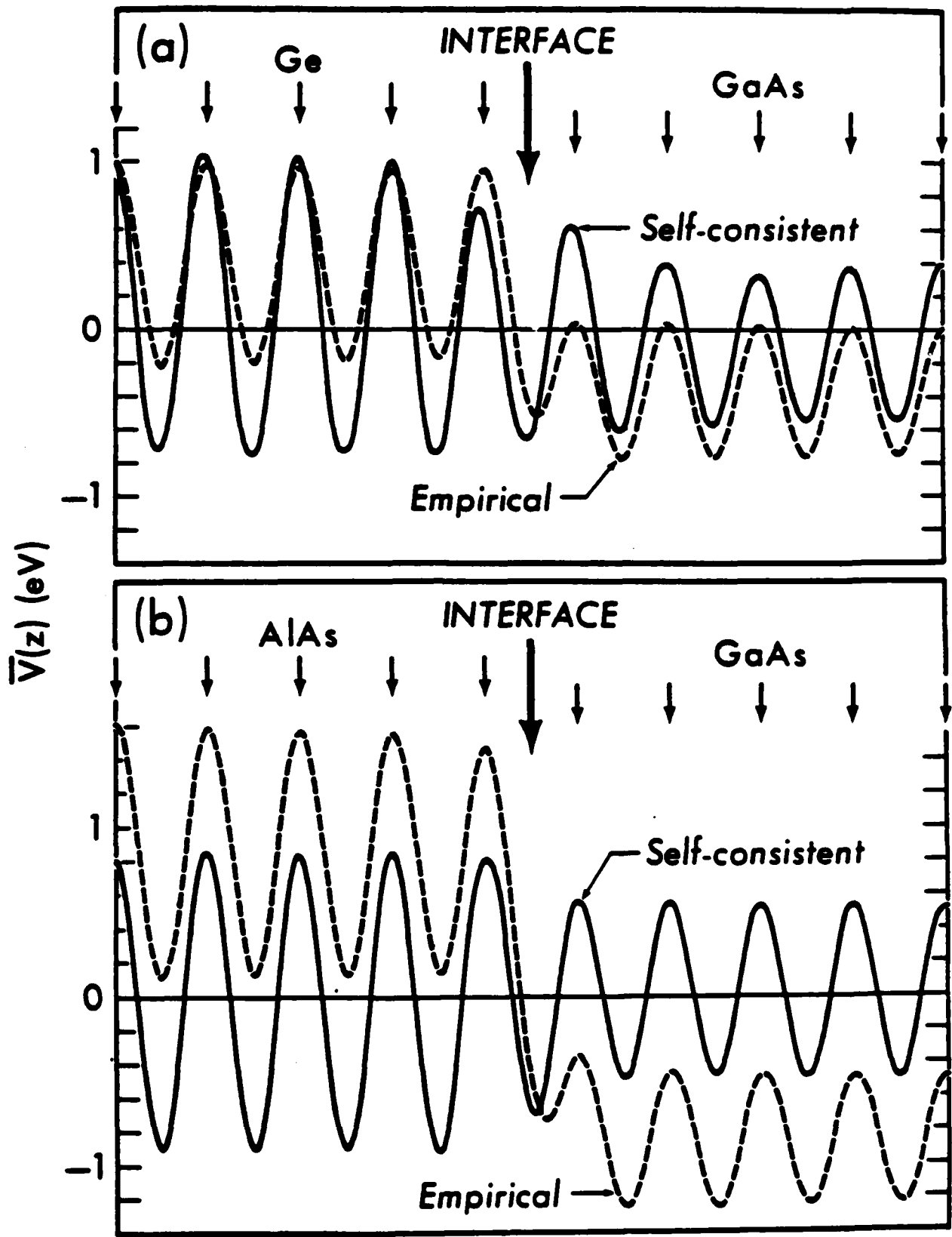


Fig.

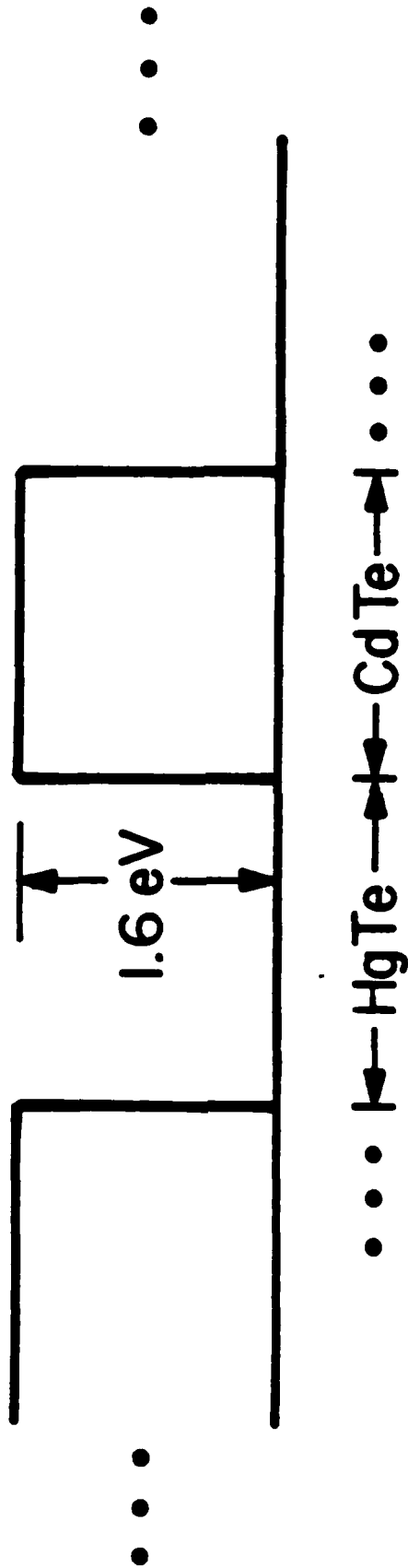


Fig.

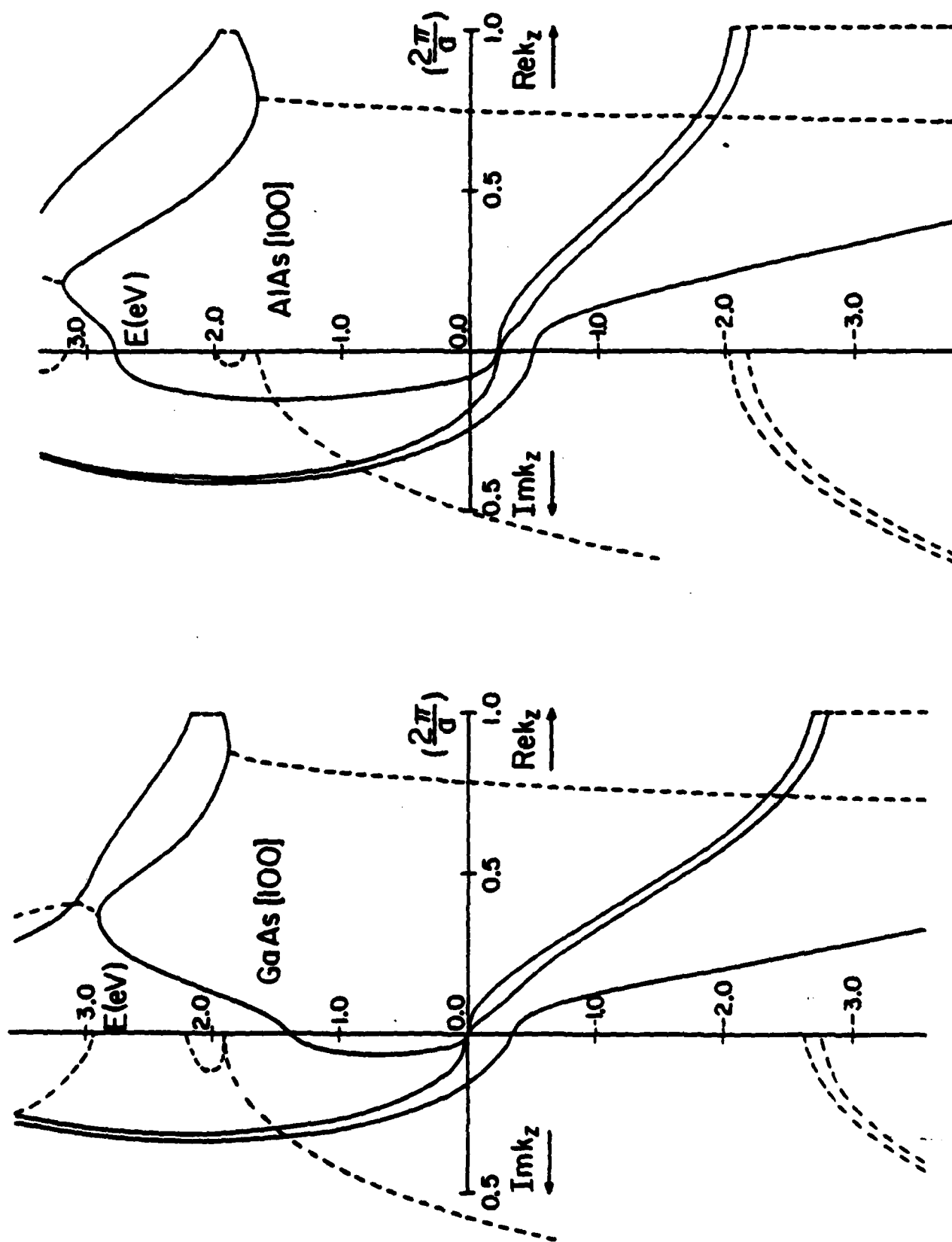


Fig. 9

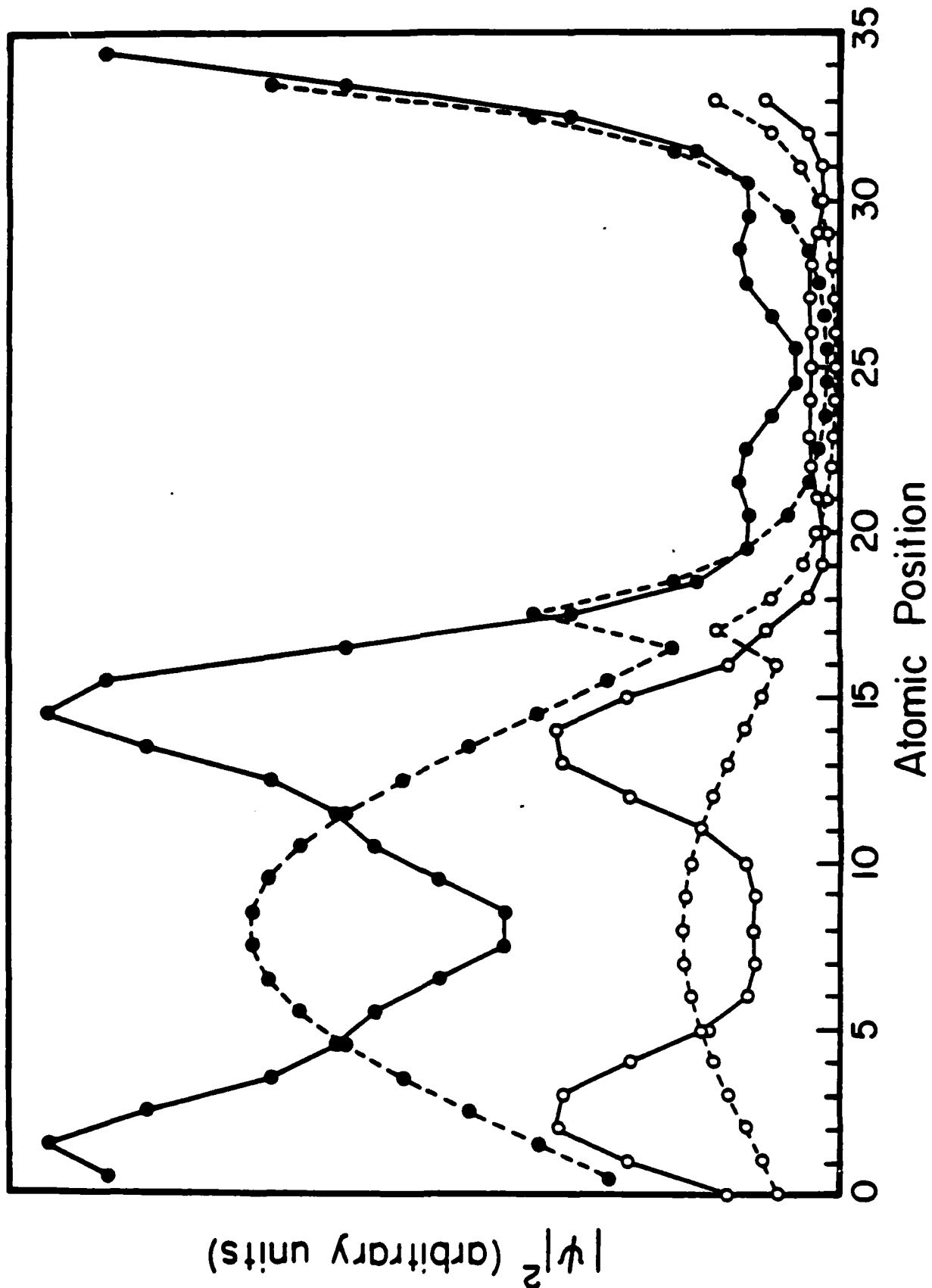


Fig. 10

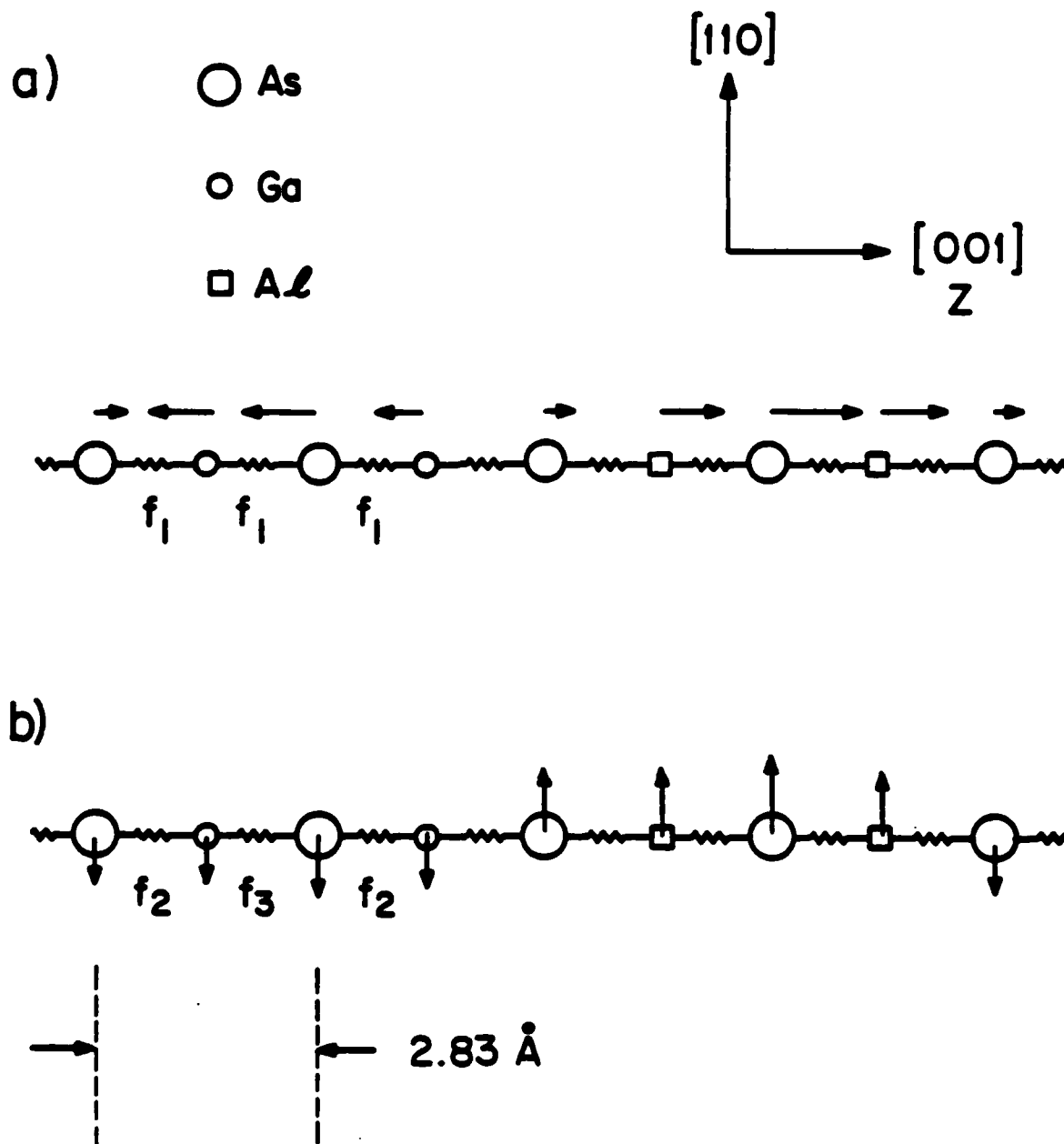


Fig. 11

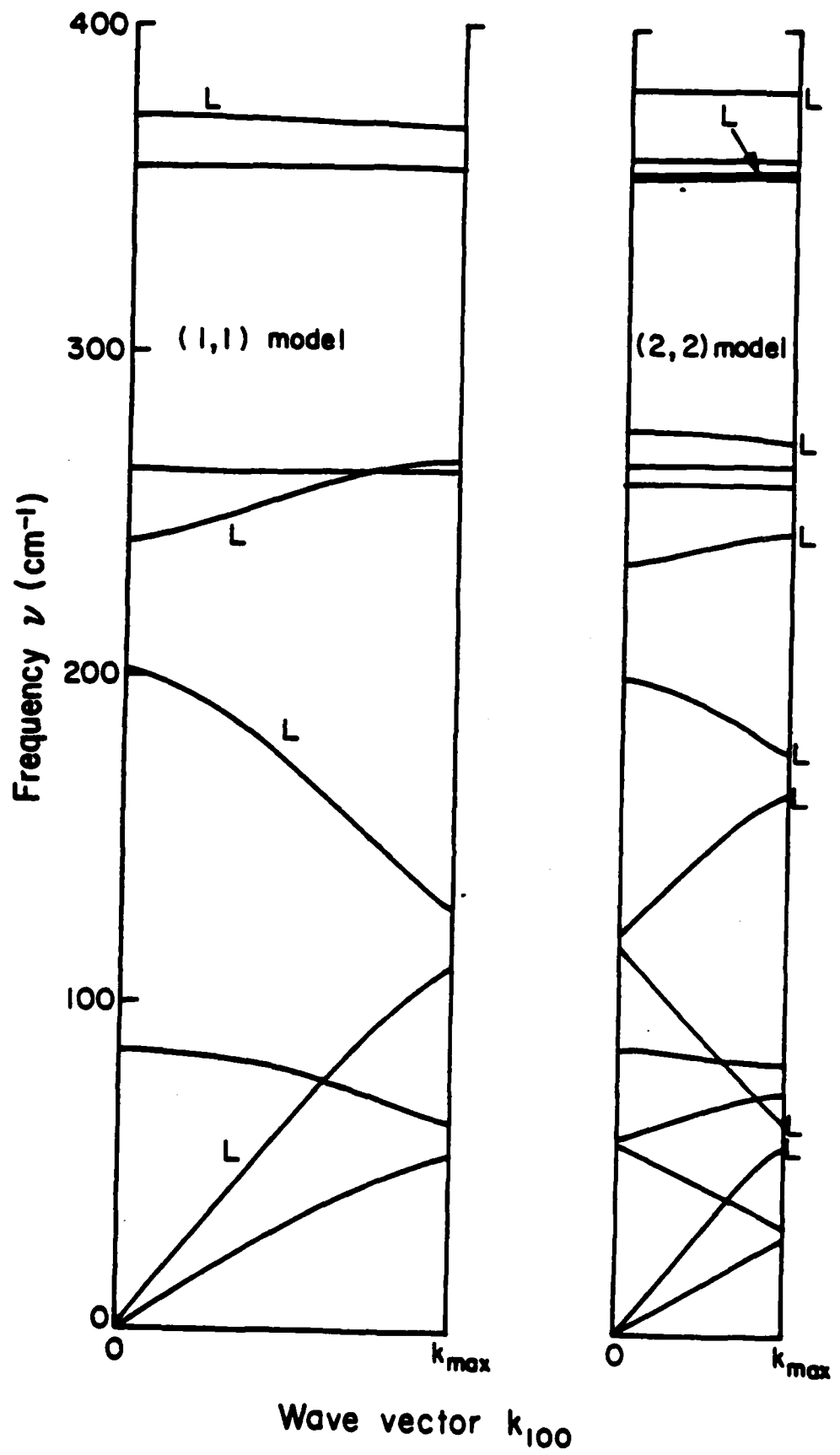


Fig. 12

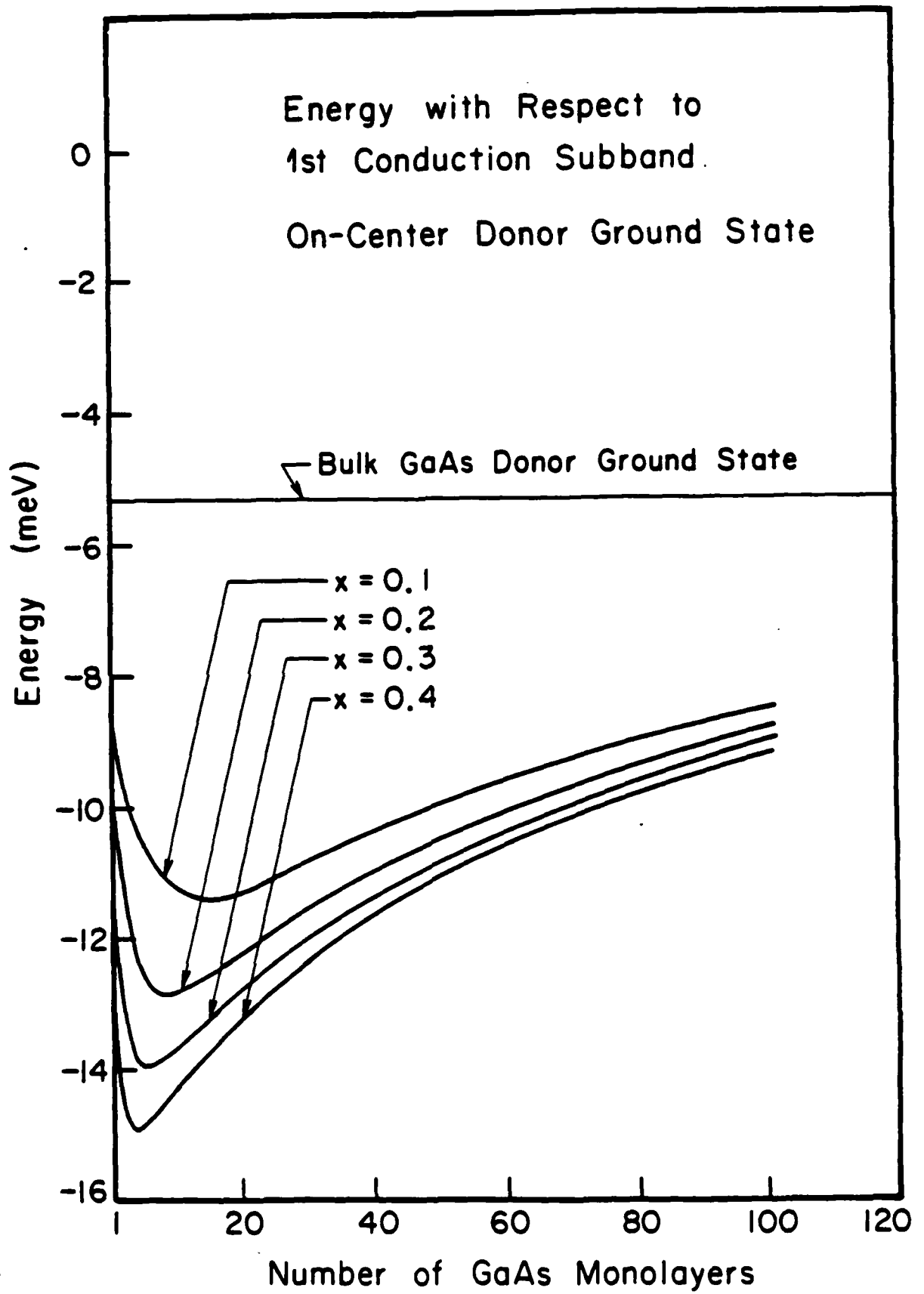


Fig.

D. L. Smith

Honeywell Systems and Research Center, Minneapolis, Minnesota 55440

T. C. McGill

T. J. Watson, Sr. Laboratory of Applied Physics, California Institute of Technology, Pasadena, California 91125

J. N. Schulman

Department of Physics and Astronomy, University of Hawaii, Honolulu, Hawaii 96822

(Received 11 February 1983; accepted for publication 29 April 1983)

The HgTe-CdTe superlattice is found to exhibit properties superior to those of the (Hg, Cd)Te alloy as an infrared detector material. A calculation shows that the superlattice tunneling length is shorter than that of the alloy with the same band gap. For a given cutoff wavelength tolerance, we find that less fractional precision is needed in the superlattice control parameter (layer thicknesses) than in the alloy control parameter (composition). Also,  $p$ -side diffusion currents are expected to be reduced due to the larger superlattice electron effective mass.

PACS numbers: 85.60.Gz, 73.40.Lq, 73.40.Gk, 78.20. — e

There is at present a major effort to construct arrays of photovoltaic detectors for the purpose of infrared imaging.<sup>1</sup> The (Hg,Cd)Te alloy is the material most often used to fabricate such detector arrays. Large tunneling currents and the extremely precise composition control required to accurately determine the band gap (or equivalently the cutoff wavelength  $\lambda_c$ ) are two major difficulties in making the detectors.<sup>1</sup> These problems are especially severe for long wavelength ( $\lambda_c \geq 10 \mu\text{m}$ ) detectors. Here, we show that the HgTe-CdTe superlattice potentially offers inherent advantages compared with the (Hg,Cd)Te alloy as an infrared detector material in that (1) tunneling currents in the superlattice are found to be much less than in the alloy of the same band gap, (2) the fractional uncertainty in the band-gap control parameter (layer thickness for the superlattice, composition for the alloy) permissible in the superlattice is greater than that permissible in the alloy for fixed band-gap tolerance requirements, and (3)  $p$ -side diffusion currents in the superlattice are expected to be less than in the alloy of the same band gap. These potential advantages of the superlattice are greatest for the smaller band-gap materials.

The HgTe-CdTe superlattice was originally proposed as an IR material in Ref. 2. In that work, it was shown that the band gap of the superlattice could be controlled by selecting the superlattice layer thicknesses and that most of the useful regions of the IR spectrum could be sampled. It was predicted, however, that very thin layer superlattices were required. Very recently, the HgTe-CdTe superlattice has been fabricated.<sup>3-5</sup> Although relatively thick layer structures were grown, this work is extremely encouraging and suggests that the difficult problems associated with growing this superlattice can indeed be solved.

The calculations are performed using the two-band  $k$ - $p$  approach for the conduction and light hole band.<sup>6,7</sup> The heavy hole band dispersion is treated by including a momentum matrix element with the  $\Gamma_{15}$  conduction-band states. The result of this formal approach is an analytical expression for the superlattice dispersion relation including complex wave vector values. The band gap follows by finding the

energy range described by real superlattice wave vectors. The effective masses are obtained by differentiation and the tunneling lengths by finding the imaginary superlattice wave vector in the band-gap region. The tunneling length is defined as the reciprocal of the maximum magnitude imaginary wave vector of the dispersion curve connecting the conduction-and minimum and the valence-band maximum. The alloy is also described using the two-band  $k$ - $p$  approach in a virtual crystal-type approximation. The CdTe and HgTe  $\Gamma_6 - \Gamma_8$  splittings are taken to be 1.60 and  $-0.303$  eV and the  $\Gamma_{15c} - \Gamma_8$  splittings as 6.01 and 5.58 eV, respectively.<sup>8</sup> The  $\Gamma_6$  to light hole momentum matrix element ( $\sqrt{2/3}$  the  $\Gamma_1 - \Gamma_{15v}$  value) is taken to be 2.54.  $\sqrt{eV m_0}$  (Ref. 8) and the  $\Gamma_{15c}$  to heavy hole momentum matrix element as 2.30  $\sqrt{eV m_0}$ . This value gives a heavy hole effective mass of 0.55  $m_0$  (Ref. 9) in the constituent materials. A lattice constant of 6.472 Å was used.<sup>9,10</sup> The offset between the CdTe and HgTe valence bands was taken to be zero.<sup>2,7</sup>

In Fig. 1 we compare calculated cutoff wavelengths for

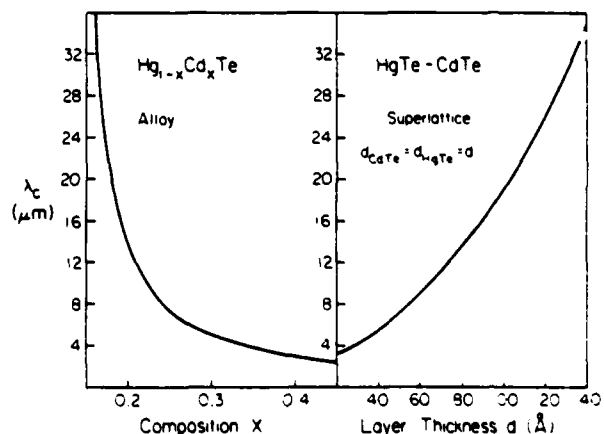


FIG. 1. Cutoff wavelength as a function of alloy composition (left panel) for the  $\text{Hg}_{1-x}\text{Cd}_x\text{Te}$  alloy (from Ref. 11 at  $T = 77$  °K) and cutoff wavelength as a function of layer thickness (right panel) for the HgTe-CdTe superlattice with equally thick HgTe and CdTe layers.

superlattices with equal CdTe and HgTe layer thicknesses with those of the alloy. Layer thicknesses of the superlattice ( $d$ ) and composition ( $x$ ) of the alloy are varied. The results for the alloy are taken from Ref. 11 for 77 °K. Notice that a large part of the IR spectrum can be sampled by the superlattice without going to extremely thin layer spacings. Although qualitatively similar to the results of Ref. 2, the results shown in Fig. 1 differ in an important quantitative way. We predict that useful regions of the IR spectrum are obtained with much thicker layer superlattices (thus, easier to fabricate) than was predicted in Ref. 2. For example, for  $\lambda_c = 12 \mu\text{m}$ , we predict a  $73\text{-}\text{\AA}$  layer thickness superlattice is required while the result of Ref. 2 would be  $20 \text{\AA}$ . This difference comes about because the tight binding parameters used in Ref. 2 gave energy bands with too little dispersion or, equivalently, too large effective masses.<sup>12</sup> The HgTe conduction-band effective mass is the most important here. The experimental value for this parameter is about  $0.026m_0$  (Ref. 8) whereas the tight binding parameters used in Ref. 2 gave a value of about  $0.27m_0$ .

An important point implied from Fig. 1 concerns the precision with which the control parameter must be determined to fix  $\lambda_c$  with a given tolerance. Because the  $\lambda_c$  versus composition curve for the alloy diverges at  $x \sim 0.14$  (Ref. 11) (where the band gap goes to zero), extremely precise control of the composition is required at the larger values of  $\lambda_c$ . The  $\lambda_c$  vs  $d$  curve for the superlattice does not diverge for finite  $d$  (the band gap asymptotically goes to zero as  $d$  approaches infinity) and less precise control of  $d$  is required to fix  $\lambda_c$ . For example, if  $\lambda_c$  must be  $12 \pm 2 \mu\text{m}$ ,  $\Delta x/x$  must be less than about one part in 20 whereas  $\Delta d/d$  must be less than about one part in seven. This advantage of the superlattice is more significant as larger  $\lambda_c$  materials are considered.

In Fig. 2 we compare the calculated results for the electron effective mass normal to the plane of the interface in the superlattice as a function of  $\lambda_c$  (controlled by changing  $d$ )<sup>13</sup> with the electron effective mass of the alloy as a function of  $\lambda_c$  (controlled by changing  $x$ ). Note the scale change in the

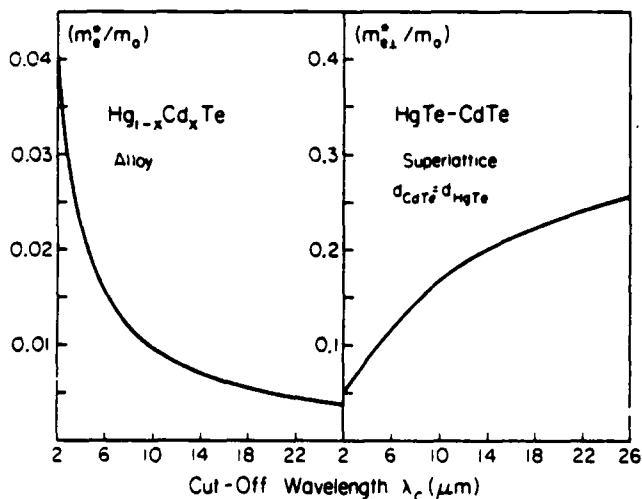


FIG. 2. Electron effective mass as a function of cutoff wavelength for the (Hg,Cd)Te alloy (left panel) and for the HgTe-CdTe superlattice (right panel). The electron effective mass for the superlattice is anisotropic, the component normal to the layer plane is shown.

two panels. In the superlattice this effective mass takes on values comparable to effective masses in Si. These modest values of the effective mass suggest that electron transport normal to the layer plane should occur fairly easily. However, the superlattice effective masses are much larger than the extremely small values which occur in the alloys, particularly in the large  $\lambda_c$  regime. The larger superlattice effective mass will reduce the electron diffusivity of the superlattice as compared with the alloy with the same  $\lambda_c$ . This in turn should reduce the  $p$ -side diffusion currents in a photovoltaic device made from the superlattice (we assume that the diode structure is such that the plane of the  $p$ - $n$  junction is parallel to the plane of the layers<sup>14</sup>). Perhaps more importantly the larger effective masses strongly suggest significantly reduced band-to-band tunneling currents across the junction.

The superlattice effective masses are somewhat sensitive to the value of the assumed valence-band offset but the value of this parameter is not well known. The most recent experimental results are consistent with the zero offset assumed here, but are not definitive.<sup>15</sup> If the offset is a significant fraction of the CdTe band gap, the superlattice perpendicular effective masses will be larger than those shown in Fig. 2.

To examine the tunneling question in more detail in Fig. 3 we compare the tunneling lengths of the superlattice and alloy as functions of  $\lambda_c$ . The tunneling length of the superlattice is seen to be significantly shorter than that of the alloy. This difference in tunneling lengths is more significant for larger  $\lambda_c$ . For example, the superlattice tunneling length in  $\lambda_c = 12 \mu\text{m}$  material is about  $50 \text{\AA}$  which is comparable to the alloy tunneling length in the  $\lambda_c = 4.5 \mu\text{m}$  alloy material. The tunneling length in  $\lambda_c = 12 \mu\text{m}$  alloy material is about  $130 \text{\AA}$ , over two and a half times that in the superlattice with this cutoff wavelength. The tunneling length gives the length scale over which the wave function decays exponentially into a forbidden energy region such as occurs at a  $p$ - $n$  junction. In calculations of tunneling currents the tunneling length appears in a decaying exponential.<sup>16</sup> Thus, the shorter tunneling lengths predicted for the superlattice as compared with the alloy with the same  $\lambda_c$  strongly suggest much smaller

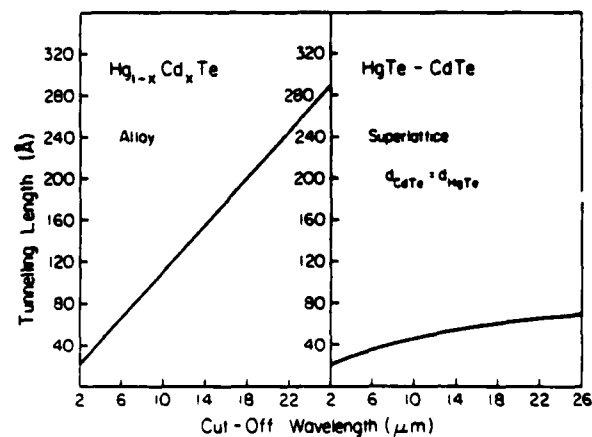


FIG. 3. Tunneling length as a function of cutoff wavelength for the (Hg,Cd)Te alloy (left panel) and for the HgTe-CdTe superlattice (right panel).

tunneling currents in device structures made from the superlattice than in corresponding structures formed from the alloy.

Summarizing, we have found that (1) HgTe-CdTe superlattice can sample useful ranges of the IR spectrum without using extremely thin layer thicknesses, (2) the fractional precision with which the superlattice  $\lambda_c$  control parameter need be determined is less than that for the alloy (given the same tolerance requirements for  $\lambda_c$ ), (3) the superlattice perpendicular electron effective masses are significantly larger than the extremely small values for the electron effective masses in the small band-gap alloys, suggesting reduced  $p$ -side diffusion currents, and (4) the superlattice tunneling length is much reduced as compared with that of the alloy with the same  $\lambda_c$ , implying greatly reduced tunneling currents. These results suggest that the HgTe-CdTe superlattice may be superior to the alloy as an IR detector material, especially at the longer IR wavelengths.

In this letter we have specifically contrasted the HgTe-CdTe superlattice with the (Hg,Cd)Te alloy. However, many of our conclusions are more general than just for this particular system. Very small electron effective masses and long tunneling lengths are a general property of small band-gap zinc blende crystal structure semiconductors. Large tunneling and  $p$ -side diffusion currents are an almost inevitable consequence in devices made from these materials. Small band-gap superlattices (of which HgTe-CdTe is only one possibility) will have significantly larger electron effective masses normal to the interface planes and significantly shorter tunneling lengths. Thus, the small band-gap super-

lattices offer an attractive alternative to small band-gap zinc blende materials in devices, such as IR detectors and sources, which require small band-gap materials.

The authors wish to acknowledge valuable discussions with G. C. Osbourn. This work was supported in part by the Army Research Office under contract NO. DAAG-80-C-0103.

- <sup>1</sup>See, for example, M. B. Reine, A. K. Sood, and T. J. Tredwell, in *Semiconductors and Semimetals* edited by R. K. Willardson and A. C. Beer (Academic, New York, 1981), Vol. 18.
- <sup>2</sup>J. N. Schulman and T. C. McGill, *Appl. Phys. Lett.* **34**, 663 (1979).
- <sup>3</sup>J. P. Faurier, A. Million, and J. Piagnet, *Appl. Phys. Lett.* **41**, 713 (1982).
- <sup>4</sup>J. T. Cheung, *J. Vac. Sci. Technol.* (to be published).
- <sup>5</sup>P. P. Chow (private communication).
- <sup>6</sup>S. R. White and L. J. Sham, *Phys. Rev. Lett.* **47**, 879 (1981).
- <sup>7</sup>G. Bastard, *Phys. Rev. B* **25**, 7584 (1982).
- <sup>8</sup>P. Lawaetz, *Phys. Rev. B* **4**, 3460 (1971).
- <sup>9</sup>R. Dornhaus and G. Nimtz, *Springer Tracts Mod. Phys.* **78**, 1 (1976).
- <sup>10</sup>The momentum matrix elements and lattice constant are averages of the HgTe and CdTe values.
- <sup>11</sup>J. L. Schmit and E. L. Stelzer, *J. Appl. Phys.* **40**, 4865 (1969).
- <sup>12</sup>A simple square well model suggests that the band gap is approximately proportional to  $1/md^2$ , where  $m$  is the HgTe electron effective mass and  $d$  the layer thickness.
- <sup>13</sup>The light hole effective mass normal to the interface plane is found to be slightly less than that of the electron and the heavy hole effective mass is found to be insensitive to the layer thickness and nearly equal to that of the constituent materials.
- <sup>14</sup>For superlattice whose layer spacings are small compared to the depletion width of the  $p$ - $n$  junction ( $\sim 0.1 \mu\text{m}$ ), we view the superlattice as a composite material with macroscopic fields from the junction superposed. We are currently investigating the range of validity in this viewpoint.
- <sup>15</sup>T. F. Kuech and J. O. McCaldin, *J. Appl. Phys.* **53**, 3121 (1982).
- <sup>16</sup>See, for example, C. B. Duke, *Tunneling in Solids* (Academic, New York, 1969).

## HgTe-CdTe SUPERLATTICES

D. L. Smith and T. C. McGill  
 California Institute of Technology  
 Pasadena, California 91125

**Résumé**— Nous présentons une étude théorique se rapportant aux propriétés électroniques des super-réseaux HgTe-CdTe. Nous calculons, en fonction de la période du super-réseau, les valeurs de gap d'énergie, de masses effectives normales aux interfaces et de longueurs caractéristiques d'effet tunnel. Les mêmes quantités sont aussi calculées pour un alliage (Hg,Cd)Te et comparées avec celles obtenues pour le super-réseau HgTe-CdTe. Il est démontré qu'en général, les super-réseaux HgTe-CdTe possèdent des propriétés supérieures à celles des alliages pour les applications en détection infra-rouge.

**Abstract**— We report on a theoretical study of the electronic properties of HgTe-CdTe superlattices. The band gap as a function of layer thickness, effective masses normal to the layer plane and tunneling length are compared to the corresponding (Hg, Cd)Te alloys. We find that the superlattice possesses a number of properties that may make it superior to the corresponding alloy as an infrared material.

### 1-Introduction

Superlattices formed of HgTe and CdTe have been proposed as materials for application in the infrared /1-3/. In the last couple of years a number of groups have made serious attempts to fabricate these superlattices /4-6/.

In elemental and alloy based ( $\text{Hg}_x\text{Cd}_{1-x}\text{Te}$ - $\text{Hg}_y\text{Cd}_{1-y}\text{Te}$ ) superlattices, the material is made up of alternating layers of the compounds or alloys. The simplest case is illustrated by concentrating on the elemental superlattice. In this case, the superlattice can be viewed in a Kronig-Penney square well model like that schematically illustrated in Fig. 1. In drawing this figure, the valence band offset has been taken to be zero. This value is consistent with all of the measured results and the few empirical ideas for estimating valence band offsets /7,8/. In this schematic the holes do not experience a barrier in going from one layer to another. However, the electrons see the full difference in the band gaps. As noted originally in Ref. 1, this superlattice has the property that the band gap is dependent on thickness of the layers. In the limit of very thick HgTe layers the band gap is zero since it originates in the HgTe. As the thickness of the HgTe layer is reduced, the band gap increases as a result of the confinement of the conduction band wavefunction. In the limit of very thin layers the superlattice bandgap approaches that of the alloy with the same composition. Another property of such a structure was noted in the original papers by Schulman and McGill /1-3/. The close proximity of the valence band edge of CdTe implies that the tunneling length in the CdTe for electrons at the conduction band edge is quite long and that the masses for electrons at the conduction band edge normal to the layers is relatively small. For thinner CdTe layers, the superlattice can behave as a three-dimensional bulk material as opposed to the two dimensional character of many of the other materials and systems.

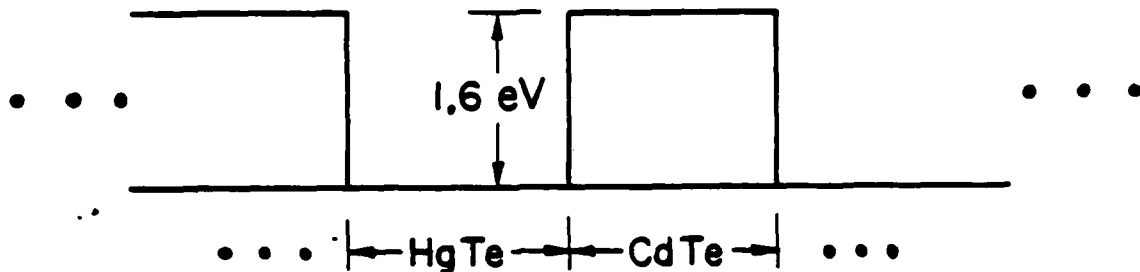


Fig. 1- Schematic illustration of the HgTe-CdTe heterojunction. Repetition of this heterojunction produces the superlattice. The valence band offset is taken to be zero.

In this paper we report on a more accurate study of the near band edge properties of the HgTe-CdTe superlattices and make detailed comparisons with the corresponding properties of the alloys. Section II contains a brief description of the theoretical technique used to make the calculations. Section III gives the results and compares them with those corresponding to the alloys. Section IV presents our conclusions.

## II-Calculational Method

In the original papers by Schulman and McGill /1-3/, the calculations were carried out using the empirical tight-binding technique. This technique had one deficiency in that it aimed at reproducing the optical transitions for the HgTe and CdTe but did not give an accurate description of the near band edge properties such as effective masses. In this report, we give the results of k-p calculations that reproduce the near band edge properties very accurately. The calculational approach is similar to those reported by White and Sham /9/, and Bastard /10/. A two-band k-p approach is applied to the conduction and light hole band. The heavy hole band is also treated using this formalism. It is taken to connect through the momentum matrix element with the  $\Gamma_{15}$  conduction band states. The potential is assumed to be constant in the two layers with a discontinuity at the interface for the s-like potential (the conduction band offset). An analytical expression for the superlattice energy-wavevector relation is obtained. The alloy is also described using a 2-band k-p approach. The parameters in the k-p are obtained using a virtual crystal type approximation.

The splittings  $\Gamma_6-\Gamma_8$  and  $\Gamma_{15;c}-\Gamma_8$  are taken to be 1.60 eV and 6.01 eV for CdTe and -0.303 eV and 5.58 eV for HgTe. The  $\Gamma_6$  to light hole momentum matrix element is taken to be  $2.54\sqrt{eV m_0}$  and the  $\Gamma_{15;c}$  to heavy hole matrix element is taken to be  $2.30\sqrt{eV m_0}$ , resulting in a heavy hole effective mass of  $0.55m_0$  in both materials. The lattice constant was taken to be 6.472 Å. The valence band offset was taken to be zero.

The effective masses are obtained by differentiating the resulting energy-wavevector relation. The tunneling length is obtained by finding the imaginary superlattice wavevector in the bandgap of the superlattice.

## III-Results

In Fig. 2 we present the results for cutoff wavelength as a function of composition for the alloy

and layer thickness for superlattices in which the thickness of the HgTe is the same as the CdTe. The result for the alloy shows the characteristic singularity at  $x = 0.14$ . In contrast the result for the bandgap of the superlattice shows no such singularity. The cutoff wavelength smoothly approaches infinity as the thickness of the HgTe layer approaches infinity. This result implies an obvious advantage for the superlattice. To reach a given cutoff wavelength, the parameters which must be controlled are the thickness of the layers. Since in the case of the superlattice the cutoff wavelength is not singular in this parameter, the precision with which this parameter must be controlled to reach a given cutoff is much less in the superlattices than in the alloys.

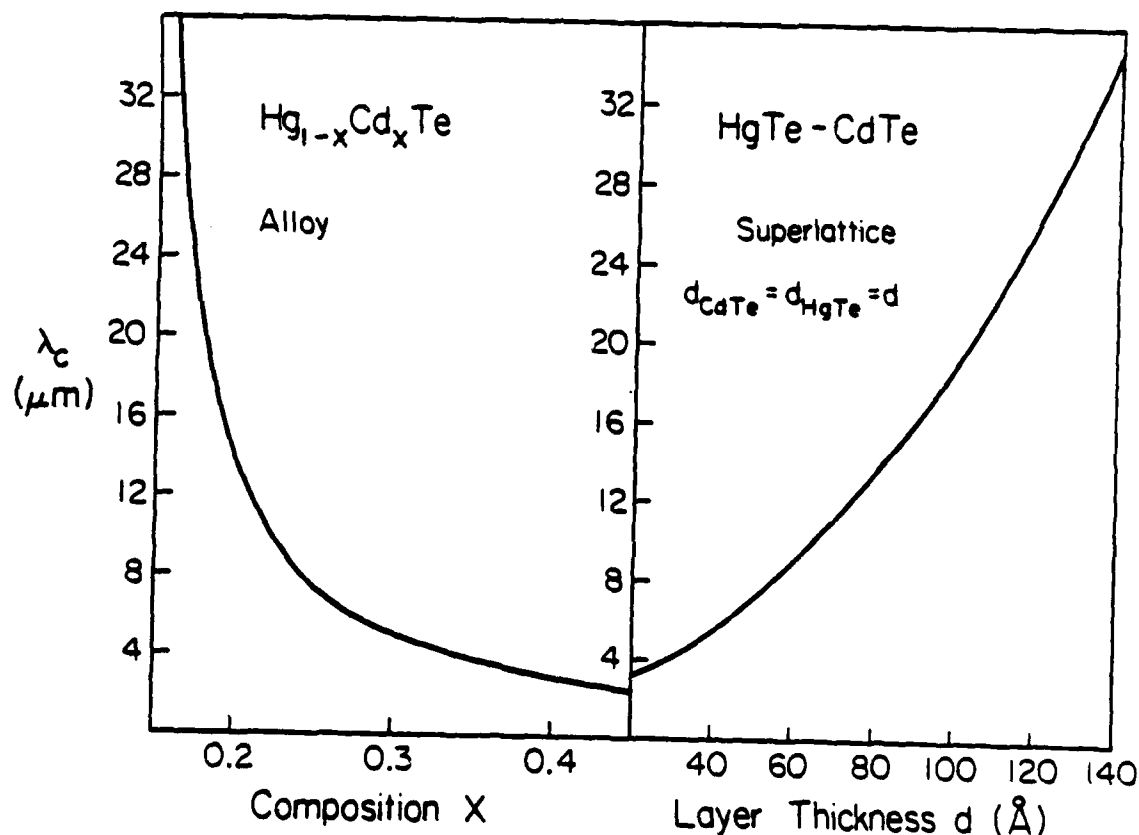


Fig. 2- The cutoff wavelength or the reciprocal of the bandgap for the alloy as a function of composition and the superlattice as a function of layer thickness. The thicknesses of the HgTe and CdTe layers in the superlattice are assumed to be the same.

One characteristic of narrow-band-gap, zincblende-crystal-structure material is the very small effective mass [11]. In Fig. 3, we have plotted the effective mass of the conduction band for the alloy and the superlattice normal to the layers as function of the cutoff wavelength or the reciprocal of the band gap. To illustrate our point the results for equal HgTe and CdTe layer thicknesses are presented. This figure shows a very interesting property of the superlattice as compared to the alloy. The effective mass of the superlattice is much larger than that for the corresponding alloy.

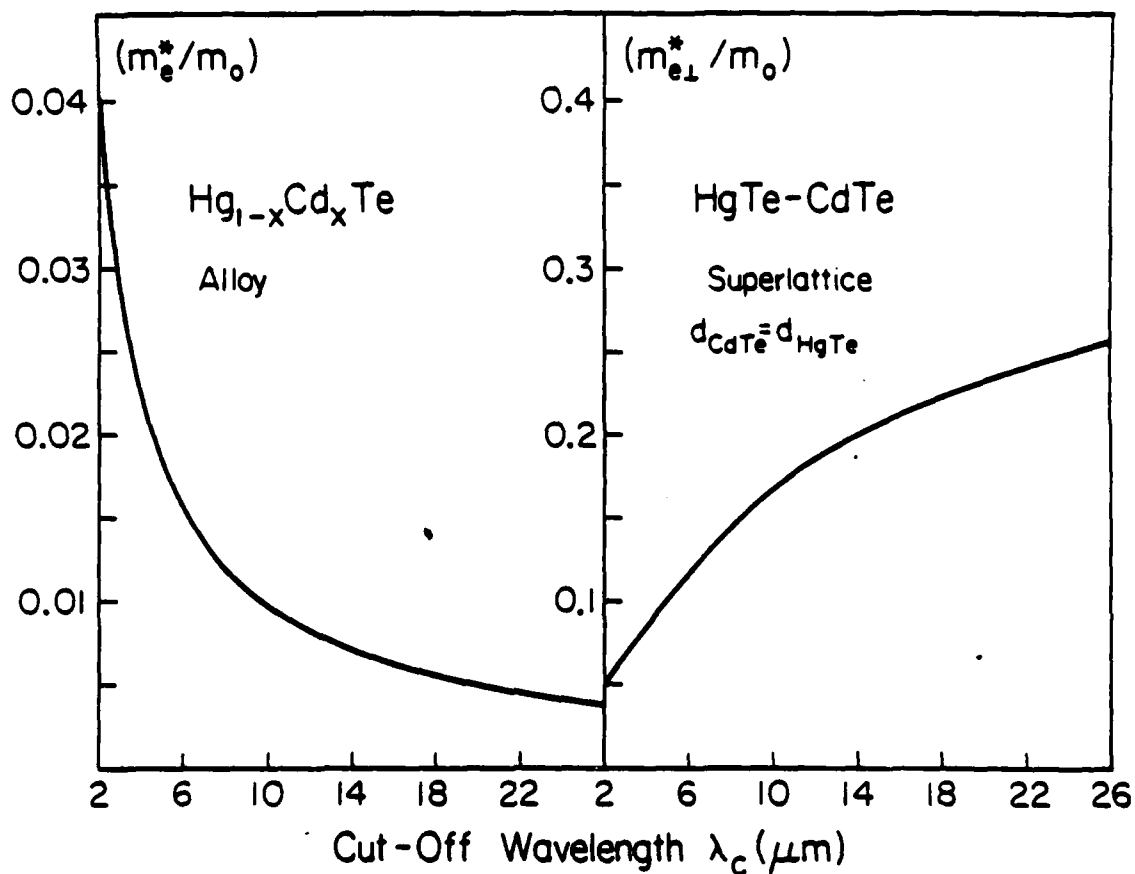


Fig. 3- The electron effective mass as a function of the cutoff wavelength for the alloys and a superlattice with equal thicknesses of HgTe and CdTe. The effective mass for the superlattice is that normal to the layers. Note the scale change on the effective masses for the two graphs.

In most device structures employing narrow band gap semiconductors, the very small electron effective mass is an obvious disadvantage. The small effective mass leads to large diffusion currents and large tunneling currents through the depletion region of the devices. In the case of the superlattices the effective mass and the band gap are not strongly coupled. Hence, one can obtain values for the effective mass in the appropriate direction that are large compared to those for the same band gap in the alloy.

To illustrate this point quantitatively, we have plotted a characteristic length governing the tunneling as a function of the cut-off wavelength for a superlattice and alloy in Fig. 4. We have selected the characteristic length to be the reciprocal of the imaginary part of the wavevector at its maximum in the forbidden gap. Again for convenience we have chosen the case when the superlattice is made of layers of HgTe and CdTe with the same thickness. The important point to note from this figure is the rather large values of the tunneling length for the alloy that are obtained when the cut-off wavelength is large and the rather small values that are obtained in the superlattice.

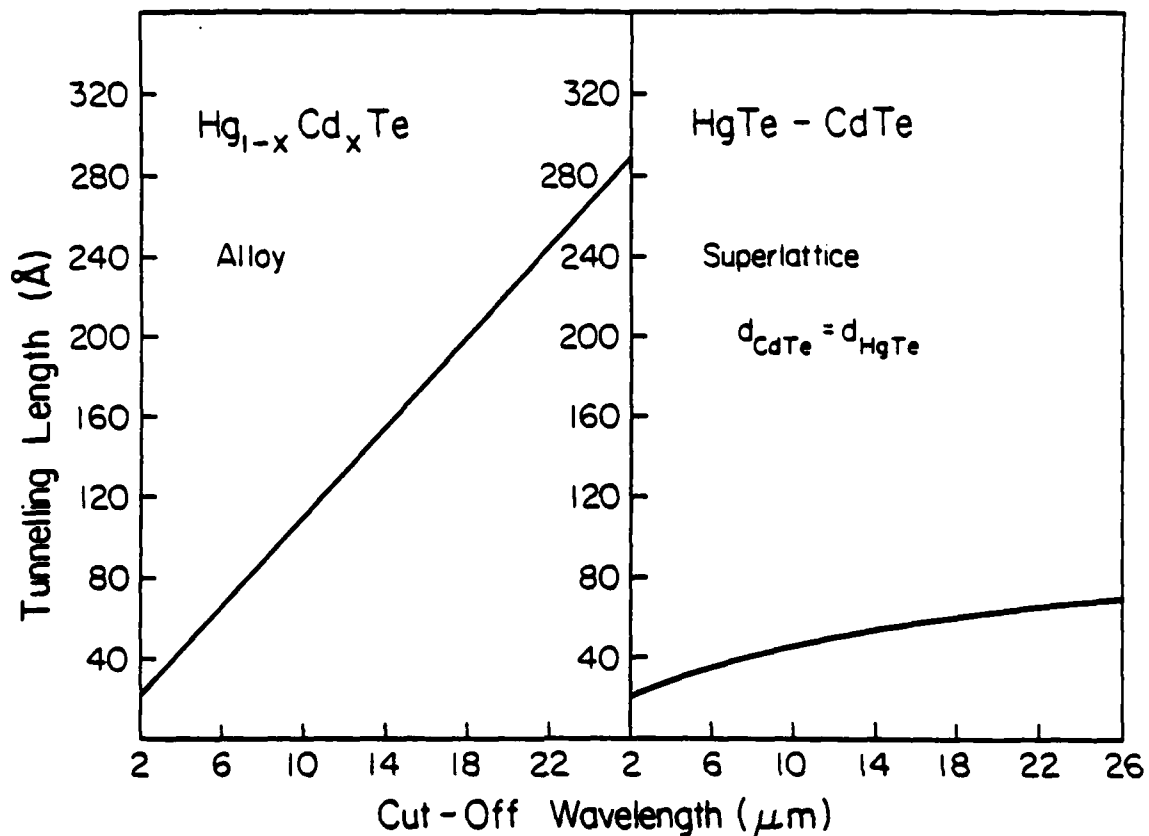


Fig. 4— The tunneling length as a function of cutoff wavelength for the alloy and superlattice. The tunneling length is defined to be the reciprocal of the imaginary part of the wavevector at its maximum in the forbidden gap. The superlattice consists of HgTe layers and CdTe layers with the same thickness.

#### IV-Conclusions

In this short note we have presented an accurate study of the narrow band edge properties of the HgTe-CdTe superlattices. The theoretical results suggest three very important properties of this superlattice as an infrared material: First, the band gap is continuously adjustable from the value of the alloy to zero for a fixed ratio of HgTe to CdTe. Second, for moderate thicknesses of the CdTe layers, the superlattice can behave as a three-dimensional material with a reasonable value for the mass of the electrons normal to the layer. Third, the electron tunneling is significantly reduced compared to that for the alloy of the same bandgap.

These properties make the superlattices of HgTe-CdTe one of the most exciting recent developments in infrared materials.

#### Acknowledgement

The authors gratefully acknowledge the support of the United States Army Research Office under Contract No. DAAG-80-C-0103.

#### References

1. Schulman, J. N. and McGill, T. C., , *Appl. Phys. Lett.* **34** (1979) 663 .

2. Schulman, J. N. and McGill, T. C., , *J. Vac. Sci. Technol.* **16** (1979) 1513.
3. Schulman, J. N. and McGill, T. C., , *Phys. Rev.* **B23** (1981) 4149.
4. Faurie, J. P., Million, A., and Piagnet, J., , *Appl. Phys. Lett.* **41** (1982)713.
5. Chow, P. P., Greenlaw, D. K., and Johnson, D.,, *J. Vac. Sci. Technol.* **A1** (1982)562.
6. Cheung, J. T. **Proceedings of the HgCdTe Workshop** *J. Vac. Sci. Technol.* (to be published).
7. Kuesch, T. F. and McCaldin, J. O., , *J. Appl. Phys.* **53** (1982) 3121.
8. Faurie, J. P.,**Proceedings of Electronic Materials Conference 1983** *J. Electronic Materials* **13** (to be published).
9. White, S. R. and Sham, L. J., , *Phys. Rev. Lett.* **47** (1981)879.
10. Bastard, G., , *Phys. Rev.* **B25** (1982) 7584.
11. C. Kittel, **Quantum Theory of Solids**(John Wiley and Sons, Inc., New York, 1963)pp. 186ff.

T. C. McGill and D. L. Smith

California Institute of Technology, Pasadena, California 91125

(Received 25 February 1983; accepted 3 March 1983)

PACS numbers: 71.25.Tn, 72.80.Ey, 68.55.+b, 73.60.Fw

In their seminal paper on superlattices, Esaki and Tsu<sup>1</sup> indicated that superlattices involving II-VI compounds and their alloys, could be of interest along with superlattices involving group IV and III-V semiconductors. Independently, Schulman and McGill<sup>2</sup> identified the HgTe-CdTe superlattice as an interesting case to study. HgTe and CdTe have the same crystal structure and lattice constant to 0.3%.<sup>3</sup> CdTe is a conventional zinc blende semiconductor with a band gap of about 1.6 eV; HgTe is a zero band gap semiconductor.<sup>3</sup> Hence, HgTe-CdTe superlattices are expected to span a wide range of properties.

Schulman and McGill<sup>2,4</sup> carried out extensive theoretical studies of this superlattice and concluded that this superlattice could have significant application in infrared devices. For fixed Hg to Cd ratio, they found that the band gap of the superlattice could be adjusted from zero in the limit of thick HgTe layers to a value that is approximately that of the corresponding alloy for thin HgTe layers. This band gap variation should be contrasted with that of the alloy where a single value is obtained for fixed Hg to Cd ratio. One could also make superlattices from alloys  $Hg_{(1-x)}Cd_xTe-Hg_{(1-y)}Cd_yTe$ . Hence, one could vary both the thickness of the two layers and  $x$  and  $y$ . These four independent parameters can be used to control the materials properties.

An important question is the value of the offset between the valence band in the two materials. This parameter is particularly important in governing the properties of the superlattices. Classical arguments based on the electron affinity differences,<sup>5</sup> the common anion rule,<sup>6</sup> and Harrison's model<sup>7</sup> suggest that valence band offsets should be small. Schulman and McGill<sup>8</sup> found that if they took the band offset between the valence bands of the HgTe and CdTe to be zero, then the decay of the wave function near the valence band and conduction band edges into the CdTe was slow. Therefore, transport normal to the layers was possible even for rather thick layers of CdTe in the superlattice. Hence, the material would behave as a true three-dimensional material, in that transport normal to the layers would take on a reasonable value. Experimentally, the value of the band offsets for this structure has not been determined unequivocally. However, the results of experiments by Kuech and McCallidin<sup>9</sup> suggest that the band offsets for the valence band may indeed be small.

In a recent paper, Smith, McGill, and Schulman<sup>10</sup> have presented a number of reasons for considering HgTe-CdTe superlattices for application in the infrared. Using a much improved calculation of the band gap of the superlattice as a function of the layer thickness, they find that interesting cutoff wavelengths (8-12  $\mu\text{m}$ ) can be reached by working with superlattices with thickness as great as 55-75  $\text{\AA}$ . Further-

more, they find that the band gap of the superlattice can be determined with less fractional precision in the layer thickness than the fractional precision in composition required for the alloy. This makes it easier to reach a given cutoff wavelength with the superlattice than with the alloy.

They also find that the CdTe layers in the superlattice tend to confine the electronic wave functions for energies in the forbidden gap better than in the alloy. To illustrate this point, we have plotted the complex band structure for  $Hg_{(1-x)}Cd_xTe$  alloys in Fig. 1 and that for HgTe-CdTe superlattices with the same band gaps. The important point to be noted here is the much larger value of the  $k_i$  for the superlattice as compared to the alloy with the same band gap. This difference in the imaginary part suggests significantly reduced tunneling in junctions formed in the superlattice as compared to those in alloys. Hence, the HgTe-CdTe superlattice has a number of properties that could make it interesting in comparison to the alloy for infrared applications.

The fabrication of these structures is difficult owing to the high Hg vapor pressure. A number of groups have been attempting to fabricate HgTe-CdTe superlattices. Very recently Faurie and co-workers<sup>11</sup> have reported the first growth of these structures. Using molecular beam epitaxy, this group has succeeded in fabricating as many as 100 layers. The thickness of the HgTe layers ranged from 180-1600  $\text{\AA}$ , and the thickness of the CdTe layers ranged from 44-600  $\text{\AA}$ . While these experimental results are very preliminary, they indicate that HgTe-CdTe superlattices can, in fact, be

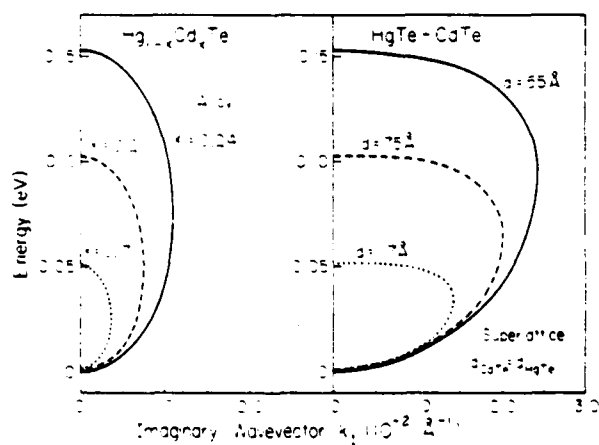


FIG. 1. Complex band structure of the  $Hg_{(1-x)}Cd_xTe$  alloy and the HgTe-CdTe superlattice. The abscissa is the imaginary part of the wave vector which governs the decay of the wave function in the forbidden energy range which is given on the ordinate. The results for a number of different alloy compositions  $x$  are given. To make comparison possible, the results are also given for the superlattice with equal amounts of CdTe and HgTe, with the thickness of the layers adjusted to give the same value for the band gap as for the alloy.

grown. Only future experiments will show whether or not they have the desired properties.

In summary, HgTe-CdTe superlattices are extremely interesting materials, whose properties are only beginning to be explored.

The authors gratefully acknowledge the support of the Army Research Office under Contract No. DAAG29-80-C-0103.

<sup>1</sup>L. Esaki and R. Tsu, *IBM J. Res. Dev.* 14, 61 (1970).

<sup>2</sup>J. N. Schulman and T. C. McGill, *Appl. Phys. Lett.* 34, 663 (1979).

<sup>3</sup>R. Dornhaus and G. Nimtz, *Springer Tracts in Modern Physics* (Springer, New York, 1976), Vol. 78.

<sup>4</sup>J. N. Schulman and T. C. McGill, *J. Vac. Sci. Technol.* 16, 1513 (1979).

<sup>5</sup>R. L. Anderson, *Proceedings of the International Conference on Semiconductors Prague, 1960* (Academic, New York, 1961), p. 563. The values and calculations are given in Ref. 4.

<sup>6</sup>J. O. McCaldin, T. C. McGill, and C. A. Mead, *J. Vac. Sci. Technol.* 13, 802 (1976).

<sup>7</sup>W. A. Harrison, *J. Vac. Sci. Technol.* 14, 1016 (1977).

<sup>8</sup>J. N. Schulman and T. C. McGill, *Phys. Rev. B* 23, 4149 (1981).

<sup>9</sup>T. F. Kuech and J. O. McCaldin, *J. Appl. Phys.* 53, 3121 (1982).

<sup>10</sup>D. L. Smith, T. C. McGill, and J. N. Schulman, *Appl. Phys. Lett.* (submitted for publication).

<sup>11</sup>J. P. Faurie, A. Million, and J. Piagnet, *Appl. Phys. Lett.* 41, 713 (1982).

**ENERGY SPECTRA OF DONORS IN GaAs-Ga<sub>1-x</sub>Al<sub>x</sub>As QUANTUM WELL STRUCTURES\***

C. MAILHIOT\*\*, Yia-Chung CHANG\*\*\* and T.C. MCGILL

*California Institute of Technology, Pasadena, California 91125, USA*

Received 10 July 1981; accepted for publication 26 August 1981

We present the results of a theoretical study of the variation of the binding energy for shallow donor states in quantum well structures consisting of a single slab of GaAs sandwiched between two semi-infinite slabs of Ga<sub>1-x</sub>Al<sub>x</sub>As. The alloy composition,  $x$ , is varied between 0.1 and 0.4. In this range, the Ga<sub>1-x</sub>Al<sub>x</sub>As is direct and the single-valley effective mass theory is a valid technique for treating shallow states. Calculations are carried out in the case of finite potential barrier determined by realistic conduction band offsets. We find that the binding energy varies from about 5 meV at infinite GaAs slab thickness to a maximum value between 15 and 5 monolayers depending on the alloy composition. The maximum binding energy varies from about 12 meV for the  $x=0.1$  alloy to about 16 meV for the  $x=0.4$  alloy.

**1. Introduction**

The unique nature of electronic states associated with semiconductor superlattices has been the subject of a great deal of interest [1-3]. In view of the potential applications of these structures [4-7], the understanding of impurity states found within these systems is an issue of technical as well as scientific importance.

In this paper, we report on a study of donor states in a single GaAs-Ga<sub>1-x</sub>Al<sub>x</sub>As quantum well, i.e., a structure formed with a central GaAs slab (well material) flanked by two semi-infinite Ga<sub>1-x</sub>Al<sub>x</sub>As slabs (barrier material). The binding energy of a donor state centered in the GaAs slab is studied as a function of the width of the rectangular potential well formed by the conduction band offset at the GaAs-Ga<sub>1-x</sub>Al<sub>x</sub>As interface. The effect of the alloy composition,  $x$ , in the barrier material is also investigated. We find that the binding energy is considerably modified as the dimension of the confining quantum well is varied. Since we treat a single quantum well, the results discussed below should apply to superlattices in which the Ga<sub>1-x</sub>Al<sub>x</sub>As barriers are thick enough so that there is little overlap between the states confined within adjacent GaAs quantum wells.

\* Work supported in part by the Army Research Office under Contract No. DAAG29-80-C-0103.

\*\* Supported by the NSERC of Canada and by the Fonds FCAC of Quebec.

\*\*\* Present address: Department of Physics, University of Illinois, Urbana, Illinois 61801, USA.

## 2. Calculation method

Calculations are based on the effective mass approximation. The composition of the Ga<sub>1-x</sub>Al<sub>x</sub>As alloy was varied in the range where the alloy remains direct, so that single-valley effective mass theory still holds. Realistic conduction band offsets of finite values were used, thereby allowing the wavefunction to penetrate into the barrier material.

Taking into account the finite magnitude of the potential barrier, the effective mass Hamiltonian corresponds to that of a Coulomb center at the middle of a finite quantum well of width  $2a$  (along the  $z$  direction) and height  $V_0$ :

$$H = \frac{-\hbar^2 \nabla^2}{2m_1^*} - \frac{e^2}{\epsilon_1 r}, \quad \text{for } |z| < a, \quad (1a)$$

$$H = \frac{-\hbar^2 \nabla^2}{2m_2^*} - \frac{e^2}{\epsilon_2 r} + V_0, \quad \text{for } |z| > a. \quad (1b)$$

$m_1^*$  and  $\epsilon_1$  refer to the bulk GaAs values and  $m_2^*$  and  $\epsilon_2$  refer to the interpolated values in Ga<sub>1-x</sub>Al<sub>x</sub>As. Since the dielectric constants of the two semiconductors are similar, the potential energy contribution due to the image charges of the impurity ion [8] was found to be at most of the order of 3% and were therefore neglected in the present calculation. The conduction band offset,  $V_0$ , was taken to be 85% of the difference in the band gaps of GaAs and Ga<sub>1-x</sub>Al<sub>x</sub>As [9]. Since the alloy composition range studied was such that the alloy was direct ( $x < 0.45$ ) [9], both the effective mass  $m_2^*$  and the conduction band offset  $V_0$  were determined using the  $\Gamma$ -point values in Ga<sub>1-x</sub>Al<sub>x</sub>As. Using room temperature values, we obtain for GaAs and Ga<sub>1-x</sub>Al<sub>x</sub>As [9]:  $m_1^* = 0.067m_0$ ,  $m_2^* = (0.067 + 0.083x)m_0$ ,  $\epsilon_1 = 13.1\epsilon_0$ ,  $\epsilon_2 = (13.1(1-x) + 10.1x)\epsilon_0$ , and  $V_0 = 1.06x$  eV, where  $m_0$  and  $\epsilon_0$  are the free electron mass and the vacuum static dielectric constant, respectively.

The calculations made use of the variational principle. The basis set used consists of solutions to the one-dimensional finite quantum well Hamiltonian multiplied by a set of nineteen two-dimensional Gaussian-type orbitals. The boundary conditions imposed on the one-dimensional solutions to the finite quantum well were continuity of the wavefunction and of the velocity operator since the two effective masses differ across the well boundary. The donor state envelope function is allowed to leak into the barrier material as the width of the well is reduced. To confirm the validity of this basis set, we have also carried out the calculation using another basis set [10], consisting of three-dimensional Gaussian-type orbitals defined in an ellipsoidal coordinate system so as to retain the non-spherical character of the Hamiltonian (eq. (1)). This basis set has the advantage of reproducing reasonably well the Coulomb center at large slab thicknesses where the cosine-like character of the well states basis set does not produce a good description. For slab thicknesses less than about 40 GaAs monolayers, this ellipsoidal basis set produces results similar to those reported here.

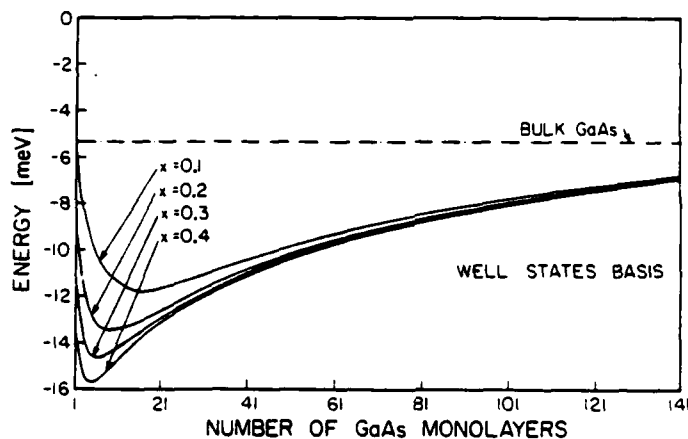


Fig. 1. Variation of the energy measured with respect to the first subband for the donor ground state in GaAs-Ga<sub>1-x</sub>Al<sub>x</sub>As quantum well structure as a function of the GaAs slab thickness. Calculations were carried out for four alloys compositions. The dash-dotted line indicates the binding energy for bulk GaAs. A GaAs monolayer is 2.83 Å thick.

### 3. Results

The energy of the ground state with respect to the first conduction subband as a function of GaAs slab thickness is shown in fig. 1 for four alloy compositions:  $x = 0.1, 0.2, 0.3, 0.4$ . The binding energy versus GaAs slab thickness curve presents a maximum whose magnitude and position depend on the alloy composition of the barrier material. The position of the maximum varies from about 15 monolayers to about 5 monolayers as the Al content in the alloy is increased from 10% to 40%. The corresponding maximum binding energy increases from about 12 to about 16 meV as the Al content in the alloy is augmented from 10% to 40%. Greater Al concentration in the barrier material leads to larger conduction band offsets and therefore more effective confinement of the donor envelope function. Since a greater confinement of the donor state leads to a more sharply peaked wavefunction around the impurity center, the attractive Coulomb potential is more effective in binding the donor state when the Al content in the Ga<sub>1-x</sub>Al<sub>x</sub>As barriers is increased.

### 4. Conclusions

We have calculated the binding energy of shallow donor states in GaAs-Ga<sub>1-x</sub>Al<sub>x</sub>As quantum well structures using the effective mass approximation scheme. Realistic values for conduction band offsets were used. The impurity

center was located in the middle of the GaAs slab. The variation in binding energy of the donor ground state was studied as a function of the central GaAs slab thickness. Calculations were done for four alloy compositions of Ga<sub>1-x</sub>Al<sub>x</sub>As in a range in which the alloy remains direct.

It was found that the binding energy of the donor ground state is considerably modified as the thickness of the GaAs slab containing the impurity was varied. This variation in binding energy should be easily observed experimentally since molecular-beam epitaxy (MBE) techniques [11] now allow for the fabrication of superlattices consisting of alternating slabs of few monolayers of GaAs-Ga<sub>1-x</sub>Al<sub>x</sub>As. It seems then possible to adjust the binding energy of a Coulomb center in a superlattice by varying the thickness of the slab containing the impurity center.

### References

- [1] J.N. Schulman and T.C. McGill, *Phys. Rev.* B19 (1979) 6341.
- [2] J.N. Schulman and T.C. McGill, *Phys. Rev. Letters* 39 (1977) 1680.
- [3] R.N. Nucho and A. Madhukar, *J. Vacuum Sci. Technol.* 15 (1978) 1530.
- [4] L. Esaki and R. Tsu, *IBM J. Res. Develop.* 14 (1970) 61.
- [5] R. Dingle, H.L. Störmer, A.C. Gossard and W. Wiegmann, *Appl. Phys. Letters* 33 (1978) 665.
- [6] J.N. Schulman and T.C. McGill, *Appl. Phys. Letters* 34 (1979) 663.
- [7] J.P. van der Ziel, R. Dingle, R.C. Miller, W. Wiegmann and W.A. Nordland, Jr., *Appl. Phys. Letters* 26 (1975) 463.
- [8] N.O. Lipari, *J. Vacuum Sci. Technol.* 15 (1978) 1412.
- [9] H.C. Casey and M.B. Panish, *Heterostructure Lasers* (Academic Press, New York, 1978) Part A, p. 192.
- [10] C. Mailhot, Y.-C. Chang and T.C. McGill, to be published.
- [11] A.C. Gossard, P.M. Petroff, W. Wiegmann, R. Dingle and A. Savage, *Appl. Phys. Letters* 29 (1976) 323.

HD-A138 149

SUPERLATTICES AND SEMICONDUCTOR/SEMICONDUCTOR  
INTERFACES(U) CALIFORNIA INST OF TECH PASADENA  
T C MCGILL 17 JAN 84 ARO-17257.6-EL DRAG29-80-C-0103

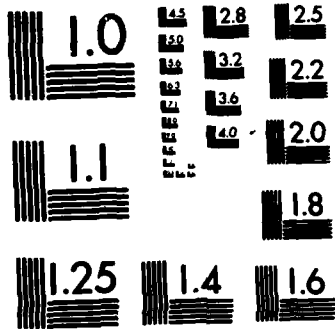
2/2

UNCLASSIFIED

F/G 20/12

NL


END  
PAGES  
3  
ETC



MICROCOPY RESOLUTION TEST CHART  
NATIONAL BUREAU OF STANDARDS-1963-A

## Energy spectra of donors in GaAs-Ga<sub>1-x</sub>Al<sub>x</sub>As quantum well structures in the effective-mass approximation

C. Mailhot, Yia-Chung Chang,\* and T. C. McGill

California Institute of Technology, Pasadena, California 91125

(Received 22 January 1982; revised manuscript received 14 May 1982)

We present the results of a study of the energy spectrum of the ground state and the low-lying excited states for shallow donors in quantum well structures consisting of a single slab of GaAs sandwiched between two semi-infinite layers of Ga<sub>1-x</sub>Al<sub>x</sub>As. The effect of the position of the impurity atom within central GaAs slab is investigated for different slab thicknesses and alloy compositions. Two limiting cases are presented: one in which the impurity atom is located at the center of the quantum well (on-center impurity), the other in which the impurity atom is located at the edge of the quantum well (on-edge impurity). Both the on-center and the on-edge donor ground state are bound for all values of GaAs slab thicknesses and alloy compositions. The alloy composition  $x$  is varied between 0.1 and 0.4. In this composition range, Ga<sub>1-x</sub>Al<sub>x</sub>As is direct, and the single-valley effective-mass theory is a valid technique for treating shallow donor states. Calculations are carried out in the case of finite potential barriers determined by realistic conduction-band offsets.

### I. INTRODUCTION

The unique nature of electronic states associated with semiconductor superlattices has been the subject of a great deal of interest both from the theoretical<sup>1-6</sup> and experimental<sup>7-10</sup> viewpoints. In view of the potential applications of these structures,<sup>11-14</sup> the understanding of impurity states found within these systems is an issue of technical as well as scientific importance.

In this paper we report on study of the energy spectrum of shallow donor states in a single GaAs-Ga<sub>1-x</sub>Al<sub>x</sub>As quantum well, i.e., a structure formed by a central GaAs slab (well material) flanked by two semi-infinite Ga<sub>1-x</sub>Al<sub>x</sub>As layers (barrier material). The energy spectrum of a donor state located within the GaAs slab is studied as a function of the width of the rectangular potential well formed by the conduction-band offset at the GaAs-Ga<sub>1-x</sub>Al<sub>x</sub>As interface. The effect of the alloy composition  $x$  in the barrier material as well as the position of the donor atom within the well are also investigated. To illustrate the effect of the position of the donor on the electronic spectra, two positions of the donor ion were studied: (1) donor ion at the center of the quantum well (on-center impurity) and (2) donor ion on the edge of the quantum well boundary (on-edge impurity). We find that the donor energy spectrum, both for the on-center and the on-edge impurity, is considerably modified as the dimension of the quantum well is

varied. Both the on-center and the on-edge donor energies with respect to the first conduction sub-band versus GaAs slab thickness present a maximum (in absolute value) whose magnitude depends on the alloy composition. The on-edge impurity produces a more shallow donor ground state than the on-center impurity. This reduction of binding of the on-edge donor ground state results from the fact that the repulsive barrier potential tends to push the electronic charge distribution away from the attractive ionized center thereby leading to a reduced effective Coulomb attraction. This finding is in accord with previous calculations carried in the case of infinite confining potential.<sup>15</sup>

In Sec. II we present the calculation techniques. We discuss first the effective-mass Hamiltonian used for treating the shallow states and its validity; then we describe the basis orbitals on which the donor state is expanded. In Sec. III, the main results are presented. First we discuss the energy spectrum for the on-center impurity; then we treat the case of the on-edge impurity. A comparison is made between these two limiting cases. A summary of the results and a conclusion are presented in Sec. IV.

### II. CALCULATION METHOD

Calculations are based on the effective-mass approximation (EMA). The GaAs-Ga<sub>1-x</sub>Al<sub>x</sub>As sys-

tem was chosen since the EMA is known to hold to a high degree of accuracy for shallow donor states in GaAs.<sup>16</sup> As shown by Ando and Mori,<sup>17</sup> the boundary condition that the donor envelope function and the particular current are continuous across the interface is sufficient in the case of GaAs-Ga<sub>1-x</sub>Al<sub>x</sub>As quantum well structures. For other systems, one would have to go beyond the EMA and use the complex band structure of the superlattice to provide a complete theoretical description of shallow donor states.<sup>18</sup> Since we treat a single quantum well, the results discussed below should apply to superlattices in which the Ga<sub>1-x</sub>Al<sub>x</sub>As barriers are thick enough so that there is little overlap between the states confined to adjacent GaAs quantum wells. In the case of thin superlattices, one should take into account the spreading of the donor envelope function into the adjacent quantum wells.

The composition of the Ga<sub>1-x</sub>Al<sub>x</sub>As alloy was varied in the range where the alloy remains direct, so that the single-valley effective-mass theory still holds. Realistic conduction-band offsets of finite magnitude were used, thereby allowing the wave function to penetrate into the barrier material as the dimensions of the confining quantum well are reduced. The use of finite conduction-band offsets has a large effect on the binding energy of the donor state in the thin GaAs slab limit and should be compared with approximate calculations carried out using infinitely high barrier height (quantum box case).<sup>19,20</sup> For example, as first shown by Levine,<sup>21</sup> hydrogenic donor states at a semiconductor surface cannot exist unless the sum of the Coulomb quantum numbers,  $l + m$ , is an odd integer if the potential discontinuity is assumed to be infinite at the surface. In this case, the ground state corresponds to a  $2p_z$  hydrogenic state. In particular, spherically symmetric states are not allowed since the donor envelope function is required to vanish at the interface. When finite conduction-band offsets are taken into account, the condition that the wave function vanish at the interface is relaxed and penetration in the barrier material is allowed. The infinite barrier case should be viewed as a limiting case valid only for very wide quantum wells for which the penetration of the donor state into the barrier material is small.

The effective-mass Hamiltonian corresponding to a Coulomb center located at a distance  $c$  from the center of a finite quantum well of width  $2a$  along the  $\hat{z}$  direction (the  $\hat{z}$  axis is normal to the interface plane) and height  $V_0$  (see Fig. 1 for geometry) is

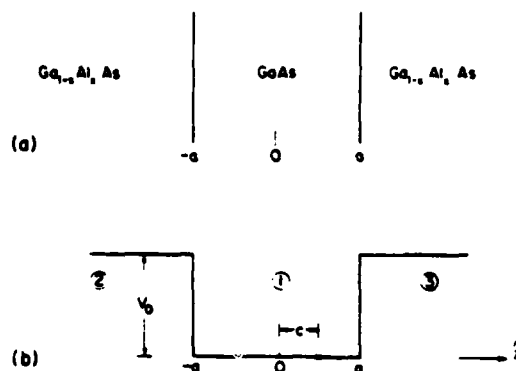


FIG. 1. Geometry of a Coulomb center located at a distance  $c$  from the center of a finite quantum well of width  $2a$  (along the  $\hat{z}$  direction) and height  $V_0$ . (a) Physical structure. (b) Quantum well potential profile along the  $\hat{z}$  axis normal to the interfaces.

$$\hat{H}(1) = \frac{-\hbar^2}{2m_1^*} \nabla^2 + V_1(\vec{r}) \quad (1a)$$

in region (1),

$$\hat{H}(2) = \frac{-\hbar^2}{2m_2^*} \nabla^2 + V_2(\vec{r}) + V_0 \quad (1b)$$

in region (2), and

$$\hat{H}(3) = \frac{-\hbar^2}{2m_2^*} \nabla^2 + V_3(\vec{r}) + V_0 \quad (1c)$$

in region (3), where  $m_1^*$  refers to the bulk GaAs (well material) effective mass and  $m_2^*$  refers to the interpolated effective mass in Ga<sub>1-x</sub>Al<sub>x</sub>As (barrier material). Since the bulk dielectric constants of GaAs and Ga<sub>1-x</sub>Al<sub>x</sub>As,  $\epsilon_1$  and  $\epsilon_2$ , respectively, differ slightly, the Hamiltonian must include terms due to electrostatic image charges.<sup>22,23</sup> The potentials  $V_1(\vec{r})$ ,  $V_2(\vec{r})$ , and  $V_3(\vec{r})$  represent the Coulomb interaction between the electron and the impurity ion as well as the ion image charge. When the origin is taken to be on the ionized donor, the left and right boundaries of the quantum well are, respectively,  $z_0 = -(a+c)$  and  $z_0 = (a-c)$ . We let the dielectric mismatch between GaAs and Ga<sub>1-x</sub>Al<sub>x</sub>As be expressed as

$$p \equiv \frac{(\epsilon_1 - \epsilon_2)}{(\epsilon_1 + \epsilon_2)}, \quad (2a)$$

$$p' \equiv \frac{2\epsilon_1}{(\epsilon_1 + \epsilon_2)}, \quad (2b)$$

and the positions of the ion image charges along the  $\hat{z}$  axis to be

$$z_0^+(n) = 2 \left\{ \left[ n - \left\lfloor \frac{n+1}{2} \right\rfloor \right] (a+c) + \left\lfloor \frac{n+1}{2} \right\rfloor (a-c) \right\}, \quad (3a)$$

$$z_0^-(n) = -2 \left\{ \left\lfloor \frac{n+1}{2} \right\rfloor (a+c) + \left[ n - \left\lfloor \frac{n+1}{2} \right\rfloor \right] (a-c) \right\}, \quad (3b)$$

where

$$[x] \equiv \text{int} x. \quad (3c)$$

Letting

$$\rho = (x^2 + y^2)^{1/2} \quad (4a)$$

and

$$r = (\rho^2 + z^2)^{1/2}, \quad (4b)$$

the potential energy in region (1) can be written as

$$V_1(\vec{r}) = \frac{-e^2}{4\pi\epsilon_1} \frac{1}{r} + v_1^+(\vec{r}) + v_1^-(\vec{r}), \quad (4c)$$

where

$$v_1^+(\vec{r}) = \frac{-e^2}{4\pi\epsilon_1} \sum_{n=1}^{\infty} p^n [\rho^2 + [z - z_0^+(n)]^2]^{-1/2}, \quad (4d)$$

$$v_1^-(\vec{r}) = \frac{-e^2}{4\pi\epsilon_1} \sum_{n=1}^{\infty} p^n [\rho^2 + [z - z_0^-(n)]^2]^{-1/2}, \quad (4e)$$

for the electron-ion potential.

In region (2), the potential energy can be expressed as

$$V_2(\vec{r}) = \frac{-e^2}{4\pi\epsilon_2} p' \sum_{n=0}^{\infty} p^n [\rho^2 + [z - z_0^+(n)]^2]^{-1/2}, \quad (4f)$$

for the electron-ion potential.

In region (3), the potential energy can be expressed as

$$V_3(\vec{r}) = \frac{-e^2}{4\pi\epsilon_2} p' \sum_{n=0}^{\infty} p^n [\rho^2 + [z - z_0^-(n)]^2]^{-1/2}, \quad (4g)$$

for the electron-ion potential.

A finite number of image charges were included in the expansion of Eqs. (4). Since the dielectric mismatch  $p$  is at most of the order of 5% for the  $x=0.4$  alloy, the contributions due to higher-order image charge terms are negligible. In the present calculation, we included only four image charge

terms.

The conduction-band offset  $V_0$  was taken to be 85% of the difference of the  $k=0$  band gaps of GaAs and Ga<sub>1-x</sub>Al<sub>x</sub>As.<sup>24</sup> Since the alloy composition range studied was such that the alloy was direct ( $x < 0.45$ ),<sup>24</sup> both the effective mass  $m_2^*$  and the conduction-band offset  $V_0$  were determined using the  $k=0$  values in Ga<sub>1-x</sub>Al<sub>x</sub>As (Ref. 24):

$$m_1^* = 0.067m_0, \quad (5a)$$

$$m_2^* = (0.067 + 0.083x)m_0, \quad (5b)$$

$$\epsilon_1 = 13.1\epsilon_0, \quad (5c)$$

$$\epsilon_2 = [13.1(1-x) + 10.1x]\epsilon_0, \quad (5d)$$

$$V_0 = 1.06x \text{ eV}, \quad (5e)$$

where  $m_0$  and  $\epsilon_0$  are the free electron mass and the vacuum static dielectric constant, respectively.

To calculate binding energies, we must solve for the Hamiltonian defined in Eqs. (1) without the impurity potentials  $V_1(\vec{r})$ ,  $V_2(\vec{r})$ , and  $V_3(\vec{r})$ . That is, we must find the ground state of an electron in the quantum well without the impurity potential. The Hamiltonian for the particle in this problem is given by

$$\hat{H}_0(1) = \frac{-\hbar^2}{2m_1^*} \nabla^2 \quad (6a)$$

in region (1),

$$\hat{H}_0(2) = \frac{-\hbar^2}{2m_2^*} \nabla^2 + V_0 \quad (6b)$$

in region (2), and

$$\hat{H}_0(3) = \frac{-\hbar^2}{2m_2^*} \nabla^2 + V_0 \quad (6c)$$

in region (3). The energies ( $E$ ) of the Coulomb states with respect to the first conduction-subband edge are given by the difference between the donor energy  $E(\hat{H})$  and the subband energy  $E(\hat{H}_0)$ :

$$E = E(\hat{H}) - E(\hat{H}_0). \quad (7)$$

Since the Hamiltonian without the Coulomb center,  $\hat{H}_0$ , is even with respect to reflection through the  $xy$  plane, eigenstates of  $\hat{H}_0$  must have definite parity. In particular, eigenstates of  $\hat{H}_0$  belonging to odd-number subbands ( $n=1,3,5,\dots$ ) must be even with respect to reflection through the  $xy$  plane. Eigenstates of  $\hat{H}_0$  belonging to even-number subbands ( $n=2,4,6,\dots$ ) must be odd with respect to reflection through the  $xy$  plane.

Calculations were carried out using a variational method. To preserve the cylindrical geometry of the system, the trial basis orbitals on which the donor-state envelope function is expanded are of

$$\langle \bar{r}' | nlm \rangle \equiv \phi_{nlm}(\bar{r}') = \sum_{i=1,2,3} N_i(n,l) [r(\lambda, d_i)]^i \exp\{-\zeta_i(n,l)[r(\lambda, d_i)]^2\} Y_l^m(\Omega'), \quad (8)$$

where  $r(\lambda, d_i) \equiv [x^2 + y^2 + \lambda^2(z - d_i)^2]^{1/2}$ , and  $N_i(n,l)$  is a normalization constant. The index  $i=1,2,3$  labels the region of space where the GTO orbital is defined. The boundary conditions that both the wave function and the particle current are continuous across the interface<sup>24</sup> determine relations between the normalization constants  $N_i(n,l)$  and the orbital exponents,  $\zeta_i(n,l)$ , in the barrier material ( $i=2,3$ ) in terms of those in the well material ( $i=1$ ). To produce an accurate description of the donor envelope wave function, a shape parameter, or eccentricity ( $\lambda$ ), as well as a shift parameter ( $d_i$ ), were incorporated in the variational basis set  $\{|nlm\rangle\}$ . The shape parameter  $\lambda$  determines the compression of the envelope function along the quantum well axis ( $\hat{z}$ ). The shift parameter  $d_i$  determines the location of the electron charge distribution when the impurity ion is moved towards the quantum well edge. In the calculation presented here we chose (1)  $d_i \equiv 0$  in the case of the on-center impurity and (2)  $d_0 \neq 0$  for  $l=0$  and  $d_i=0$  for  $l \neq 0$  in the case of the on-edge impurity. The GTO orbital exponents  $\zeta_i(n,l)$  appearing in Eq. (8) are fixed and taken to be of the form, in atomic rydberg units,<sup>25</sup>

$$\zeta_i(n,l) = \frac{\zeta_0}{b(n)(l+1)}, \quad (9)$$

with  $b(n) = \{1, 2, 4, 8, 16, 32, \frac{1}{2}\}$  and  $\zeta_0 = 8/(9\pi)$  bohr<sup>-2</sup>. The choice of  $\zeta_0$  is dictated by the fact that if one solves the hydrogen-atom Hamiltonian for the ground state with a trial Gaussian orbital of the form  $N \exp(-\zeta_0 r^2)$ , then one easily finds that the orbital exponent  $\zeta_0$  that minimizes the expectation value of the energy is  $\zeta_0 = 8/(9\pi)$  bohr<sup>-2</sup>. To make the particle current continuous, we impose continuity of the wave function and of the velocity operator across the quantum well boundary.<sup>26</sup> The boundary condition that  $(\nabla \phi_{nlm} \cdot \hat{z})/m^*$  must be continuous across the interface is required since the difference in effective masses was taken into account in the expression of the Hamiltonian. As shown by Ando and Mori,<sup>17</sup> there are adequate boundary conditions in the case

of GaAs-Ga<sub>1-x</sub>Al<sub>x</sub>As quantum well structures. The donor envelope function  $|\Psi\rangle$  is expanded on this set of trial orbitals:

$$|\Psi\rangle = \sum_{nlm} C(nlm) |nlm\rangle, \quad (10)$$

where the set of basis orbitals  $\{|nlm\rangle\}$  are the ellipsoidal GTO's defined above in Eq. (8).

The problem of solving the EMA Schrödinger equation for the donor envelope function

$$\hat{H}|\Psi\rangle = E(\hat{H})|\Psi\rangle \quad (11)$$

reduces to that of solving the generalized eigenvalue problem

$$\sum_{n'l'm'} \{ \langle nlm | \hat{H} | n'l'm' \rangle - E(\hat{H}) \langle nlm | n'l'm' \rangle \} C(n'l'm') = 0, \quad (12)$$

for the eigenenergy  $E(\hat{H})$  and the expansion coefficients  $C(nlm)$  appearing in the expansion equation (10).

Calculations were carried out using both  $s$ -like ( $l=0$ ) and  $p$ -like ( $l=1$ ) GTO's. In the case of the on-center impurity ( $c=0$ ), the Hamiltonian in Eqs. (1) mixes only orbitals whose angular momenta  $l$  differ by an even integer. For the on-center impurity, only  $s$ -like GTO's were included in the expansion equation (10). However, for the on-edge impurity ( $c=a$ ), the mixing between  $s$ - and  $p$ -like orbitals becomes appreciable and must be included to provide an accurate description of the neutral donor. For the on-edge impurity, seven  $s$ -like GTO's and seven  $p$ -like GTO's were included in the expansion equation (10). The calculation of the subband energy  $E(\hat{H}_0)$  was carried through using seven  $s$ -like GTO's. As mentioned above, eigenstates of  $\hat{H}_0$  belonging to the first conduction subband are even with respect to reflection through the  $xy$  plane and thus the donor envelope function can be fairly well described by  $s$ -like basis orbitals. For each value of GaAs slab thickness ( $2a$ ), impurity position ( $c$ ), and barrier height  $V_0$ , the shape parameter  $\lambda$  as well as the shift parameter  $d_i$  were

determined by minimizing the energy expectation value in the ground state,  $E_0(\lambda, d_1)$ .

This shifted ellipsoidal Gaussian set has the advantage of reproducing reasonably well the Coulomb center at both the small ( $a \rightarrow 0$ ) and the large ( $a \rightarrow \infty$ ) slab thickness limit where the binding energy reduces, in the case of the on-center donor, to that of the barrier material or the well material bulk values, respectively. At the same time, it retains the nonspherical character of the problem and allows the basis orbitals to reshape themselves in order to minimize the total energy. The inclusion of a shift parameter  $d_1$  in the variational basis set allows the electronic charge distribution associated with the donor ground-state envelope function to be shifted away from the position of the impurity ion. This degree of freedom appears to be most important in the case of the on-edge donor where the Coulomb potential tends to pull the charge distribution towards the ionized center whereas the repulsive barrier potential tends to push it away from the ionized center.

Figure 2 shows the eccentricity (shape parameter  $\lambda$ ) for the on-center donor state as a function of the GaAs slab thickness for different alloy compositions  $x$ . As shown in the figure, greater values of  $x$  (i.e., greater conduction-band offset) result in larger shape parameter and therefore tighter GTO's. Furthermore, the shape-parameter-versus-slab-thickness curve presents a maximum corresponding to a maximum confinement of the donor envelope function around the impurity atom. For both very large and very small slab thicknesses, the shape parameter  $\lambda$  reduces to unity as it should in order to describe the isotropic case corresponding to bulk GaAs or bulk Ga<sub>1-x</sub>Al<sub>x</sub>As, respectively.

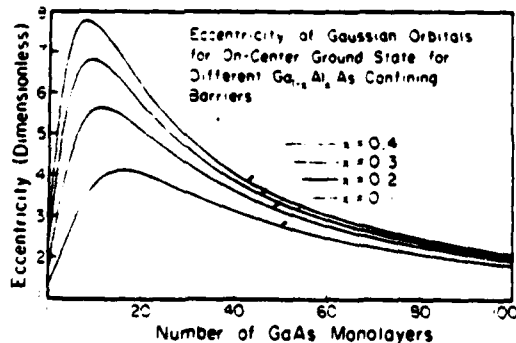


FIG. 2. Eccentricity (shape parameter)  $\lambda$  of ellipsoidal Gaussian type orbitals as a function of GaAs slab thickness for four alloy compositions,  $x = 0.1, 0.2, 0.3, 0.4$ , of Ga<sub>1-x</sub>Al<sub>x</sub>As.

### III. RESULTS

We first treat the results obtained for the on-center impurity case ( $c = 0$ ). Then we treat the on-edge impurity case ( $c = a$ ). Comparisons are made between these two limiting cases.

Figure 3 shows the on-center donor ground-state envelope function through the Coulomb center and normal to the interface plane for the different GaAs slab thicknesses and alloy compositions. Greater Al composition produces higher conduction-band offsets which, in turn, tend to localize the donor envelope function more effectively. As shown in Fig. 3, for very thin GaAs slab, the envelope function leaks appreciably into the barrier material (Ga<sub>1-x</sub>Al<sub>x</sub>As). In the limit of very thin GaAs slab thicknesses, one should recover the binding energy corresponding to bulk Ga<sub>1-x</sub>Al<sub>x</sub>As. Conversely, for large GaAs slab thicknesses, the on-center donor ground state is mostly confined within the quantum well and one

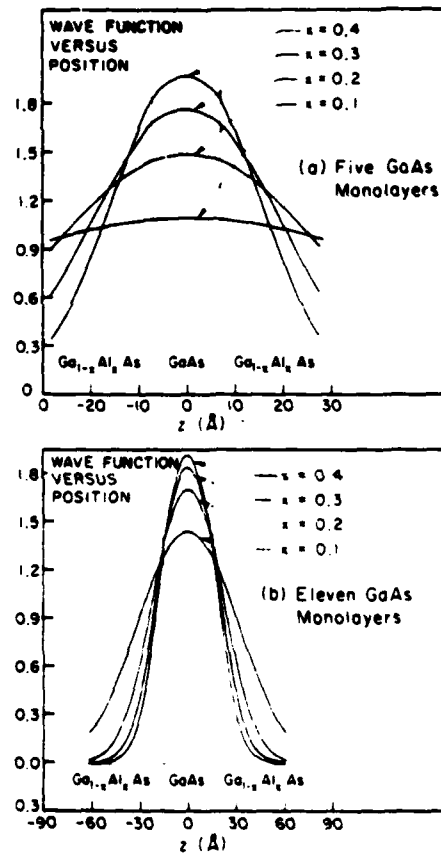


FIG. 3. On-center donor ground-state envelope function plotted along the axis normal to the interfaces for different GaAs slab thicknesses and four alloy compositions,  $x = 0.1, 0.2, 0.3, 0.4$ , of Ga<sub>1-x</sub>Al<sub>x</sub>As.

should recover the binding energy for bulk GaAs. As mentioned above, the EMA Hamiltonian for the on-center impurity mixes only orbitals whose angular momenta  $l$  differ by an even integer. As shown in Fig. 3, the total on-center impurity wave function does not acquire a  $p$ -like character.

Figure 4 shows the energy, with respect to the first conduction subband, for the on-center donor ground state as a function of GaAs slab thickness for four alloy compositions,  $x=0.1, 0.2, 0.3, 0.4$ . For the on-center impurity, the energy with respect to the first conduction subband versus GaAs slab thickness presents a maximum (in absolute value) whose magnitude depends on the alloy composition of the barrier material. Greater Al composition in the barrier material leads to larger conduction-band offsets and therefore more complete confinement of the donor envelope function. Since greater confinement of the donor state leads to a more sharply peaked wave function as the envelope function builds up amplitude around the impurity ion, the attractive Coulomb potential is more effective in binding the donor state when the Al content in the  $\text{Ga}_{1-x}\text{Al}_x\text{As}$  barrier is increased. For large GaAs

slab thicknesses, the effect of the alloy composition  $x$  or, equivalently, of the barrier height  $V_0$ , on the on-center donor ground-state energy and wave function is greatly reduced since the envelope function is strongly localized around the impurity ion in the center of the quantum well and does not feel much the repulsive barrier potential.

Figure 5 shows the energy, with respect to the first conduction subband, for the on-center low-lying excited states of even parity as a function of GaAs slab thickness for four alloy compositions,  $x=0.1, 0.2, 0.3, 0.4$ . The qualitative dependence of the GaAs slab thickness on the energy with respect to the first conduction subband of the even-parity excited states is similar, though not as important, to that of the ground state as can be seen by comparing Figs. 4 and 5. The envelope functions corresponding to these excited states are even with respect to reflection through the  $xy$  plane since these are made up from states derived from the first conduction subband.

Figure 6 shows the on-edge donor ground-state envelope function through the Coulomb center and normal to the interface plane. As mentioned

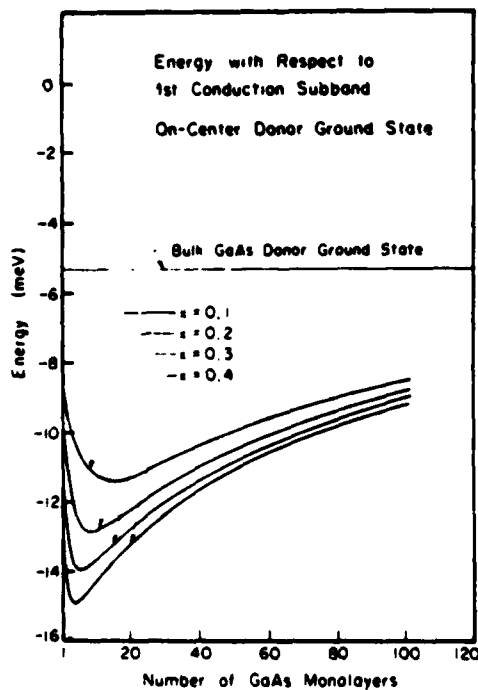


FIG. 4. Energy of the on-center donor ground state with respect to the first conduction subband as a function of GaAs slab thickness for four alloy compositions,  $x=0.1, 0.2, 0.3, 0.4$ , of  $\text{Ga}_{1-x}\text{Al}_x\text{As}$ . Calculations are carried through using seven  $s$ -like ellipsoidal Gaussian-type orbitals as defined in the text.

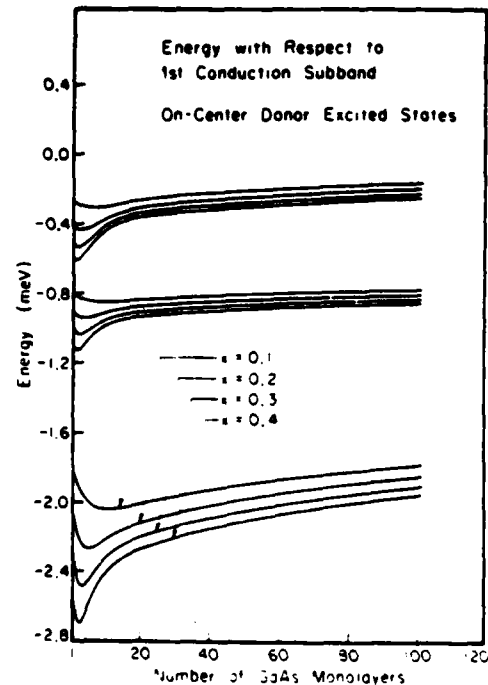


FIG. 5. Energy of the on-center low-lying excited states of even parity with respect to the first conduction subband as a function of GaAs slab thickness for four alloy compositions,  $x=0.1, 0.2, 0.3, 0.4$ , of  $\text{Ga}_{1-x}\text{Al}_x\text{As}$ . Calculations are carried through using seven  $s$ -like ellipsoidal Gaussian-type orbitals as defined in the text.

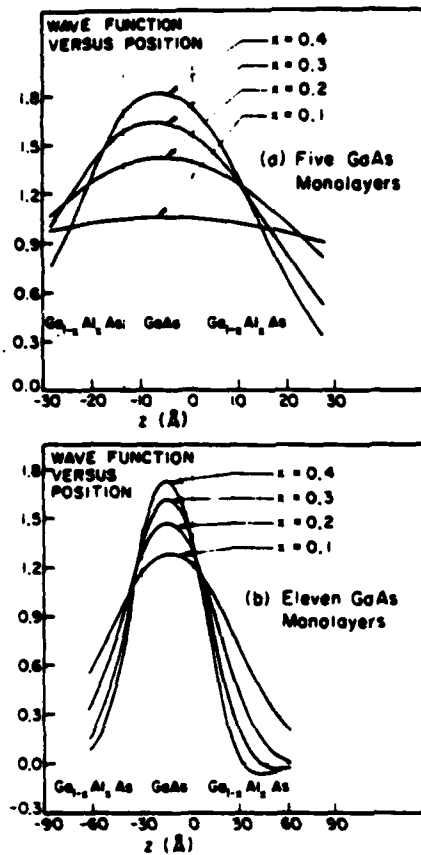


FIG. 6. On-edge donor ground-state envelope function plotted along the axis normal to the interfaces for different GaAs slab thicknesses and four alloy compositions,  $x = 0.1, 0.2, 0.3, 0.4$ , of Ga<sub>1-x</sub>Al<sub>x</sub>As.

above, although the on-center donor wave function is entirely  $s$ -like, the on-edge wave function develops a strong  $p$ -like character. The  $p$ -like character of the on-edge wave function increases as the height of the conduction-band offset  $V_0$  increases.

Figure 7 shows the energy, with respect to the first conduction subband, of the on-edge donor ground state as a function of the GaAs slab thickness for four alloy compositions,  $x = 0.1, 0.2, 0.3, 0.4$ . The on-edge donor energy curve presents qualitatively the same features as the on-center donor energy curve. In the thin GaAs slab limit, the energy curves for the on-center and the on-edge donor are very similar. In the thick GaAs slab limit, the on-edge donor is less tightly bound than the on-center donor. This is mainly due to the fact that, as the impurity ion approaches the quantum well edge, the donor ground-state envelope function should be constructed more and more from Bloch states derived from the Ga<sub>1-x</sub>Al<sub>x</sub>As conduction-

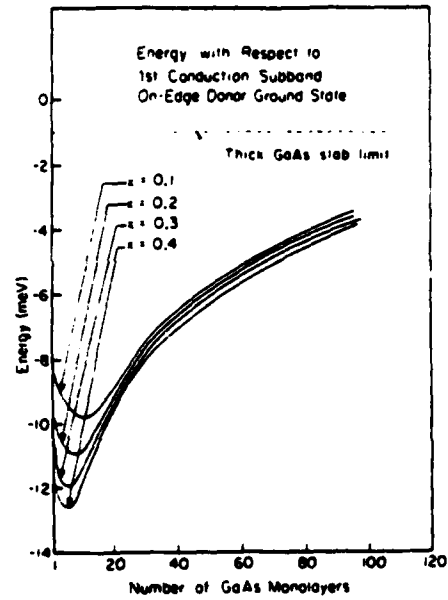


FIG. 7. Energy of the on-edge donor ground state with respect to the first conduction subband as a function of GaAs slab thickness for four alloy compositions,  $x = 0.1, 0.2, 0.3, 0.4$ , of Ga<sub>1-x</sub>Al<sub>x</sub>As. Calculations are carried through using seven  $s$ -like and seven  $p$ -like ellipsoidal Gaussian-type orbitals as defined in the text. The dashed line indicates that energy with respect to the first conduction subband in the large GaAs slab-thickness limit.

band edge. These states lie above the GaAs conduction-band edge by an energy equal to the conduction-band offset between GaAs and Ga<sub>1-x</sub>Al<sub>x</sub>As. As the on-edge donor ground-state envelope function includes more of these higher-energy states, the on-edge donor ground state becomes more shallow than the on-center donor ground state. Furthermore, in the case of the on-edge center, the repulsive barrier potential tends to push the electronic charge distribution away from the ionized donor, leading to a reduced Coulomb attraction. For the on-edge impurity, the results presented here using finite conduction-band offsets are qualitatively similar to the case where infinite conduction-band offsets are assumed,<sup>15</sup> thereby preventing the donor envelope function from leaking out of the quantum well. The dashed line in Fig. 7 indicates the binding energy in the limit of large GaAs slab. The boundary conditions on the wave function at the interface in the finite conduction-band offset case gives the donor envelope function a  $d$ -like character as the slope of the wave function is vanishingly small on the donor center. In the large slab limit, the  $p$ -like character of the

donor envelope function is less important for the finite conduction-band offset case and the donor ground state mostly consists of shifted *s*-like orbitals.

#### IV. SUMMARY AND CONCLUSION

We have calculated the energy spectrum of shallow donor states in GaAs-Ga<sub>1-x</sub>Al<sub>x</sub>As quantum well structures using the effective-mass approximation scheme. The variation in energy with respect to the first conduction subband of the donor ground state and the low-lying excited states was studied as a function of the central GaAs slab thickness, the position of the impurity atom within the GaAs slab and the alloy composition *x* of Ga<sub>1-x</sub>Al<sub>x</sub>As. Calculations were done for four alloy compositions of Ga<sub>1-x</sub>Al<sub>x</sub>As in a range in which the alloy remains direct (*x* < 0.45). Realistic values for conduction-band offsets of finite magnitude were used. The effect of the impurity position on the binding energy of the donor state was investigated in the two limit cases where the impurity ion was at the center of the quantum well (on-center impurity) and at the edge of the quantum well (on-edge impurity).

In the case of both the on-center and the on-edge impurities, the energy with respect to the first conduction subband versus slab thickness presents a maximum (in absolute value) corresponding to a maximum confinement of the donor-state envelope wave function. In the case of the on-edge impurity, the donor ground state is not as tightly bound

as the on-center ground state. The reduction in the binding for the on-edge impurity is a direct consequence of the repulsive interface potential which tends to push the electronic charge distribution away from the Coulomb center.

For both the on-center and the on-center impurity, it was found that the energy spectrum of the donor ground state and the low-lying excited states is considerably modified as the thickness of the GaAs slab containing the impurity was varied. This variation in binding energy should be easily observed experimentally since molecular-beam epitaxy techniques<sup>27</sup> now allow for the fabrication of superlattices consisting of alternating slabs of few monolayers of GaAs-Ga<sub>1-x</sub>Al<sub>x</sub>As. It seems possible to adjust the binding of a Coulomb center in a superlattice by varying the thickness of the slab containing the impurity center.

#### ACKNOWLEDGMENTS

This work was supported by the Army Research Office under Contract No. DAAG29-80-C-0103. One of us (C.M.) has been supported by the National Science and Engineering Research Council (NSERC) of Canada and by the Fonds F.C.A.C. pour l'aide et le soutien à la recherche of Québec. The authors are greatly indebted to G. Bastard and to F. Stern for pointing out the deficiencies of a previous calculation using a less adequate variational basis set than the one presented here. The authors also wish to acknowledge C.A. Swarts for many very helpful discussions.

\*Present address: Department of Physics, University of Illinois, Urbana, Illinois 61801.

<sup>1</sup>J. N. Schulman and T. C. McGill, Phys. Rev. Lett. **39**, 1680 (1977).

<sup>2</sup>R. N. Nucho and A. Madhukar, J. Vac. Sci. Technol. **15**, 1530 (1978).

<sup>3</sup>J. N. Schulman and T. C. McGill, Phys. Rev. B **19**, 6341 (1979).

<sup>4</sup>D. Mukherji and B. R. Nag, Phys. Rev. B **12**, 4338 (1975).

<sup>5</sup>G. A. Sai-Halasz, L. Esaki, and W. A. Harrison, Phys. Rev. B **18**, 2812 (1978).

<sup>6</sup>S. Satpathy and M. Alterelli, Phys. Rev. B **23**, 2977 (1981).

<sup>7</sup>R. Dingle, W. Wiegmann, and C. Henry, Phys. Rev. Lett. **33**, 827 (1974).

<sup>8</sup>R. Tsu, A. Koma, and L. Esaki, J. Appl. Phys. **46**, 842 (1975).

<sup>9</sup>Y. Guldner, J. P. Vieren, P. Voisin, M. Voos, L. L. Chang and L. Esaki, Phys. Rev. Lett. **45**, 1719 (1980).

<sup>10</sup>L. L. Chang, H. Sakaki, C. A. Chang, and L. Esaki, Phys. Rev. Lett. **38**, 1489 (1977).

<sup>11</sup>L. Esaki and R. Tsu, IBM J. Res. Develop. **14**, 61 (1970).

<sup>12</sup>R. Dingle, H. L. Strörmer, A. C. Gossard, and W. Wiegmann, Appl. Phys. Lett. **33**, 665 (1978).

<sup>13</sup>J. N. Schulman and T. C. McGill, Appl. Phys. Lett. **34**, 663 (1979).

<sup>14</sup>J. P. van der Ziel, R. Dingle, R. C. Miller, W. Wiegmann, and W. A. Nordland Jr., Appl. Phys. Lett. **26**, 463 (1975).

<sup>15</sup>G. Bastard, Surf. Sci. **113**, 165 (1982).

<sup>16</sup>G. E. Stilman, C. M. Larsen, C. M. Wolfe, and C. R. Brandt, Solid State Commun. **9**, 51 (1967).

<sup>17</sup>T. Ando and S. Mori, Surf. Sci. **113**, 124 (1982).

- <sup>18</sup>J. N. Schulman and Y. C. Chang, *Phys. Rev. B* **24**, 4445 (1981).
- <sup>19</sup>P. Voisin, G. Bastard, C. E. T. Gonçalves da Silva, M. Voos, L. L. Chang, and L. Esaki, *Solid State Commun.* **39**, 79 (1981).
- <sup>20</sup>R. C. Miller, D. A. Kleinman, W. T. Tsang, and A. C. Gossard, *Phys. Rev. B* **24**, 1134 (1981).
- <sup>21</sup>J. D. Levine, *Phys. Rev.* **140**, A586 (1965).
- <sup>22</sup>B. V. Pethukov, V. L. Pokrovskii, and A. V. Shaplik, *Fiz. Tverd. Tela (Leningrad)* **9**, 70 (1967) [*Soviet Phys.—Solid State* **9**, 51 (1967)].
- <sup>23</sup>N. O. Lipari, *J. Vac. Sci. Technol.* **15**, 1412 (1978).
- <sup>24</sup>H. C. Casey and M. B. Panish, *Heterostructure Lasers* (Academic, New York, 1978), Part A, Chap. 4.
- <sup>25</sup>Atomic units are defined here with respect to GaAs bulk values. Energy is measured in units of  $(m_1^* e^4)/(2\hbar^2 \epsilon_1^2)$  (donor rydberg) and distance is measured in units of  $(\hbar^2 \epsilon_1)/(m_1^* e^2)$  (donor bohr). The effective mass  $m_1^*$  and the static dielectric constant  $\epsilon_1$  both refer to GaAs bulk values.
- <sup>26</sup>W. A. Harrison, *Phys. Rev.* **123**, 85 (1961).
- <sup>27</sup>A. C. Gossard, P. M. Petroff, W. Wiegmann, R. Dingle, and A. Savage, *Appl. Phys. Lett.* **29**, 323 (1976).

# Energy spectra of donors in GaAs-Ga<sub>1-x</sub>Al<sub>x</sub>As quantum well structure: the effective mass approximation

C. Mailliot, Yia-Chung Chang,<sup>ab</sup> and T. C. McGill

*California Institute of Technology, Pasadena, California 91125*

(Received 27 January 1982; accepted 5 April 1982)

We present the results of a study of the energy spectrum of the ground state for shallow donors in quantum well structures, consisting of a single slab of GaAs sandwiched between two semi-infinite layers of Ga<sub>1-x</sub>Al<sub>x</sub>As. The effect of the position of the impurity atom within the central GaAs slab is investigated for different slab thicknesses and alloy compositions. Two limiting cases are presented: One in which the impurity atom is located at the center of the quantum well (on-center impurity), the other in which the impurity atom is located at the edge of the quantum well (on-edge impurity). Both the on-center and the on-edge donor ground state are bound for all values of GaAs slab thicknesses and alloy compositions. The alloy composition  $x$  is varied between 0.1 and 0.4. In this composition range, Ga<sub>1-x</sub>Al<sub>x</sub>As is direct and the single-valley effective mass theory is a valid technique for treating shallow donor states. Calculations are carried out in the case of finite potential barriers determined by realistic conduction band offsets.

PACS numbers: 73.40.Lq, 71.25.Jd, 71.55.Ht

## I. INTRODUCTION

The unique nature of electronic states associated with semiconductor superlattices has been the subject of a great deal of interest both from the theoretical<sup>1-6</sup> and experimental<sup>7-10</sup> viewpoints. In view of the potential applications of these structures,<sup>11-14</sup> the understanding of impurity states found within these systems is an issue of technical as well as scientific importance.

In this paper, we report on a study of the energy spectrum of shallow donor states in a single GaAs-Ga<sub>1-x</sub>Al<sub>x</sub>As quantum well, i.e., a structure formed by a central GaAs slab (well material) flanked by two semi-infinite Ga<sub>1-x</sub>Al<sub>x</sub>As layers (barrier material). The energy spectrum of a donor state located within the GaAs slab is studied as a function of the width of the rectangular potential well formed by the conduction band offset at the GaAs-Ga<sub>1-x</sub>Al<sub>x</sub>As interface. The effect of the alloy composition  $x$  in the barrier material, as well as the position of the donor atom within the well, are also investigated. Two positions of the donor were studied: (1) donor ion at the center of the quantum well (on-center impurity) and (2) donor ion on the edge of the quantum well boundary (on-edge impurity). We find that the donor energy spectrum, both for the on-center and the on-edge impurity, is considerably modified as the dimension of the quantum well is varied. Both the on-center and the on-edge donor energies, with respect to the first conduction subband versus GaAs slab thickness, present a maximum (in absolute value) whose magnitude depends on the alloy composition. The on-edge impurity, produces a more shallow donor ground state than the on-center impurity. This reduction of binding of the on-edge donor ground state results from the fact that the repulsive barrier potential tends to push the electronic charge distribution away from the attractive ionized center, thereby leading to a reduced effective Coulomb attraction. This finding is in accord with previous calculations carried in the case of infinite confining potential.<sup>15</sup>

In Sec. II, we present the calculation techniques. We discuss first the effective mass Hamiltonian used for treating the shallow states and its validity, then we describe the basis orbitals on which the donor state is expanded. In Sec. III, the main results are presented. First, we discuss the energy spectrum for the on-center impurity, then we treat the case of the on-edge impurity. A comparison is made between these two limiting cases. A summary of the results and a conclusion are presented in Sec. IV.

## II. CALCULATIONAL METHOD

Calculations are based on the effective mass approximation (EMA). The GaAs-Ga<sub>1-x</sub>Al<sub>x</sub>As system was chosen since the EMA is known to hold to a high degree of accuracy for shallow donor states in GaAs.<sup>16</sup> As shown by Ando and Mori,<sup>17</sup> the boundary conditions that the donor envelope function and the particle current are continuous across the interface are adequate in the case of GaAs-Ga<sub>1-x</sub>Al<sub>x</sub>As quantum well structures.

The composition of the Ga<sub>1-x</sub>Al<sub>x</sub>As alloy was varied in the range where the alloy remains direct, so that the single-valley effective mass theory still holds. Realistic conduction band offsets of finite magnitude were used, thereby allowing the wave function to penetrate into the barrier material as the dimensions of the confining quantum well are reduced. The use of finite conduction band offsets has a large effect on the binding energy of the donor state in the thin GaAs slab limit and should be compared with approximate calculations carried out using infinitely high barrier height (quantum box),<sup>18,19</sup> in which case the donor wave function is required to vanish at the interface. When finite conduction band offsets are taken into account, the condition that the wave function vanishes at the interface is relaxed and penetration in the barrier material is allowed. The infinite barrier case should be viewed as a limiting case valid only for very

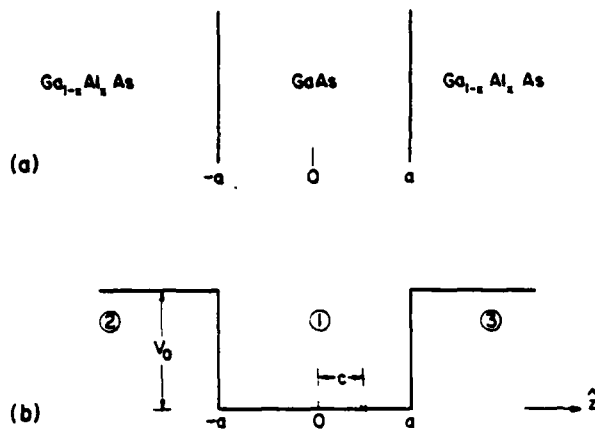


FIG. 1. Geometry of a Coulomb center located at a distance  $c$  from the center of a finite quantum well of width  $2a$  (along the  $z$  direction) and height  $V_0$ . (a) physical structure; (b) quantum well potential profile along the  $z$  axis normal to the interfaces.

wide quantum wells for which the penetration of the donor state into the barrier material is small.

The effective mass Hamiltonian corresponding to a Coulomb center located at a distance  $c$  from the center of a finite quantum well of width  $2a$  along the  $z$  direction (the  $z$  axis is normal to the interface plane) and height  $V_0$  (see Fig. 1 for geometry) is

$$\hat{H}(1) = \frac{-\hbar^2}{2m_1^*} \nabla^2 + V_1(r), \quad \text{in region (1)}, \quad (1a)$$

$$\hat{H}(2) = \frac{-\hbar^2}{2m_2^*} \nabla^2 + V_2(r) + V_0, \quad \text{in region (2)}, \quad (1b)$$

$$\hat{H}(3) = \frac{-\hbar^2}{2m_2^*} \nabla^2 + V_3(r) + V_0, \quad \text{in region (3)}, \quad (1c)$$

where  $m_1^*$  refers to the bulk GaAs (well material) effective mass and  $m_2^*$  refers to the interpolated effective mass in  $\text{Ga}_{1-x}\text{Al}_x\text{As}$  (barrier material). The origin of the coordinates is taken on the ionized donor. Since the bulk dielectric constants of GaAs and  $\text{Ga}_{1-x}\text{Al}_x\text{As}$ ,  $\epsilon_1$  and  $\epsilon_2$ , respectively, differ slightly, the Hamiltonian must include terms due to electrostatic image charges.<sup>20,21</sup> The potentials  $V_1(r)$ ,  $V_2(r)$ , and  $V_3(r)$  represent the Coulomb interaction between the electron and the impurity ion as well as the ion image charge. The expressions for the electron-ion potential [ $V_i(r)$ ] will be given elsewhere.<sup>22</sup>

The conduction band offset  $V_0$  was taken to be 85% of the difference of the  $k=0$  band gaps of GaAs and  $\text{Ga}_{1-x}\text{Al}_x\text{As}$ .<sup>23</sup> Since the alloy composition range studied was such that the alloy was direct ( $x < 0.45$ ),<sup>23</sup> both the effective mass  $m_2^*$  and the conduction band offset  $V_0$  were determined using the  $k=0$  values of  $\text{Ga}_{1-x}\text{Al}_x\text{As}$ <sup>23</sup>

$$m_1^* = 0.067 m_0, \quad (2a)$$

$$m_2^* = (0.067 + 0.083x)m_0, \quad (2b)$$

$$\epsilon_1 = 13.1\epsilon_0, \quad (2c)$$

$$\epsilon_2 = [13.1(1-x) + 10.1x]\epsilon_0, \quad (2d)$$

$$V_0 = 1.06x \text{ eV}, \quad (2e)$$

where  $m_0$  and  $\epsilon_0$  are the free electron mass and the vacuum static dielectric constant, respectively.

To calculate energies with respect to the first conduction subband, we must solve for the Hamiltonian in Eqs. (1) without the impurity potentials  $V_1(r)$ ,  $V_2(r)$ , and  $V_3(r)$ . Letting  $\hat{H}_0$  be the Hamiltonian without the impurity potential, the energies ( $E$ ) of the Coulomb states with respect to the first conduction subband edge are given by the difference between the donor energy  $E(\hat{H})$ , and the subband energy  $E(\hat{H}_0)$ :  $E = E(\hat{H}) - E(\hat{H}_0)$ .

Calculations were carried out using a variational method. To preserve the cylindrical geometry of the system, the trial basis orbitals on which the donor state envelope function is expanded is of the form of Gaussian-type orbitals (GTO's), defined in an ellipsoidal coordinate system and shifted with respect to the ionized donor taken to be at the origin

$$\langle r' | nlm \rangle = \phi_{nlm}(r') = \sum_{i=1,2,3} N_i(n,l) [r(\lambda, d_i)]^i \exp\{-\zeta_i(n,l)[r(\lambda, d_i)]^2\} Y_l^m(\Omega'), \quad (3)$$

where  $r(\lambda, d_i) = [x^2 + y^2 + \lambda^2(z - d_i)^2]^{1/2}$ , and  $N_i(n,l)$  is a normalization constant. The index  $i = 1, 2, 3$  labels the region of space where the GTO orbital is defined. The boundary conditions that both the wave function and the particle current are continuous across the interface<sup>24</sup> determine relations between the normalization constants  $N_i(n,l)$  and the orbital exponents  $\zeta_i(n,l)$  in the barrier material ( $i = 2, 3$ ) in terms of those in the well material ( $i = 1$ ). To produce an accurate description of the donor envelope wave function, a shape parameter ( $\lambda$ ), as well as a shift parameter ( $d_i$ ), were incorporated in the variational basis set  $\{|nlm\rangle\}$ . The shape parameter  $\lambda$  determines the compression of the envelope function along the quantum well axis ( $z$ ). The shift parameter  $d_i$  determines the location of the electron charge distribution when the impurity ion is moved towards the quantum well edge. In the calculation presented here, we chose: (1)  $d_i = 0$  in the case of the on-center impurity and (2)  $d_0 \neq 0$  for  $l = 0$  and  $d_i = 0$  for  $l \neq 0$  in the case of the on-edge impurity. The GTO orbital exponents  $\zeta_i(n,l)$  appearing in the Eq. (3) are fixed and taken to be of the form (in atomic Rydberg units<sup>25</sup>)  $\zeta_i(n,l) = \zeta_0/b(n)(l+1)$ , with  $b(n) = \{1, 2, 4, 8, 16, 32, 1/2\}$  and  $\zeta_0 = 8/(9\pi) \text{ bohr}^{-2}$ . The donor envelope function  $|\Psi\rangle$  is expanded on the set of basis orbitals  $\{|nlm\rangle\}$  defined in Eq. (3). We then solve the EMA Schrödinger equation for the donor envelope function

$$\hat{H}|\Psi\rangle = E(\hat{H})|\Psi\rangle, \quad (4)$$

for the eigenenergy  $E(\hat{H})$ .

Calculations were carried out using seven  $s$ -like ( $l = 0$ ) and seven  $p$ -like ( $l = 1$ ) GTO's. In the case of the on-center impurity ( $c = 0$ ), the Hamiltonian in Eqs. (1) mixes only orbitals whose angular momentum  $l$  differ by an even integer. For the on-center impurity, only  $s$ -like GTO's were included in the expansion of the donor wave function. However, for the on-edge impurity ( $c = a$ ), the mixing between  $s$ - and  $p$ -like orbitals becomes appreciable and must be included to provide an accurate description of the neutral donor. The calculation of the subband energy  $E(\hat{H}_0)$  was carried through using only  $s$ -like GTO's. For each value of GaAs slab thickness

(2a), impurity position ( $c$ ), and barrier height  $V_0$ , the shape parameter  $\lambda$ , as well as the shift parameter  $d$ , were determined by minimizing the energy expectation value in the ground state  $E_0(\lambda, d)$ .

This shifted ellipsoidal Gaussian set has the advantage of reproducing reasonably well the Coulomb center at both the small ( $a \rightarrow 0$ ) and the large ( $a \rightarrow \infty$ ) slab thickness limit where the binding energy reduces, in the case of the on-center donor, to that of the barrier material or the well material bulk values, respectively. At the same time, it retains the nonspherical character of the problem and allows the basis orbitals to reshape themselves in order to minimize the total energy. The inclusion of a shift parameter  $d$ , in the variational basis set allows the electronic charge distribution associated with the donor ground state envelope function to be shifted away from the position of the impurity ion. This degree of freedom appears to be most important in the case of the on-edge donor where the Coulomb potential tends to pull the charge distribution towards the ionized center, whereas the repulsive barrier potential tends to push it away from the ionized center.

### III. RESULTS

We first treat the results obtained for the on-center impurity case ( $c = 0$ ). Then we treat the on-edge impurity case ( $c = a$ ). Comparisons are made between these two limiting cases for the donor ground state.

Figure 2 shows the energy, with respect to the first conduction subband, for the on-center donor ground state as a function of GaAs slab thickness for four alloy compositions  $x = 0.1, 0.2, 0.3, 0.4$ . For the on-center impurity, the energy with respect to the first conduction subband versus GaAs slab thickness presents a maximum (in absolute value) whose magnitude depends on the alloy composition of the barrier material. Greater Al composition in the barrier material leads to larger conduction band offsets and therefore more complete confinement of the donor envelope function. Since greater confinement of the donor state leads to a more sharply peaked wave function as the envelope function builds up amplitude around the impurity ion, the attractive Coulomb potential is more effective in binding the donor state when the Al content in the  $\text{Ga}_{1-x}\text{Al}_x\text{As}$  barrier is increased. For large GaAs slab thicknesses, the effect of the alloy composition  $x$  or, equivalently, of the barrier height  $V_0$ , on the on-center donor ground state energy and wave function is greatly reduced since the envelope function is strongly localized around the impurity ion in the center of the quantum well and does not feel much the repulsive barrier potential.

Figure 3 shows the energy, with respect to the first conduction subband, of the on-edge donor ground state as a function of the GaAs slab thickness for four alloy compositions  $x = 0.1, 0.2, 0.3, 0.4$ . The on-edge donor energy curve presents qualitatively the same features as the on-center donor energy curve. In the thin GaAs slab limit, the energy curves for the on-center and the on-edge donor are very similar. In the thick GaAs slab limit, the on-edge donor is less tightly bound than the on-center donor. This is mainly due to the fact that, as the impurity ion approaches the quantum

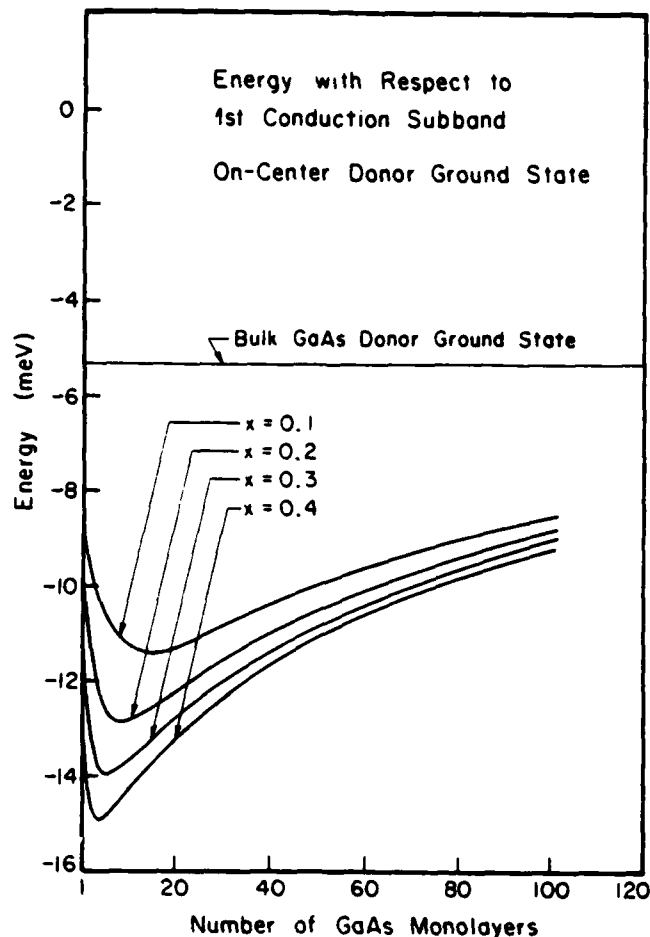


FIG. 2. Energy of the on-center donor ground state with respect to the first conduction subband as a function of GaAs slab thickness for four alloy compositions  $x = 0.1, 0.2, 0.3, 0.4$ , of  $\text{Ga}_{1-x}\text{Al}_x\text{As}$ . Calculations are carried through using seven  $s$ -like ellipsoidal Gaussian-type orbitals, as defined in the text.

well edge, the donor ground state envelope function should be constructed more and more from Bloch states derived from the  $\text{Ga}_{1-x}\text{Al}_x\text{As}$  conduction band edge. These states lie above the GaAs conduction band edge by an energy equal to the conduction band offset between GaAs and  $\text{Ga}_{1-x}\text{Al}_x\text{As}$ . As the on-edge donor ground state envelope function includes more of these higher energy states, the on-edge donor ground state becomes more shallow than the on-center donor ground state. Furthermore, in the case of the on-edge center, the repulsive barrier potential tends to push the electronic charge distribution away from the ionized donor, leading to a reduced Coulomb attraction. For the on-edge impurity, the results presented here using finite conduction band offsets are qualitatively similar to the case where infinite band offsets are assumed,<sup>15</sup> thereby preventing the donor envelope function from leaking out of the quantum well. The dashed line in Fig. 3 indicates the energy with respect to the first conduction subband in the limit of large GaAs slab. The boundary conditions on the wave function at the interface for the finite conduction band offset case gives the donor envelope function a  $d$ -like character as the slope of the wave function is vanishingly small on the donor center. In the large slab limit, the  $p$ -like character of the

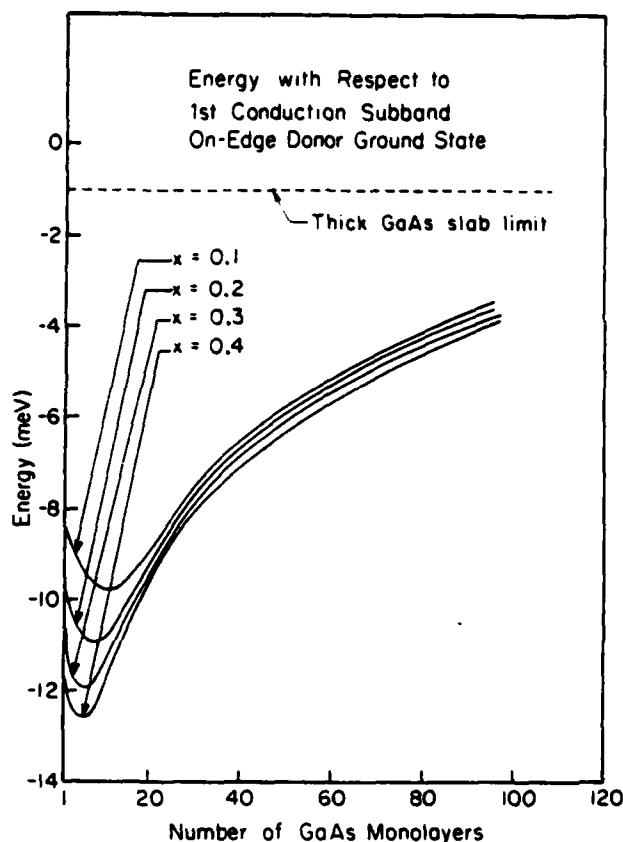


FIG. 3. Energy of the on-edge donor ground state with respect to the first conduction subband as a function of GaAs slab thickness for four alloy compositions  $x = 0.1, 0.2, 0.3, 0.4$ , of  $\text{Ga}_{1-x}\text{Al}_x\text{As}$ . Calculations are carried through using seven  $s$ -like and seven  $p$ -like ellipsoidal Gaussian-type orbitals, as defined in the text. The dashed line indicates the energy with respect to the first conduction subband in the large GaAs slab thickness limit.

donor envelope function is less important and the donor ground state mostly consists of shifted  $s$ -like orbitals.

#### IV. SUMMARY AND CONCLUSION

We have calculated the energy spectrum of shallow donor states in  $\text{GaAs-Ga}_{1-x}\text{Al}_x\text{As}$  quantum well structures using the effective mass approximation scheme. The variation in energy with respect to the first conduction subband of the donor ground state was studied as a function of the central GaAs slab thickness, the position of the impurity atom within the GaAs slab and the alloy composition  $x$  of  $\text{Ga}_{1-x}\text{Al}_x\text{As}$ . Calculations were done for four alloy compositions of  $\text{Ga}_{1-x}\text{Al}_x\text{As}$  in a range in which the alloy remains direct ( $x < 0.45$ ). Realistic values for conduction band offsets of finite magnitude were used. The effect of the impurity position on the binding energy of the donor state was investigated in the two limit cases where the impurity ion was at the center of the quantum well (on-center impurity) and at the edge of the quantum well (on-edge impurity).

In the case of both the on-center and the on-edge impurities, the energy with respect to the first conduction subband versus slab thickness presents a maximum (in absolute value) corresponding to a maximum confinement of the donor state envelope wave function. In the case of the on-edge impurity,

the donor ground state is not as tightly bound as the on-center ground state. The reduction in the binding for the on-edge impurity is a direct consequence of the repulsive interface potential which tends to push the electronic charge distribution away from the Coulomb center.

For both the on-center and the on-edge impurity, it was found that the energy spectrum of the donor ground state is considerably modified as the thickness of the GaAs slab containing the impurity was varied. This variation in binding energy should be easily observed experimentally, since molecular-beam epitaxy (MBE) techniques<sup>26</sup> now allow for the fabrication of superlattices consisting of alternating slabs of few monolayers of  $\text{GaAs-Ga}_{1-x}\text{Al}_x\text{As}$ . It seems possible to adjust the binding of a Coulomb center in a superlattice by varying the thickness of the slab containing the impurity center.

#### ACKNOWLEDGMENTS

This work was supported by the Army Research Office under Contract No. DAAG29-80-C-0103. One of us (CM) has been supported by the NSERC of Canada and by the Fonds F.C.A.C. pour l'aide et le soutien à la recherche of Québec. The authors are greatly indebted to G. Bastard and to F. Stern for pointing out the deficiencies of a previous calculation using a less adequate variational basis set than the one presented here. The authors also wish to acknowledge C. A. Swarts for many very helpful discussions.

<sup>24</sup> Present address: Department of Physics, University of Illinois, Urbana, Illinois 61801.

<sup>1</sup>J. N. Schulman and T. C. McGill, *Phys. Rev. Lett.* **39**, 1680 (1977).

<sup>2</sup>R. N. Nuchto and A. Madhukar, *J. Vac. Sci. Technol.* **15**, 1530 (1978).

<sup>3</sup>J. N. Schulman and T. C. McGill, *Phys. Rev. B* **19**, 6341 (1979).

<sup>4</sup>D. Mukherji and B. R. Nag, *Phys. Rev. B* **12**, 4338 (1975).

<sup>5</sup>G. A. Sai-Halasz, L. Esaki, and W. A. Harrison, *Phys. Rev. B* **18**, 2812 (1978).

<sup>6</sup>S. Satpathy and M. Altarelli, *Phys. Rev. B* **23**, 2977 (1981).

<sup>7</sup>R. Dingle, W. Wiegmann, and C. Henry, *Phys. Rev. Lett.* **33**, 827 (1974).

<sup>8</sup>R. Tsu, A. Koma, and L. Esaki, *J. Appl. Phys.* **46**, 842 (1975).

<sup>9</sup>Y. Guldner, J. P. Vieren, P. Voisin, M. Voos, L. L. Chang, and L. Esaki, *Phys. Rev. Lett.* **45**, 1719 (1980).

<sup>10</sup>L. L. Chang, H. Sakaki, C. A. Chang, and L. Esaki, *Phys. Rev. Lett.* **38**, 1489 (1977).

<sup>11</sup>L. Esaki and R. Tsu, *IBM J. Res. Develop.* **14**, 61 (1970).

<sup>12</sup>R. Dingle, H. L. Störmer, A. C. Gossard, and W. Wiegmann, *Appl. Phys. Lett.* **33**, 665 (1978).

<sup>13</sup>J. N. Schulman and T. C. McGill, *Appl. Phys. Lett.* **34**, 663 (1979).

<sup>14</sup>J. P. van der Ziel, R. Dingle, R. C. Miller, W. Wiegmann, and W. A. Nordland, Jr., *Appl. Phys. Lett.* **26**, 463 (1975).

<sup>15</sup>G. Bastard, *Proceedings of the Fourth International Conference on Electronic Properties of Two-Dimensional Systems*, August 24–28 1981, New Hampshire, Surf. Sci. **113**, 165 (1982).

<sup>16</sup>G. E. Stilman, C. M. Larsen, C. M. Wolfe, and C. R. Brandt, *Solid State Commun.* **9**, 51 (1967).

<sup>17</sup>T. Ando and S. Mori, *Proceedings of the Fourth International Conference on Electronic Properties of Two-Dimensional Systems*, August 24–28 1981, New Hampshire, Surf. Sci. **113**, 124 (1982).

<sup>18</sup>P. Voisin, G. Bastard, C. E. T. Gonçalves da Silva, M. Voos, L. L. Chang, and L. Esaki, *Solid State Commun.* **39**, 79 (1981).

<sup>19</sup>R. C. Miller, D. A. Kleinman, W. T. Tsang, and A. C. Gossard, *Phys. Rev. B* **24**, 1134 (1981).

<sup>20</sup>B. V. Pethukov, V. L. Pokrovskii, and A. V. Shaplik, *Sov. Phys. Solid*

State 9, 51 (1967).

<sup>21</sup>N. O. Lipari, *J. Vac. Sci. Technol.* **15**, 1412 (1978).

<sup>22</sup>C. Mailhot, Y. C. Chang, and T. C. McGill (to be published).

<sup>23</sup>H. C. Casey and M. B. Panish, *Heterostructure Lasers* (Academic, New York, 1978), Part A, Chap. 4.

<sup>24</sup>W. A. Harrison, *Phys. Rev.* **123**, 85 (1961).

<sup>25</sup>Atomic units are defined here with respect to GaAs bulk values. Energy is measured in units of  $(m_0^* e^4) / (2 \hbar^2 \epsilon_1^2)$  (donor Rydberg) and distance is measured in units of  $(\hbar^2 \epsilon_1) / (m_0^* e^2)$  (donor bohr). The effective mass  $m_0^*$  and the static dielectric constant  $\epsilon_1$  both refer to GaAs bulk values.

<sup>26</sup>A. C. Gossard, P. M. Petroff, W. Wiegmann, R. Dingle, and A. Savage, *Appl. Phys. Lett.* **29**, 323 (1976).

# Tunneling and propagating transport in GaAs-Ga<sub>1-x</sub>Al<sub>x</sub>As-GaAs double heterojunctions<sup>a)</sup>

C. Mailhot and T. C. McGill

California Institute of Technology, Pasadena, California 91125

J. N. Schulman<sup>b)</sup>

Department of Physics and Astronomy, University of Hawaii, Honolulu, Hawaii 96822

(Received 8 February 1983; accepted 21 February 1983)

We present a study of the transport characteristics of electrons through abrupt GaAs-Ga<sub>1-x</sub>Al<sub>x</sub>As-GaAs(100) double heterojunctions. The theoretical apparatus uses complex-k-band structures in the tight-binding approximation and transfer matrices. States on each side of the Ga<sub>1-x</sub>Al<sub>x</sub>As central barrier are expanded in terms of a complex-k-bulk state basis so as to provide a description of the wave function at the GaAs-Ga<sub>1-x</sub>Al<sub>x</sub>As(100) interface. We treat the case where the incoming state in GaAs is derived from near the conduction band  $\Gamma$  point. Transmission through the Ga<sub>1-x</sub>Al<sub>x</sub>As barrier is either tunneling or propagating depending on the nature of the Bloch states available for strong coupling in the alloy. States derived from the same extremum of the conduction band appear to couple strongly to each other across the GaAs-Ga<sub>1-x</sub>Al<sub>x</sub>As interface. Transport characteristics of incoming states derived from near the conduction band  $\Gamma$  point are examined as a function of the energy of the incoming state, thickness of the Ga<sub>1-x</sub>Al<sub>x</sub>As barrier, and alloy composition  $x$ . Transmission through the Ga<sub>1-x</sub>Al<sub>x</sub>As barrier is either tunneling or propagating, depending on the nature of the Bloch states available for strong coupling in the alloy.

PACS numbers: 73.40.Gk, 73.40.Lq

## I. INTRODUCTION

The introduction of new device fabrication technologies has allowed the realization of planar electronic devices in which the dimension perpendicular to the growth plane is of the order of a few lattice spacings. The understanding of electron states at semiconductor interfaces is of great importance regarding the performance of these very small-scale electronic devices. The work presented here is concerned with the transport of electrons through a GaAs-Ga<sub>1-x</sub>Al<sub>x</sub>As-GaAs(100) double heterojunction structure (DHS).

The mode of transport in these structures is either *tunneling* (energy less than the potential barrier height) or *propagating* (energy greater than the potential barrier height). In the former, the Bloch states available for transmission in the Ga<sub>1-x</sub>Al<sub>x</sub>As are *evanescent* and the wave vector  $k$  is complex. In the latter, the Bloch states available for transmission in the alloy are *propagating* and the wave vector  $k$  takes on real values.

The theoretical framework exploits the bulk properties of the constituent semiconductors forming the DHS. The transport of electrons through a region of space in which the energy of the electron is such that free propagation is not allowed is best described in terms of the complex-k-bulk band structure. The breakdown of translational invariance induced by the interface implies a new set of boundary conditions that do not exclude the component of the wave vector  $k$  normal to the interface to take on complex values. The bulk Bloch states associated with complex  $k$  provide then a suitable basis for a full description of the wave function. The problem of calculating the transport coefficients of Bloch

states at an abrupt interface using complex-k-band structure, cast in a tight-binding band calculation scheme, has been addressed in the past.<sup>1-4</sup> It is only recently that an expedient method, applicable to tight-binding, pseudopotential, and  $k \cdot p$  band calculation formalisms, has been devised to reduce the problem of calculating the complex-k-band structure to that of an associated eigenvalue problem.<sup>5,6</sup>

The paper is organized as follows: In Sec. II, the basic ingredients of the technique used to calculate the transport coefficients are presented. The major results are discussed in Sec. III. A summary and conclusions are given in Sec. IV.

## II. CALCULATIONAL METHOD

The system studied consists of a barrier of Ga<sub>1-x</sub>Al<sub>x</sub>As located between two semi-infinite layers of GaAs. Figure 1 illustrates the system studied. An electron incoming from bulk region I (GaAs) at an energy  $E$ , above the GaAs conduction band minimum, is scattered at the boundaries of the barrier region II (Ga<sub>1-x</sub>Al<sub>x</sub>As) and is finally transmitted in another bulk region III (GaAs). The  $\Gamma$ -point conduction band potential barrier at the interface,  $\Delta E_{\Gamma}$ , is taken to be a fraction of the difference in the  $\Gamma$ -point band gaps between GaAs and Ga<sub>1-x</sub>Al<sub>x</sub>As. Depending on whether we describe the total wave function in a bulk region or a barrier region, different representations are used accordingly. We now discuss these two representations.

Systems which exhibit two-dimensional periodicity are best described in a planar orbital representation.<sup>7-10</sup> A planar orbital is a two-dimensional Bloch sum consisting of localized atomic functions. Let  $\hat{z}$  be the direction normal to the interface and  $k_{\parallel} = \hat{z}k_x + \hat{y}k_y$  be the two-dimensional

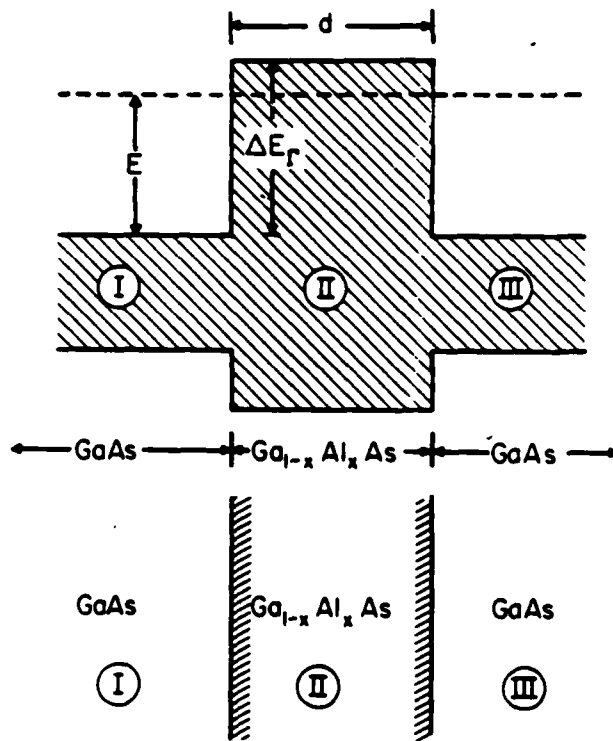


FIG. 1. Energy band diagram of GaAs-Ga<sub>1-x</sub>Al<sub>x</sub>As-GaAs DHS and corresponding physical structure. The electron is derived from the GaAs  $\Gamma$  point and has a total energy  $E$  measured with respect to the GaAs  $\Gamma$ -point conduction band minimum. The  $\Gamma$ -point conduction band offset is indicated by  $\Delta E_{\Gamma}$ . The thickness of the Ga<sub>1-x</sub>Al<sub>x</sub>As barrier is  $d$ .

wave vector parallel to the interface. Let  $\phi_{\alpha}(\mathbf{k}_{\parallel}; \sigma)$  designate the planar orbital corresponding to a given atomic orbital type  $\alpha$  within the layer  $\sigma$ . The Bloch states  $\psi(\mathbf{k}_{\parallel}, k_{\perp})$ , labeled by the wave vector  $\mathbf{k} = \mathbf{k}_{\parallel} + \hat{z}k_{\perp}$ , are expanded in terms of this set of planar orbitals  $\{\phi_{\alpha}(\mathbf{k}_{\parallel}; \sigma)\}$ . For interface systems,  $k_{\perp}$  is complex in general.

Where the total Hamiltonian is bulklike, the wave function is expanded in a set of bulk Bloch states  $\{\psi(\mathbf{k}_{\parallel}, k_{\perp})\}$ . On each side of an interface connecting two bulklike regions, the wave function is described in a planar orbital representation  $\{\phi_{\alpha}(\mathbf{k}_{\parallel}; \sigma)\}$ , and transferred across the interface using a transfer matrix. The connection between the bulk Bloch states representation  $\{\psi(\mathbf{k}_{\parallel}, k_{\perp})\}$  and the planar orbital representation,  $\{\phi_{\alpha}(\mathbf{k}_{\parallel}; \sigma)\}$  is described in Ref. 6 and will not be repeated here.

The total number  $N$  of Bloch states  $\psi(\mathbf{k}_{\parallel}, k_{\perp})$  with  $k_{\perp} = k_{\lambda}$  ( $\lambda = 1, \dots, N$ ) corresponding to a given parallel wave vector  $\mathbf{k}_{\parallel}$  and energy  $E$  depends on the particular tight-binding model used and on the orientation of the interface plane. More specifically, the total number of Bloch states  $\psi(\mathbf{k}_{\parallel}, k_{\perp})$  with real or complex wave vector  $k_{\perp}$  is equal to the product of the number of atomic orbitals per atom times the number of layers interacting with a given layer.<sup>1</sup> In the tight-binding representation used here, we have five orbitals per atom ( $s^{\uparrow}, s, p_x, p_y, p_z$ )<sup>11</sup> and only first nearest-neighbor interactions were included. There are, therefore, ten Bloch states ( $N = 10$ ) for each parallel wave vector  $\mathbf{k}_{\parallel}$  and total energy  $E$ . Half of the states have to be discarded because they either

grow away from the interface, if  $\text{Im}(k_{\perp})$  does not have the proper sign, or are propagating in the wrong direction when  $k_{\perp}$  is real.

Let the incoming Bloch state  $\psi(\mathbf{k}_{\parallel}, k_0)$  with real wave vector  $k_0$  be incident from the left in GaAs onto the GaAs-Ga<sub>1-x</sub>Al<sub>x</sub>As interface. The total wave function on a given layer  $\sigma$  can be written as<sup>1</sup>

$$\Psi(\mathbf{k}_{\parallel}, E; \sigma) = \psi(\mathbf{k}_{\parallel}, k_0; \sigma)$$

$$+ \sum_{k_{\perp}} A_{k_{\perp}}^{(I)}(\mathbf{k}_{\parallel}, E) \psi(\mathbf{k}_{\parallel}, k_{\perp}; \sigma), \text{ in region I,} \quad (1a)$$

$$\Psi(\mathbf{k}_{\parallel}, E; \sigma) = \sum_{\alpha} B_{\alpha}^{(II)}(\mathbf{k}_{\parallel}, E, \sigma) \phi_{\alpha}(\mathbf{k}_{\parallel}; \sigma), \text{ in region II,} \quad (1b)$$

$$\Psi(\mathbf{k}_{\parallel}, E; \sigma) = \sum_{k_{\perp}} A_{k_{\perp}}^{(III)}(\mathbf{k}_{\parallel}, E) \psi(\mathbf{k}_{\parallel}, k_{\perp}; \sigma), \text{ in region III.} \quad (1c)$$

At fixed energy  $E$  and parallel wave vector  $\mathbf{k}_{\parallel}$ , we denote by  $R_{\lambda}(\mathbf{k}_{\parallel}, E)$  and  $T_{\lambda}(\mathbf{k}_{\parallel}, E)$  the  $k_{\perp}$ -resolved reflection and transmission coefficients corresponding to the Bloch state  $\psi(\mathbf{k}_{\parallel}, k_{\lambda})$ . The total transport coefficients  $R(\mathbf{k}_{\parallel}, E)$  and  $T(\mathbf{k}_{\parallel}, E)$  are just the sum of the transport coefficients  $R_{\lambda}(\mathbf{k}_{\parallel}, E)$  and  $T_{\lambda}(\mathbf{k}_{\parallel}, E)$ . Flux conservation requires  $R(\mathbf{k}_{\parallel}, E) + T(\mathbf{k}_{\parallel}, E) = 1$ .

As shown in Ref. 1, the transmission coefficient for the Bloch state  $\psi(\mathbf{k}_{\parallel}, k_{\lambda})$  vanishes when the wave vector of the incoming Bloch state  $k_0$  approaches a critical point such that  $[\partial E(\mathbf{k})/\partial k_{\perp}]_{k_{\perp}=k_0} = 0$ . In that case, the incoming state is identical with the reflected state. At this critical point, the incoming state  $\psi(\mathbf{k}_{\parallel}, k_0)$  carries no momentum across the interface and does not couple to any Bloch states in Ga<sub>1-x</sub>Al<sub>x</sub>As. Therefore, transmission starts to occur as the incident wave vector  $k_0$  moves away from the critical point.

The transport states originate in the complex-k-band structure of GaAs and Ga<sub>1-x</sub>Al<sub>x</sub>As. The complex-k-band structure for GaAs and AlAs is well known.<sup>1,12</sup> We have used similar techniques to obtain the complex-k-band structure for Ga<sub>1-x</sub>Al<sub>x</sub>As within the virtual crystal approximation. Within the ten-band tight-binding description used here, the GaAs  $\Gamma$ -point conduction band minimum is at an energy  $E_{\Gamma}^{\text{GaAs}} \approx 1.51$  eV above the GaAs  $\Gamma$ -point valence band maximum, and the GaAs  $X$ -point conduction band valley is at an energy  $E_X^{\text{GaAs}} \approx 0.52$  eV above the GaAs  $\Gamma$ -point conduction band minimum.

We denote the bulk states with  $k_{\perp} = k_{\lambda}$  in spatial region  $\mu$  by  $\psi(\mathbf{k}_{\parallel}, k_{\lambda}^{\mu})$ . In the discussion that follows, the incident Bloch state is derived from near the GaAs conduction band  $\Gamma$  point with real wave vector  $k_0 = k_{\Gamma}^I$ , e.g.,  $\psi(\mathbf{k}_{\parallel}, k_0) = \psi(\mathbf{k}_{\parallel}, k_{\Gamma}^I)$ . The  $k_{\perp}$  values of interest are those near the conduction band extrema  $\Gamma(\cdot)_{\Gamma}$  and  $X(k_X)$ . In the energy range between the bottom of the GaAs conduction band and the GaAs  $X$ -point valley,  $k_{\Gamma}^I$  is real and  $k_X^I$  is complex such that  $\psi(\mathbf{k}_{\parallel}, k_{\Gamma}^I)$  has a traveling character and  $\psi(\mathbf{k}_{\parallel}, k_X^I)$  has an evanescent character. However, in the energy range above the  $X$ -point valley, both  $k_{\Gamma}^I$  and  $k_X^I$  are real such that  $\psi(\mathbf{k}_{\parallel}, k_{\Gamma}^I)$  and  $\psi(\mathbf{k}_{\parallel}, k_X^I)$  have traveling character. Similar considerations apply to the Bloch states available for transport in the alloy Ga<sub>1-x</sub>Al<sub>x</sub>As.

For an alloy composition  $x < 0.45$ ,<sup>13</sup> Ga<sub>1-x</sub>Al<sub>x</sub>As is di-

rect and  $E_{\Gamma}^{\text{Ga}_{1-x}\text{Al}_x\text{As}} < E_x^{\text{Ga}_{1-x}\text{Al}_x\text{As}}$  in this composition range. Throughout the calculations, the conduction band offset  $\Delta E_{\Gamma}$  was taken to be equal to 85% of the difference of  $\Gamma$ -point band gaps between GaAs and  $\text{Ga}_{1-x}\text{Al}_x\text{As}$ .<sup>13,14</sup> The dependence on the alloy composition  $x$  of the  $\Gamma$ -point energy edge in  $\text{Ga}_{1-x}\text{Al}_x\text{As}$  is, in the virtual crystal approximation:  $E_{\Gamma}^{\text{Ga}_{1-x}\text{Al}_x\text{As}} \approx 1.35x$  eV, above the GaAs  $\Gamma$ -point conduction band minimum.

### III. RESULTS

We present the main results for the transmission coefficients of electrons through a  $\text{GaAs-Ga}_{1-x}\text{Al}_x\text{As-GaAs}$  DHS. The incident Bloch state is derived from near the GaAs conduction band  $\Gamma$  point with real wave vector  $k_0 \equiv k_{\Gamma}^i$ , e.g.,  $\psi(k_{\parallel}, k_0) \equiv \psi(k_{\parallel}, k_{\Gamma}^i)$ . We discuss the transport across the central  $\text{Ga}_{1-x}\text{Al}_x\text{As}$  barrier as a function of the energy  $E$ , of the incoming Bloch state  $\psi(k_{\parallel}, k_0)$ , thickness of the barrier and alloy composition  $x$  in the central  $\text{Ga}_{1-x}\text{Al}_x\text{As}$  barrier.

#### A. Qualitative features of transport

Figure 2 shows the total transmission and reflection coefficients  $T(k_{\parallel}, E)$  and  $R(k_{\parallel}, E)$  as a function of the energy  $E$  of the incoming Bloch state. Energy is measured with respect

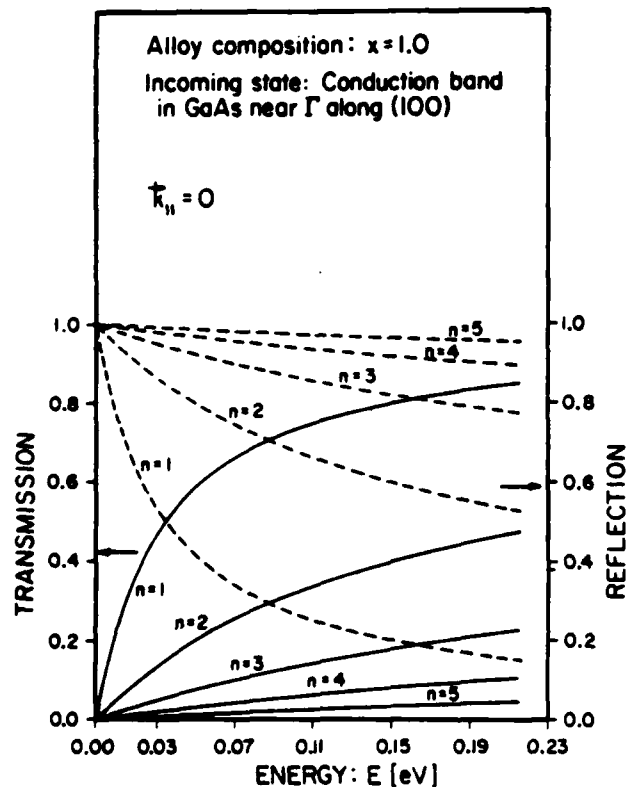


FIG. 2. Total transmission (solid line) and reflection (dashed line) coefficients  $T(k_{\parallel}, E)$  and  $R(k_{\parallel}, E)$  as a function of the energy  $E$  of the incident Bloch state  $\psi(k_{\parallel}, k_{\Gamma}^i)$  for different  $\text{Ga}_{1-x}\text{Al}_x\text{As}$  barrier thicknesses with an alloy composition of  $x = 1.0$ . Energy is measured with respect to the GaAs conduction band minimum and  $k_{\parallel} = 0$ . The number of  $\text{Ga}_{1-x}\text{Al}_x\text{As}$  barrier layers is  $n$ . Incoming state: Conduction band in GaAs near  $\Gamma$  along (100).

to the GaAs conduction band minimum. We consider the case of vanishing parallel wave vector  $k_{\parallel} = 0$  and composition of  $x = 1.0$ . Calculations were carried out for different AlAs barrier thicknesses.

For energies of the incoming states near the GaAs conduction band  $\Gamma$  point, transmission through the AlAs barrier occurs mostly via the coupling to evanescent states that connect to the AlAs conduction band at the  $\Gamma$  point. In the energy range considered, no propagating Bloch states are available in AlAs and the wave function has an evanescent character in the barrier. The AlAs  $\Gamma$ -point minimum is at an energy  $E_{\Gamma}^{\text{AlAs}} = 1.35$  eV above the GaAs conduction band minimum. As mentioned in Sec. II, the transmission coefficient vanishes for incoming states derived from near the conduction band  $\Gamma$  point at an energy equal to  $E_{\Gamma}^{\text{GaAs}}$ . At this energy, the component of the group velocity normal to the interface vanishes  $[\partial E(k)/\partial k_x]_{k_x=k_{\Gamma}^i} = 0$ , and the incoming state  $\psi(k_{\parallel}, k_{\Gamma}^i)$  does not couple to any states in AlAs.

We now examine the different transport regimes. Figure 3 shows the total transmission coefficient  $T(k_{\parallel}, E)$  as a function of the number of monolayers forming the central  $\text{Ga}_{1-x}\text{Al}_x\text{As}$  barrier. Layers are measured in units of  $a/2$ , where  $a$  is the GaAs lattice constant. Energies of the incoming Bloch state  $\psi(k_{\parallel}, k_{\Gamma}^i)$  range from  $0.19 \text{ eV} < E < 0.69 \text{ eV}$ , measured with respect to the GaAs conduction band minimum. The alloy composition is  $x = 0.3$  and  $k_{\parallel} = 0$ . The alloy is direct and the  $\Gamma$ -point energy edge of  $\text{Ga}_{1-x}\text{Al}_x\text{As}$  is

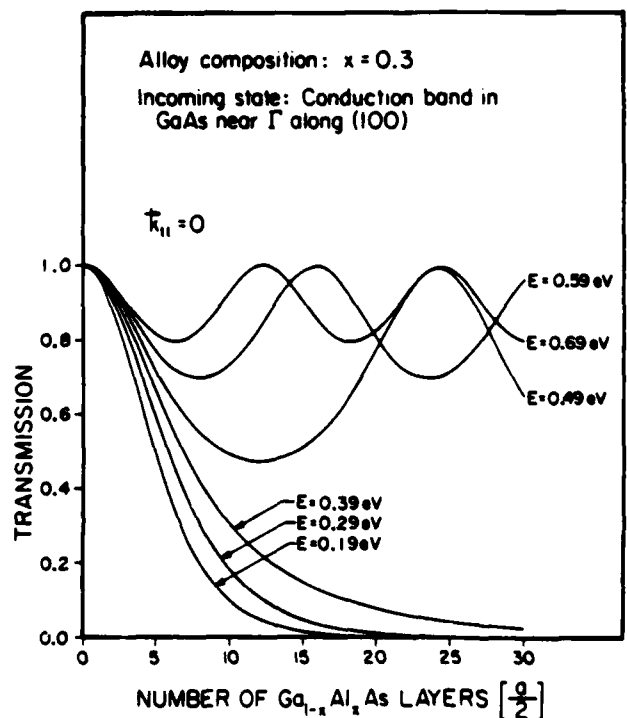


FIG. 3. Total transmission coefficient  $T(k_{\parallel}, E)$  as a function of central  $\text{Ga}_{1-x}\text{Al}_x\text{As}$  barrier thickness for different incoming energies. The incoming Bloch state has no momentum parallel to the interface  $k_{\parallel} = 0$ . The  $\text{Ga}_{1-x}\text{Al}_x\text{As}$  alloy composition is  $x = 0.3$ . Incoming state: Conduction band in GaAs near  $\Gamma$  along (100).

$E_r^{Ga_1-xAl_xAs} \approx 0.41$  eV. Transmission through the  $Ga_{1-x}Al_xAs$  barrier is either tunneling or propagating, depending on the nature of the Bloch states available for strong coupling in the alloy. For energies of the incoming state less than  $E_r^{Ga_1-xAl_xAs}$ , the available states in the alloy are *gap states* ( $k_r''$  complex) and the wave function is damped in the barrier. However, for energies of the incoming state greater than  $E_r^{Ga_1-xAl_xAs}$ , the available states in the alloy are *band states* ( $k_r''$  real) and the wave function is not damped in the barrier.

Generally, when an incoming state in GaAs is derived from a conduction band extremum, say  $\lambda$ , such that  $k_0 = k_\lambda^I$  and  $\psi(k_\parallel, k_0) = \psi(k_\parallel, k_\lambda^I)$  the mode of transport (i.e., tunneling or propagating) appears to be determined by the nature of the states in  $Ga_{1-x}Al_xAs$  derived from the same conduction band extremum  $\psi(k_\parallel, k_\lambda^I)$ . For energies of the incoming state less than the alloy conduction band edge  $E_\lambda^{Ga_1-xAl_xAs}$ , the states that couple strongly in the alloy are gap states [ $\psi(k_\parallel, k_\lambda^I)$  evanescent] and hence the wave function is damped in the barrier. However, for energies of the incoming state greater than the alloy conduction band edge  $E_\lambda^{Ga_1-xAl_xAs}$ , the states that couple strongly in the alloy are band states [ $\psi(k_\parallel, k_\lambda^I)$  propagating] and hence the wave function is not damped in the barrier.

In the tunneling regime of transport, transmission occurs mostly via the coupling to the alloy  $\Gamma$ -point *evanescent* states ( $k_r''$  complex). As seen in Fig. 3, the evanescent character of the wave function in  $Ga_{1-x}Al_xAs$  is reflected in the fact that the transmission coefficient  $T(k_\parallel, E)$  is an exponentially decaying function of the  $Ga_{1-x}Al_xAs$  barrier thickness. These observations are similar to those obtained from the thick-barrier WKB approximation.<sup>15,16</sup> For incoming states with energy greater than  $E_r^{Ga_1-xAl_xAs}$ , transmission occurs mostly via the coupling to the alloy  $\Gamma$ -point *propagating* states ( $k_r''$  real). The transmission coefficient is unity when the thickness of the  $Ga_{1-x}Al_xAs$  barrier contains an integral number of half-wavelengths (determined by  $k_r''$ ) in the barrier region. Under these resonant scattering conditions, the states derived from the conduction band  $\Gamma$  point couple strongly to each other and channeling into Bloch states derived from different conduction band extrema is found to be small. This observation is supported by the original work<sup>1,2</sup> on the transport of Bloch states at a single GaAs- $Ga_{1-x}Al_xAs$  heterojunction. For energy of the incoming state above  $E_r^{Ga_1-xAl_xAs}$ , the transmission coefficient is a periodic function of the  $Ga_{1-x}Al_xAs$  barrier thickness. Since the wave vector  $k_r''$  increases with incident Bloch state energy, the period of the transmission amplitude decreases with the energy of the incident Bloch state. The off-resonance transmission amplitudes increase with increasing incident energy. The general qualitative behavior of the transport is similar to that exhibited by plane wave states incident on a rectangular quantum-mechanical barrier.<sup>17</sup>

Figure 4 shows the total transmission and reflection coefficients  $T(k_\parallel, E)$  and  $R(k_\parallel, E)$  as a function of the number of monolayers forming a central AlAs barrier. The energy of the incoming Bloch state  $\psi(k_\parallel, k_r^I)$  is  $E = 0.51$  eV, measured with respect to the GaAs conduction band minimum. The

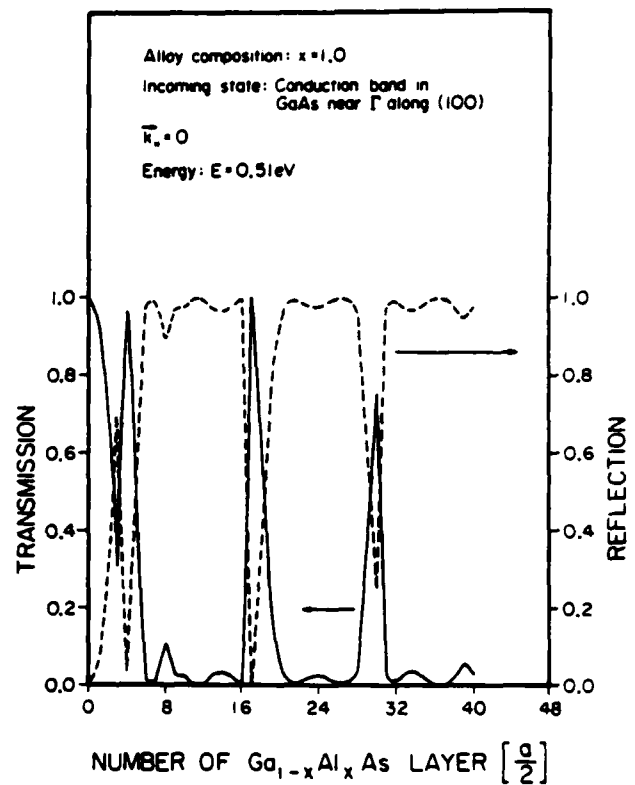


FIG. 4. Total transmission (solid line) and reflection (dashed line) coefficients  $T(k_\parallel, E)$  and  $R(k_\parallel, E)$  as a function of central AlAs barrier thickness for an energy of  $E = 0.51$  eV. Energy is measured with respect to the GaAs conduction band minimum and  $k_\parallel = 0$ . Alloy composition:  $x = 1.0$ . Incoming state: Conduction band in GaAs near  $\Gamma$  along (100).

incoming state derived from near the conduction band  $\Gamma$  point has vanishing parallel momentum  $k_\parallel = 0$ . At this energy the states available for transport in AlAs are *propagating* states near the  $X$ -point extremum ( $k_r''$  real), and *evanescent* states connecting to the  $\Gamma$  point ( $k_r''$  complex) at higher energy. Here again it is found that, for incoming states derived from the GaAs conduction band  $\Gamma$  point, transmission through the AlAs barrier occurs mostly via the coupling to evanescent states that connect to the AlAs conduction band at the  $\Gamma$  point. At small AlAs barrier thicknesses, transmission of conduction band  $\Gamma$ -point incoming states is governed by *tunneling*. In this regime, the incoming state  $\psi(k_\parallel, k_r^I)$  tunnels through the AlAs barrier by coupling to the evanescent Bloch states  $\psi(k_\parallel, k_r^I)$  associated with the conduction band  $\Gamma$ -point minimum. However, it was found that under energetically favorable conditions, transport could exhibit very sharp *resonance scattering* through available propagating  $X$ -point states  $\psi(k_\parallel, k_r^I)$ . This mode of resonant transport occurs for thick AlAs barriers when the tunneling through  $\Gamma$ -point-derived evanescent Bloch states is negligible. Resonance scattering through propagating  $X$ -point Bloch states appears to be very sharp due to the weak coupling between  $\psi(k_\parallel, k_r^I)$  and  $\psi(k_\parallel, k_r^I)$ . Similar regimes of transport have also been reported in the case of GaAs- $Ga_{1-x}P_x$ -GaAs strained (100) double heterostructures.<sup>4</sup>

### B. Admixture of states of different symmetries

We now analyze the relative contributions of the  $X$ -point and the  $\Gamma$ -point conduction band Bloch states to the transmitted wave function as a function of the alloy composition  $x$ . Figure 5 shows the transmission coefficients  $T_{\Gamma}(k_{\parallel}, E)$  and  $T_X(k_{\parallel}, E)$  as a function of alloy composition, for two different  $\text{Ga}_{1-x}\text{Al}_x\text{As}$  barrier thicknesses. The energy of the incoming state is  $E = 0.69$  eV measured with respect to the GaAs conduction band minimum. For the range of alloy compositions studied, this energy is greater than  $E_{\Gamma}^{\text{Ga}_{1-x}\text{Al}_x\text{As}}$ . At this energy the  $\Gamma$ -point and  $X$ -point states in GaAs and  $\text{Ga}_{1-x}\text{Al}_x\text{As}$  are propagating ( $k_{\Gamma}^I, k_{\Gamma}^II, k_{\Gamma}^III$  real, and  $k_X^I, k_X^II, k_X^III$  real). The incoming Bloch state has  $k_{\parallel} = 0$ .

As mentioned above, the  $\Gamma$ -point energy edge  $E_{\Gamma}^{\text{Ga}_{1-x}\text{Al}_x\text{As}}$  scales linearly with the alloy composition. The composition  $x$  is therefore proportional to the  $\Gamma$ -point barrier height at the interface. For the range of alloy compositions studied, the  $\Gamma$ -point energy edge of  $\text{Ga}_{1-x}\text{Al}_x\text{As}$  varies approximately in the range  $0 \text{ eV} < E_{\Gamma}^{\text{Ga}_{1-x}\text{Al}_x\text{As}} < 0.47$  eV, above the GaAs  $\Gamma$ -point conduction band minimum. For an energy of the incoming state of  $E = 0.69$  eV, the transport regime for incoming states derived from the conduction band  $\Gamma$  point is propagating since the coupling states in the alloy are propagating Bloch states. Since the energy of the incoming state lies above the  $\Gamma$ -point energy edge of the alloy, the transmission amplitude is a weakly dependent function of the barrier height.

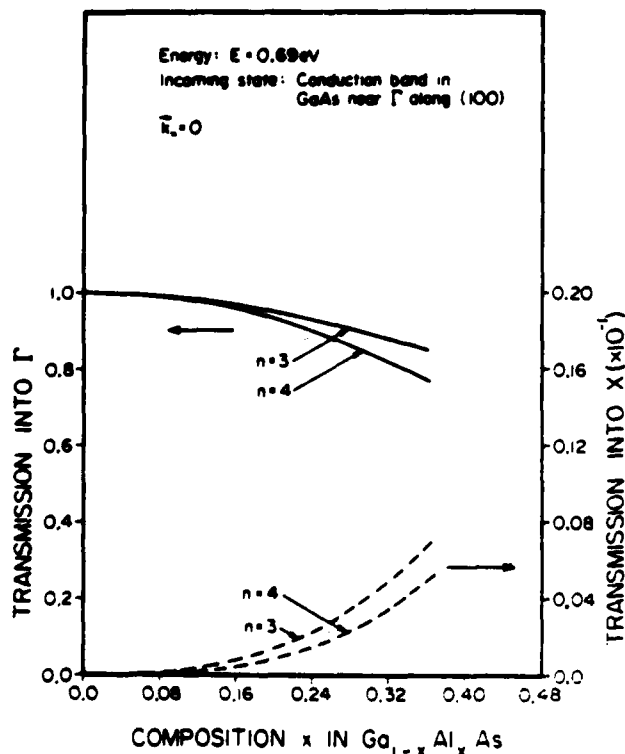


FIG. 5. Wave vector-resolved transmission coefficients  $T_{\Gamma}(k_{\parallel}, E)$  (solid line) and  $T_X(k_{\parallel}, E)$  (dashed line) as a function of  $\text{Ga}_{1-x}\text{Al}_x\text{As}$  alloy composition  $x$  for different barrier thicknesses. The energy of the incoming state is  $E = 0.69$  eV. The number of  $\text{Ga}_{1-x}\text{Al}_x\text{As}$  barrier layers is  $n$ , and  $k_{\parallel} = 0$ . Incoming state: Conduction band in GaAs near  $\Gamma$  along (100).

As the Al content of  $\text{Ga}_{1-x}\text{Al}_x\text{As}$  increases, transmission into the propagating  $X$ -point Bloch states  $\psi(k_{\parallel}, k_X^III)$  increases but remains rather small. States derived from the same extremum of the conduction band appear to couple strongly to each other across the GaAs- $\text{Ga}_{1-x}\text{Al}_x\text{As}$  interface. However, states derived from different extrema of the conduction band appear to couple weakly across the GaAs- $\text{Ga}_{1-x}\text{Al}_x\text{As}$  interface.

### IV. SUMMARY AND CONCLUSION

We have calculated the transport coefficients of Bloch states through GaAs- $\text{Ga}_{1-x}\text{Al}_x\text{As}$ -GaAs double heterojunctions. The model uses complex- $k$ -band structures and transfer matrix methods in the tight-binding approximation. With these techniques,  $k_x$ -resolved transport coefficients can be calculated. This, in turn, allows for a better understanding of the transmission coefficients of Bloch states derived from different extrema of the conduction band in GaAs. The incoming electron is derived from the GaAs conduction band  $\Gamma$  point. Calculation of transport coefficients associated with various conduction band valleys were carried through as a function of (1) energy of the incoming Bloch state, (2) thickness of the central  $\text{Ga}_{1-x}\text{Al}_x\text{As}$  barrier and, (3) alloy composition  $x$  in the central  $\text{Ga}_{1-x}\text{Al}_x\text{As}$  barrier.

States derived from the same extremum of the conduction band appear to couple strongly to each other across the GaAs- $\text{Ga}_{1-x}\text{Al}_x\text{As}$  interface. Transmission through the  $\text{Ga}_{1-x}\text{Al}_x\text{As}$  barrier is either tunneling or propagating depending on the nature of the Bloch states available for strong coupling in the alloy. For energies of the incoming states near the GaAs conduction band  $\Gamma$  point, transmission through the  $\text{Ga}_{1-x}\text{Al}_x\text{As}$  barrier occurs mostly via the coupling to states (evanescent or propagating) that connect to the alloy conduction band at the  $\Gamma$  point.

If the propagating mode of transport, resonances in the transmission could possibly be used in GaAs high-speed low-power electronic devices. In an operational mode, it is desirable to populate the low-mass high-velocity GaAs conduction band  $\Gamma$ -point minimum and to depopulate the high-mass low-velocity  $X$  and  $L$  valleys. These results could provide the basis for an interesting filter for use in high-speed devices.<sup>18</sup>

### ACKNOWLEDGMENTS

The authors wish to acknowledge D. L. Smith for clarifying their thoughts and assisting with the manuscript, and G. C. Osbourn for pointing out to them some previously published work related to the study presented here. One of us (CM) has been supported by the NSERC of Canada and by the Fonds F.C.A.C. pour l'aide et le soutien à la recherche of Québec.

<sup>1</sup> Work supported in part by the Army Research Office under Contract No. DAAG29-88-C-0103.

<sup>18</sup> Work supported in part by ONR Contract N00014-82-K-0458.

- <sup>1</sup>G. C. Osbourn and D. L. Smith, *Phys. Rev. B* **19**, 2124 (1979).  
<sup>2</sup>G. C. Osbourn and D. L. Smith, *J. Vac. Sci. Technol.* **16**, 1529 (1979).  
<sup>3</sup>G. C. Osbourn, *J. Vac. Sci. Technol.* **17**, 1104 (1980).  
<sup>4</sup>G. C. Osbourn, *J. Vac. Sci. Technol.* **19**, 592 (1981).  
<sup>5</sup>Y. C. Chang and J. N. Schulman, *Phys. Rev. B* **25**, 3975 (1982).  
<sup>6</sup>J. N. Schulman and Y. C. Chang, *Phys. Rev. B* **27**, 2346 (1983).  
<sup>7</sup>D. H. Lee and J. D. Joannopoulos, *Phys. Rev. B* **23**, 4988, 4997 (1981).  
<sup>8</sup>J. Pollmann and S. Pantelides, *Phys. Rev. B* **18**, 5524 (1978).  
<sup>9</sup>D. H. Lee and J. D. Joannopoulos, *J. Vac. Sci. Technol.* **19**, 355 (1981).  
<sup>10</sup>Y. C. Chang and J. N. Schulman, *J. Vac. Sci. Technol.* **21**, 540 (1982).  
<sup>11</sup>P. Vogl, H. P. Hjalmarson, and J. D. Dow, *J. Phys. Chem. Solids* (in press).  
<sup>12</sup>J. N. Schulman and Y. C. Chang, *Phys. Rev. B* **24**, 4445 (1981).  
<sup>13</sup>H. C. Casey and M. B. Panish, *Heterostructure Lasers* (Academic, New York, 1978), Part A, Chap. 4.  
<sup>14</sup>R. Dingle, W. Weigmann, and C. Henry, *Phys. Rev. Lett.* **33**, 827 (1974).  
<sup>15</sup>W. A. Harrison, *Phys. Rev.* **123**, 85 (1961).  
<sup>16</sup>C. B. Duke, *Tunneling Phenomena in Solids* (Plenum, New York, 1969), p. 31.  
<sup>17</sup>L. I. Schiff, *Quantum Mechanics*, 3rd ed. (McGraw-Hill, New York, 1968), pp. 102-104.  
<sup>18</sup>C. Mailhot, D. L. Smith, and T. C. McGill, *J. Vac. Sci. Technol. B* (to be published).

# Transport characteristics of $L$ -point and $\Gamma$ -point electrons through $\text{GaAs-Ga}_{1-x}\text{Al}_x\text{As-GaAs}(111)$ double heterojunctions<sup>a)</sup>

C. Mailhot, D. L. Smith, and T. C. McGill

*T. J. Watson, Sr., Laboratory of Applied Physics, California Institute of Technology, Pasadena, California 91125*

(Received 25 January 1983; accepted 21 March 1983)

We present here a study on the transport characteristics of  $L$ -point and  $\Gamma$ -point derived electrons through abrupt  $\text{GaAs-Ga}_{1-x}\text{Al}_x\text{As-GaAs}(111)$  double heterojunctions. The use of complex- $k$  band structures in the tight-binding approximation and transfer matrices provide a reasonably accurate description of the wave function at the  $\text{GaAs-Ga}_{1-x}\text{Al}_x\text{As}$  interface. A representation of the wave function in terms of bulk complex- $k$  Bloch states is used in the  $\text{GaAs}$  regions where the potential is bulklike. A representation of the wave function in terms of planar orbitals is used in the central  $\text{Ga}_{1-x}\text{Al}_x\text{As}$  region where the potential deviates from its bulk value (i.e., interfacial region). Within this theoretical framework, realistic band structure effects are taken into account and no artificial rules regarding the connection of the wave function across the interface are introduced. The ten-band tight-binding model includes admixture in the total wave function of states derived from different extrema of the  $\text{GaAs}$  conduction band. States derived from the same extremum of the conduction band appear to couple strongly to each other, whereas states derived from different extrema are found to couple weakly. Transport characteristics of incoming  $L$ -point and  $\Gamma$ -point Bloch states are examined as a function of the energy of the incoming state, thickness of the  $\text{Ga}_{1-x}\text{Al}_x\text{As}$  barrier, and alloy composition  $x$ . Transmission through the  $\text{Ga}_{1-x}\text{Al}_x\text{As}$  barrier is either tunneling or propagating depending on the nature of the Bloch states available for strong coupling in the alloy. Since Bloch states derived from different extrema of the conduction band appear to couple weakly to each other, it seems possible to reflect the low velocity  $L$ -point component of the current while transmitting the high velocity  $\Gamma$ -point component.

PACS numbers: 73.40.Lq

## I. INTRODUCTION

The introduction of new device fabrication technologies has allowed the realization of planar electronic devices in which the dimension perpendicular to the growth plane is of the order of a few lattice spacings. The understanding of the transport of electrons through semiconductor interfaces is of great importance regarding the performance of these very small-scale electronic devices. The major reason that makes  $\text{GaAs}$  a prime candidate for high speed electronic devices is the very high velocities that can be achieved by electrons derived from the  $\Gamma$ -point conduction band minimum. The small value of the  $\Gamma$ -point effective mass is in major part responsible for the very high velocities that can be achieved by these electrons. At higher energies, electrons start to populate the low velocity  $L$ -point and  $X$ -point  $\text{GaAs}$  conduction band valleys, therefore reducing the population of the high velocity  $\Gamma$ -point minimum. This has the direct effect of setting an upper limit to the speed at which the device can operate. The study of transport of electrons associated with the various  $\text{GaAs}$  conduction band valleys is therefore of crucial importance. The work presented here is concerned with the transport of  $L$ -point and  $\Gamma$ -point derived electron states through a  $\text{GaAs-Ga}_{1-x}\text{Al}_x\text{As-GaAs}(111)$  double heterojunction structure (DHS). The transport in these structures is either tunneling or propagating depending on the nature of the states with strong coupling available for transmission in the  $\text{Ga}_{1-x}\text{Al}_x\text{As}$  barrier (i.e., evanescent or propagating). In the former, the Bloch states with strong

coupling available for transmission in the  $\text{Ga}_{1-x}\text{Al}_x\text{As}$  barrier are evanescent and the wave vector  $k$  is complex. In the latter, the Bloch states with strong coupling available for transmission in the alloy are propagating and the wave vector  $k$  takes on real values.

In the following, we examine DHS in which the perpendicular dimension of the central barrier region is of the order of a few atomic layers. Since the potential varies over distances on an atomic scale, a theoretical approach beyond the effective-mass theory is needed. The theoretical framework used here exploits the bulk properties of the constituent semiconductors forming the DHS. The transport of electrons through a region of space in which the energy of the state is such that free propagation is not allowed is best described in terms of the complex- $k$  bulk band structure. The breakdown of translational invariance induced by the interface implies a new set of boundary conditions that do not exclude the component of the wave vector  $k$  normal to the interface to take on complex values. The problem of calculating the transport coefficients of Bloch states at an abrupt interface using complex- $k$  band structure, cast in a tight-binding band calculation scheme, has been addressed in the past.<sup>1-4</sup> The major result of the following theoretical study is that the mixing between  $L$ -point and  $\Gamma$ -point states appears to be small. Therefore, there seems to exist two distinctive energy barriers for  $L$ -point and  $\Gamma$ -point electrons. Given an alloy composition of the  $\text{Ga}_{1-x}\text{Al}_x\text{As}$  barrier, there is a range of energies for which the electrons incoming from the  $\Gamma$ -point minimum of  $\text{GaAs}$  are mostly transmitted, whereas the elec-

trons incoming from the  $L$ -point extremum of GaAs are mostly reflected. It seems then possible to reflect back the low velocity  $L$ -point component of the current while allowing the high velocity  $\Gamma$ -point component to be transmitted.

The paper is organized as follows: in Sec. II, the basic ingredients of the theoretical technique used to calculate the transport coefficients are presented. The major results are presented and discussed in Sec. III. A summary and conclusions are given in Sec. IV.

## II. CALCULATIONAL METHOD

The DHS studied consists of a region of  $\text{Ga}_{1-x}\text{Al}_x\text{As}$  located between two semi-infinite layers of GaAs. Figure 1 shows the energy band diagram and the physical configuration of the DHS. The energy band diagram of the structure indicates the relative positions of the  $\Gamma$ -point and the  $L$ -point conduction band edges for an alloy composition of  $x \approx 0.3$  in the  $\text{Ga}_{1-x}\text{Al}_x\text{As}$  barrier. An electron incoming in the bulk region I (GaAs) at a total energy  $E$  above the GaAs  $\Gamma$ -point minimum is scattered at the boundaries of the barrier region II ( $\text{Ga}_{1-x}\text{Al}_x\text{As}$ ) and is finally transmitted in another bulk region III (GaAs). The incoming electron is derived from the  $\Gamma$  point or from the  $L$  point in GaAs. The  $\Gamma$ -point conduc-

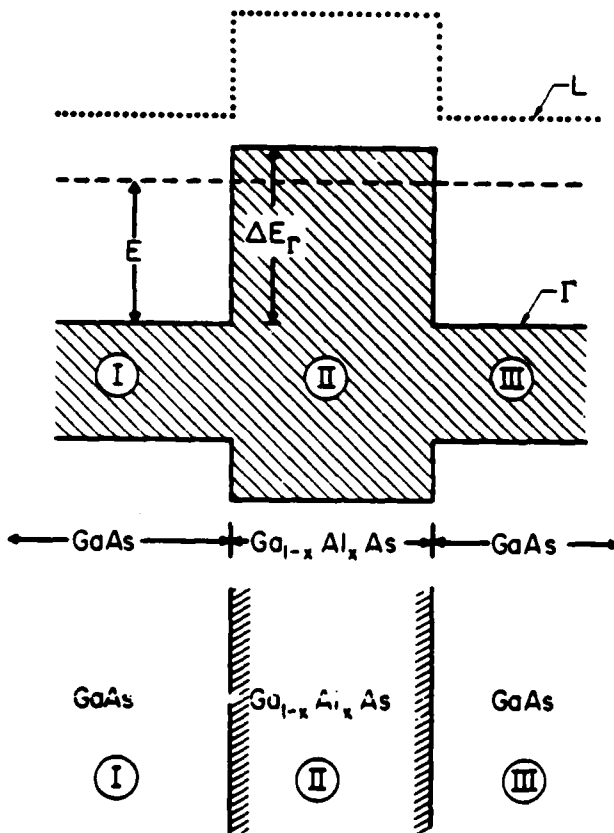


FIG. 1. Energy band diagram of GaAs- $\text{Ga}_{1-x}\text{Al}_x\text{As}$ -GaAs DHS and corresponding physical structure. The electron is derived from the  $\Gamma$ -point or from the  $L$ -point and has a total energy  $E$  measured with respect to the GaAs  $\Gamma$ -point conduction band minimum. The relative positions of the  $\Gamma$ -point (solid line) and the  $L$ -point (dotted line) conduction band edges are also shown for an alloy composition of  $x \approx 0.3$  in the  $\text{Ga}_{1-x}\text{Al}_x\text{As}$  barrier. The  $\Gamma$ -point conduction band offset is indicated by  $\Delta E_{\Gamma}$ .

tion band offset  $\Delta E_{\Gamma}$  is a fraction of the difference in the  $\Gamma$ -point conduction band gaps between GaAs and  $\text{Ga}_{1-x}\text{Al}_x\text{As}$ . Depending on whether we describe the total wave function in a bulk region or an interfacial region, different representations are used accordingly. We now discuss these two representations.

Systems which exhibit two-dimensional periodicity are best described in a planar orbital representation.<sup>5-10</sup> A planar orbital is a two-dimensional Bloch sum consisting of localized atomic functions. Let  $\hat{z}$  be the direction normal to the interface and  $\mathbf{k}_{\parallel} = \hat{x}k_x + \hat{y}k_y$  be the two-dimensional wave vector parallel to the interface. We assume that space lattice matching at the interface is such that  $\mathbf{k}_{\parallel}$  is a good quantum number for the planar orbital. Let  $\phi_{\alpha}(\mathbf{k}_{\parallel}; \sigma)$  designate the planar orbital corresponding to a given atomic orbital of symmetry  $\alpha$  within the atomic plane  $j$  of the layer  $\sigma$ . The bulk Bloch states  $\psi(\mathbf{k}_{\parallel}, k_z)$ , labeled by the wave vector  $\mathbf{k} = \mathbf{k}_{\parallel} + \hat{z}k_z$ , are expanded in terms of this set of planar orbitals  $\{\phi_{\alpha}(\mathbf{k}_{\parallel}; \sigma)\}$ . For interface systems,  $k_z$  is complex in general.

Wherever the total Hamiltonian is bulklike, the wave function is expanded in a set of bulk Bloch states  $\{\psi(\mathbf{k}_{\parallel}, k_z)\}$ . At the GaAs- $\text{Ga}_{1-x}\text{Al}_x\text{As}$  interfaces, the potential is no longer bulklike and a description in terms of bulk Bloch states is prohibited. In the interfacial regions, the wave function is described in a planar orbital representation  $\{\phi_{\alpha}(\mathbf{k}_{\parallel}; \sigma)\}$ . The connection between the bulk Bloch states representation  $\{\psi(\mathbf{k}_{\parallel}, k_z)\}$  and the planar orbital representation  $\{\phi_{\alpha}(\mathbf{k}_{\parallel}; \sigma)\}$  is described in Ref. 6 and will not be repeated here.

The total number  $N$  of Bloch states  $\psi(\mathbf{k}_{\parallel}, k_z)$  with  $k_z = k_{\lambda}$  ( $\lambda = 1, \dots, N$ ) corresponding to a given parallel wave vector  $\mathbf{k}_{\parallel}$  and total energy  $E$  depends on the particular tight-binding model used and on the orientation of the interface plane. More specifically, the total number of Bloch states  $\psi(\mathbf{k}_{\parallel}, k_{\lambda})$  with real or complex wave vector  $k_{\lambda}$  is equal to the product of the number of atomic orbitals per atom times the number of layers interacting with a given layer.<sup>1</sup> In the tight-binding representation used here, we have five orbitals per atom ( $\alpha = s^*, s, p_x, p_y, p_z$ )<sup>11</sup> and only first nearest-neighbor interactions were included. There are therefore ten Bloch states ( $N = 10$ ) for each parallel wave vector  $\mathbf{k}_{\parallel}$  and total energy  $E$ . Half of the states have to be discarded because they either grow away from the interface, if  $\text{Im}(k_z)$  does not have the proper sign, or are propagating in the wrong direction when  $k_z$  is real.

Let the incoming Bloch state  $\psi(\mathbf{k}_{\parallel}, k_0)$  with real wave vector  $k_0$  be incident from the left in GaAs onto the GaAs- $\text{Ga}_{1-x}\text{Al}_x\text{As}$  interface. The total wave function on a given layer  $\sigma$  can be written as<sup>1</sup>:

$$\Psi(\mathbf{k}_{\parallel}, E; \sigma) = \psi(\mathbf{k}_{\parallel}, k_0; \sigma) + \sum_{k_{\lambda}} A_{k_{\lambda}}^{(I)}(\mathbf{k}_{\parallel}, E) \psi(\mathbf{k}_{\parallel}, k_{\lambda}; \sigma), \text{ region I} \quad (1a)$$

$$\Psi(\mathbf{k}_{\parallel}, E; \sigma) = \sum_{\alpha} B_{\alpha}^{(I-II)}(\mathbf{k}_{\parallel}, E, \sigma) \phi_{\alpha}(\mathbf{k}_{\parallel}; \sigma), \text{ interface I-II} \quad (1b)$$

$$\Psi(\mathbf{k}_\parallel, E; \sigma) = \sum_{k_x} A_{k_x}^{(II)}(\mathbf{k}_\parallel, E) \psi(\mathbf{k}_\parallel, k_x, \sigma), \text{ region II} \quad (1c)$$

$$\Psi(\mathbf{k}_\parallel, E; \sigma) = \sum_{\sigma'} B_{\sigma'}^{(II-III)}(\mathbf{k}_\parallel, E, \sigma) \phi_{\sigma'}(\mathbf{k}_\parallel, \sigma), \text{ interface II-III} \quad (1d)$$

$$\Psi(\mathbf{k}_\parallel, E; \sigma) = \sum_{k_x} A_{k_x}^{(III)}(\mathbf{k}_\parallel, E) \psi(\mathbf{k}_\parallel, k_x, \sigma), \text{ region III.} \quad (1e)$$

The expansion coefficients  $A_{k_x}^{(I)}(\mathbf{k}_\parallel, E)$ ,  $A_{k_x}^{(II)}(\mathbf{k}_\parallel, E)$ , and  $A_{k_x}^{(III)}(\mathbf{k}_\parallel, E)$  are associated with the bulk Bloch states representation  $\{\psi(\mathbf{k}_\parallel, k_x)\}$  in regions I-III, respectively. The expansion coefficients  $B_{\sigma'}^{(II-III)}(\mathbf{k}_\parallel, E, \sigma)$  and  $B_{\sigma'}^{(III-III)}(\mathbf{k}_\parallel, E, \sigma)$  are associated with the planar orbital representation  $\{\phi_{\sigma'}(\mathbf{k}_\parallel, \sigma)\}$ , across the interfaces. At fixed total energy  $E$  and parallel wave vector  $\mathbf{k}_\parallel$ , we denote by  $R_\lambda(\mathbf{k}_\parallel, E)$  and  $T_\lambda(\mathbf{k}_\parallel, E)$  the  $k_x$ -resolved reflection and transmission coefficients corresponding to the Bloch state  $\psi(\mathbf{k}_\parallel, k_x)$  in GaAs. The  $k_x$ -resolved transport coefficients  $R_\lambda(\mathbf{k}_\parallel, E)$  and  $T_\lambda(\mathbf{k}_\parallel, E)$  are related to the expansion coefficients in the bulk Bloch state representation  $A_{k_x}^{(I)}(\mathbf{k}_\parallel, E)$  and  $A_{k_x}^{(III)}(\mathbf{k}_\parallel, E)$ , respectively. The total transport coefficients  $R(\mathbf{k}_\parallel, E)$  and  $T(\mathbf{k}_\parallel, E)$  are just the sum of the transport coefficients  $R_\lambda(\mathbf{k}_\parallel, E)$  and  $T_\lambda(\mathbf{k}_\parallel, E)$ . Flux conservation requires  $R(\mathbf{k}_\parallel, E) + T(\mathbf{k}_\parallel, E) = 1$ .

As shown in Ref. 1, the transmission coefficient for the Bloch state  $\psi(\mathbf{k}_\parallel, k_x)$  vanishes when the wave vector of the incoming Bloch state,  $k_0$ , approaches a critical point such that  $[\partial E(\mathbf{k})/\partial k_x]_{k_x=k_0} = 0$ . In that case, the incoming state is identical with the reflected state. At this critical point, the incoming state  $\psi(\mathbf{k}_\parallel, k_0)$  has no component of the group velocity perpendicular to the interface and does not couple to any Bloch states in  $\text{Ga}_{1-x}\text{Al}_x\text{As}$ . Therefore, transmission starts to occur as the incident wave vector  $k_0$  moves away from the critical point.

The transport states in the complex- $k$  band structure of GaAs and  $\text{GaAs-Ga}_{1-x}\text{Al}_x\text{As}$ . The complex- $k$  band structure for GaAs and AlAs is well known.<sup>1,12</sup> We have used similar techniques to obtain the complex- $k$  band structure for  $\text{Ga}_{1-x}\text{Al}_x\text{As}$  within the virtual crystal approximation. Within the ten-band tight-binding description used here, the GaAs  $\Gamma$ -point conduction band minimum is  $E_{\Gamma}^{\text{GaAs}} = 1.509$  eV above the GaAs  $\Gamma$ -point valence band maximum and the GaAs  $L$ -point conduction band valley is at an energy  $E_L^{\text{GaAs}} = 0.50$  eV above the GaAs  $\Gamma$ -point conduction band minimum.

The propagating or evanescent nature of the Bloch states depends on the real or complex character of the wave vector  $k_x$  normal to the (111) interface plane. Propagating Bloch states are associated with real values of  $k_x$ , whereas evanescent Bloch states are associated with complex values of  $k_x$ . We denote the bulk states with  $k_x = k_\lambda$  in spatial region  $\mu$  by  $\psi(\mathbf{k}_\parallel, k_\lambda^\mu)$ . In the discussion that follows, the incident Bloch state is derived either from near the GaAs conduction band  $L$  point with real wave vector  $k_0 = k_L$ , e.g.,  $\psi(\mathbf{k}_\parallel, k_0) = \psi(\mathbf{k}_\parallel, k_L)$ , or from the GaAs conduction band  $\Gamma$  point with real wave vector  $k_0 = k_\Gamma$ , e.g.,

$$\psi(\mathbf{k}_\parallel, k_0) = \psi(\mathbf{k}_\parallel, k_\Gamma).$$

Throughout the calculations, the conduction band offset  $\Delta E_\Gamma$  is taken to be equal to 85% of the difference of the  $\Gamma$ -point band gap between GaAs and  $\text{GaAs-Ga}_{1-x}\text{Al}_x\text{As}$ .<sup>13,14</sup> The virtual crystal approximation is used to weight the tight-binding parameters of  $\text{Ga}_{1-x}\text{Al}_x\text{As}$  according to the alloy composition  $x$ . In the following, we consider alloy compositions in the range  $x < 0.3$ , for which  $\text{Ga}_{1-x}\text{Al}_x\text{As}$  is direct. Within this composition range, the dependence of the  $\Gamma$ -point and  $L$ -point energy edges in  $\text{Ga}_{1-x}\text{Al}_x\text{As}$  on the alloy composition  $x$  is, in the virtual crystal approximation:  $E_{\Gamma}^{\text{Ga}_{1-x}\text{Al}_x\text{As}} \approx 1.35x$  eV and  $E_L^{\text{Ga}_{1-x}\text{Al}_x\text{As}} \approx (0.50 + 0.65x)$  eV, above the GaAs  $\Gamma$ -point conduction band minimum.

Throughout this study, we neglect carrier scattering by the electron-phonon interaction and by the alloy disorder. Such scattering would undoubtedly occur in the structures we consider here and will have some influence on the transport in them. We point out, however, that the thickness of the barrier in the structures we discuss is less than the scattering mean free path.<sup>15</sup> The scattering processes could be discussed in perturbation theory using the wave functions we calculate here as the unperturbed states.

### III. RESULTS

We present the main results for the transmission coefficients of electrons derived from the  $L$  point and  $\Gamma$  point of GaAs through the  $\text{GaAs-Ga}_{1-x}\text{Al}_x\text{As-GaAs(111)DHS}$ . We discuss the transport across the central  $\text{Ga}_{1-x}\text{Al}_x\text{As}$  barrier as a function of the total energy  $E$  of the incoming state, thickness of the  $\text{Ga}_{1-x}\text{Al}_x\text{As}$  barrier, and alloy composition  $x$ .

The different transport regimes (tunneling and propagating) can be demonstrated by studying the transmission coefficient for fixed barrier thickness as a function of the energy of the incoming state. Figure 2 shows the transmission coefficient  $T(\mathbf{k}_\parallel, E)$  as a function of the energy  $E$  of the incoming Bloch state. The incoming Bloch state is either derived from the GaAs  $L$  point ( $k_0 = k_L$ ), or from the GaAs  $\Gamma$  point ( $k_0 = k_\Gamma$ ). Energy is measured with respect to the GaAs  $\Gamma$ -point conduction band minimum. We consider the case of vanishing parallel wave vector  $\mathbf{k}_\parallel = 0$ . Calculations were carried out for an alloy composition of  $x = 0.1$  and a barrier thickness of seven  $\text{Ga}_{1-x}\text{Al}_x\text{As}$  layers. For the  $x = 0.1$  alloy, the  $\text{Ga}_{1-x}\text{Al}_x\text{As}$   $\Gamma$ -point and the  $L$ -point energies are:  $E_{\Gamma}^{\text{Ga}_{1-x}\text{Al}_x\text{As}} = 0.135$  eV, and  $E_L^{\text{Ga}_{1-x}\text{Al}_x\text{As}} = 0.565$  eV, above the GaAs  $\Gamma$ -point conduction band minimum. For energies of the incoming states near a given GaAs conduction band extremum ( $L$  or  $\Gamma$ ), transmission through the  $\text{Ga}_{1-x}\text{Al}_x\text{As}$  barrier appears to occur mostly via the coupling to states that connect to the alloy conduction band at the same extremum in the Brillouin zone ( $L$  or  $\Gamma$ ). Since the Bloch states derived from different extrema of the conduction band appear to couple weakly to each other, the energy barrier for the states derived from the  $L$  point is different than the energy barrier for the states derived from the  $\Gamma$  point.

The figure clearly demonstrates that there seems to exist a range of energies above the GaAs  $L$ -point valley ( $E_L^{\text{GaAs}}$ ) and

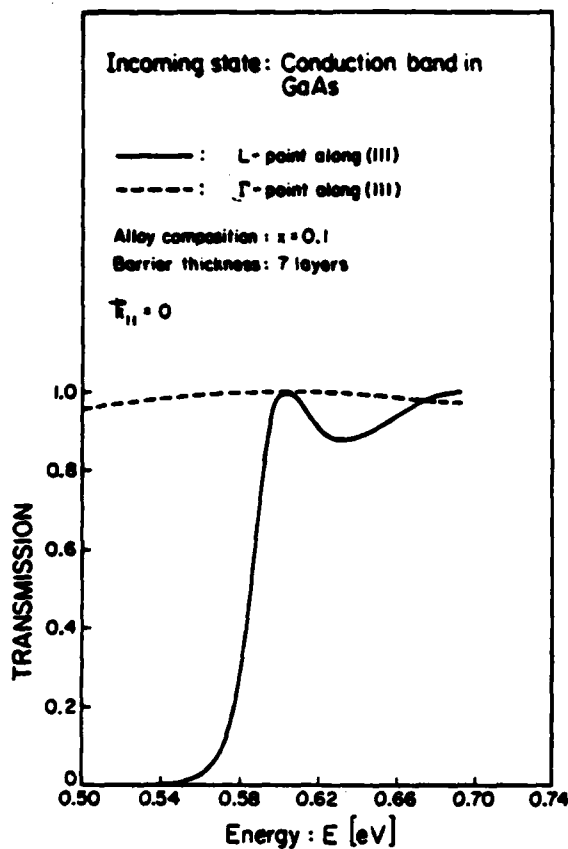


FIG. 2. Transmission coefficient  $T(k_{||}, E)$  as a function of the energy  $E$  of the incoming electron. The incoming electron is either derived from the GaAs  $L$  point (solid line), or from the GaAs  $\Gamma$  point (dashed line). The alloy composition of  $x = 0.1$  and the  $\text{Ga}_{1-x}\text{Al}_x\text{As}$  barrier is seven layers thick. Energy is measured with respect to the GaAs  $\Gamma$ -point conduction band minimum and  $k_{\perp} = 0$ .

below the  $\text{Ga}_{1-x}\text{Al}_x\text{As}$   $L$ -point valley ( $E_L^{\text{Ga}_{1-x}\text{Al}_x\text{As}}$ ), such that transmission is large for incoming Bloch states derived from the  $\Gamma$  point and small for incoming Bloch states derived from the  $L$  point. In this energy range,  $E_L^{\text{GaAs}} < E < E_L^{\text{Ga}_{1-x}\text{Al}_x\text{As}}$ , Bloch states incoming from the  $\Gamma$  point in GaAs couple mostly to *propagating*  $\Gamma$ -point states in the barrier ( $k_{\perp}^{\text{II}}$  real), and Bloch states incoming from the  $L$ -point in GaAs couple mostly to *evanescent*  $L$ -point states in the barrier ( $k_{\perp}^{\text{II}}$  complex). The energy range for which the transmission  $\psi(k_{||}, k_{\perp}^{\text{I}}) \rightarrow \psi(k_{||}, k_{\perp}^{\text{III}})$  is much greater than the transmission  $\psi(k_{||}, k_{\perp}^{\text{I}}) \rightarrow \psi(k_{||}, k_{\perp}^{\text{III}})$  roughly corresponds to the composition-dependent  $L$ -point energy barrier that the incoming  $L$ -point Bloch states have to overcome in order for them to become propagating ( $k_{\perp}^{\text{II}}$  real) in the barrier. For the  $x = 0.1$  alloy, the  $L$ -point valley of the alloy lies at  $E_L^{\text{Ga}_{1-x}\text{Al}_x\text{As}} = 0.565$  eV above the GaAs conduction band minimum, and  $\psi(k_{||}, k_{\perp}^{\text{I}}) \rightarrow \psi(k_{||}, k_{\perp}^{\text{III}})$  transmission will remain small below this energy, whereas  $\psi(k_{||}, k_{\perp}^{\text{I}}) \rightarrow \psi(k_{||}, k_{\perp}^{\text{III}})$  transmission will be important. Thus, for a given  $\text{Ga}_{1-x}\text{Al}_x\text{As}$  composition  $x$ , there is a range of energies, roughly  $E_L^{\text{GaAs}} < E < E_L^{\text{Ga}_{1-x}\text{Al}_x\text{As}}$ , for which electrons incoming in GaAs from the  $\Gamma$  point are mostly transmitted whereas electrons incoming in GaAs from the  $L$  point are

mostly reflected. Generally, when an incoming state in GaAs is derived from a conduction band extremum, say  $\lambda$ , such that  $k_{\perp} = k_{\perp}^{\lambda}$  and  $E$  is close to  $E_{\lambda}^{\text{GaAs}}$ , the mode of transport (i.e., tunneling or propagating) appears to be determined by the nature of the states in  $\text{Ga}_{1-x}\text{Al}_x\text{As}$  derived from the same conduction band extremum  $\psi(k_{||}, k_{\perp}^{\lambda})$ . For incoming state energies less than the alloy conduction band edge  $E_L^{\text{Ga}_{1-x}\text{Al}_x\text{As}}$ , the states that couple strongly in the alloy are gap states [ $\psi(k_{||}, k_{\perp}^{\lambda})$  evanescent] and hence the wave function is damped in the barrier. However, for incoming state energies greater than the alloy conduction band edge  $E_L^{\text{Ga}_{1-x}\text{Al}_x\text{As}}$ , the states that couple strongly in the alloy are band states [ $\psi(k_{||}, k_{\perp}^{\lambda})$  propagating] and hence the wave function is not damped in the barrier.

We now discuss the energy dependence of the transmission for incoming electrons derived from the GaAs  $L$ -point valley. As mentioned in Sec. II, the transmission coefficient vanishes for incoming states derived from the  $L$  point at an energy equal to the  $L$ -point extremum of GaAs,  $E_L^{\text{GaAs}}$ . At this energy, the component of the group velocity normal to the interface vanishes [ $\partial E(k)/\partial k_{\perp}|_{k_{\perp}=k_{\perp}^L} = 0$ ], and the incoming state  $\psi(k_{||}, k_{\perp}^L)$  does not couple to any Bloch states in  $\text{Ga}_{1-x}\text{Al}_x\text{As}$ . The overall energy dependence is found to be similar to that of plane waves incident on a rectangular barrier as derived from a one-dimensional quantum-mechanical treatment.<sup>16</sup> For incoming states derived from the GaAs  $L$  point with energy below  $E_L^{\text{Ga}_{1-x}\text{Al}_x\text{As}} = 0.565$  eV, transport through the barrier is tunneling and the transmission is small. However, for incoming states derived from the GaAs  $L$  point with energy above  $E_L^{\text{Ga}_{1-x}\text{Al}_x\text{As}}$ , transport through the barrier is propagating and the transmission becomes important. For a fixed barrier thickness, propagating transport exhibits maximum transmission whenever the energy of the incoming state is such the thickness of the  $\text{Ga}_{1-x}\text{Al}_x\text{As}$  barrier contains an integral number of half-wavelengths in the barrier region. At energies  $E > E_L^{\text{Ga}_{1-x}\text{Al}_x\text{As}}$ , the transmission oscillates as a function of energy and is maximum at resonance. The off-resonance transmission amplitude increases with increasing incoming energy.

The different transport regimes (tunneling and propagating) can also be demonstrated by studying the transmission coefficient for fixed incoming energy as a function of the barrier thickness. Figure 3 shows the transmission coefficient  $T(k_{||}, E)$ , as a function of the number of layers forming the central  $\text{Ga}_{1-x}\text{Al}_x\text{As}$  barrier for various energies of the incoming Bloch state. The alloy composition is  $x = 0.1$  and  $k_{\perp} = 0$ . Layers are measured in units of  $a/\sqrt{3}$ , where  $a$  is the GaAs lattice constant. For the  $x = 0.1$  alloy, the  $\Gamma$ -point and  $L$ -point conduction band energies in  $\text{Ga}_{1-x}\text{Al}_x\text{As}$  are:  $E_{\Gamma}^{\text{Ga}_{1-x}\text{Al}_x\text{As}} = 0.135$  eV and  $E_L^{\text{Ga}_{1-x}\text{Al}_x\text{As}} = 0.565$  eV, above the GaAs  $\Gamma$ -point conduction band minimum. The incoming Bloch state is either derived from the GaAs point  $L$  ( $k_{\perp} = k_{\perp}^L$ ), or from the GaAs  $\Gamma$  point ( $k_{\perp} = k_{\perp}^{\Gamma}$ ). For the case where the incoming Bloch state is derived from the GaAs  $L$ -point valley, the different types of transport (tunneling and propagating) are shown for an energy  $E = 0.54$  eV  $< E_L^{\text{Ga}_{1-x}\text{Al}_x\text{As}}$ , in which case the transport is tunneling

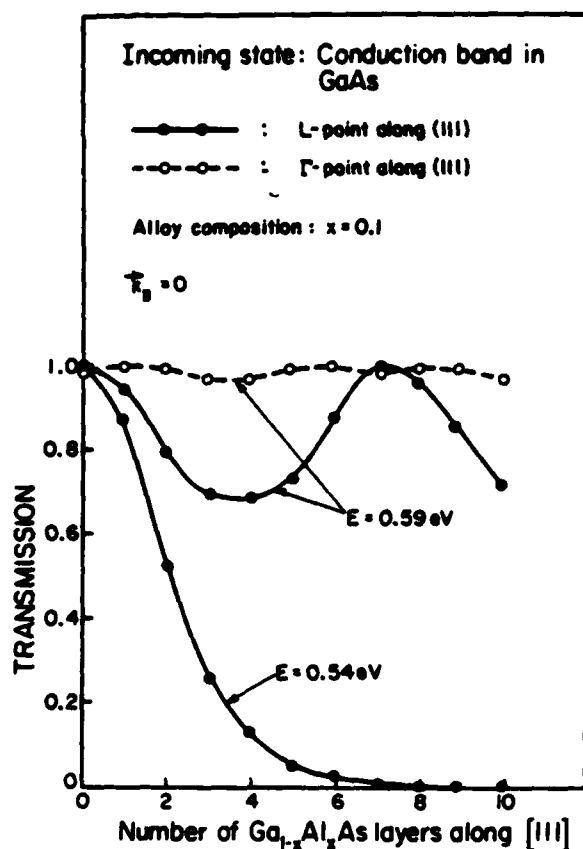


FIG. 3. Transmission coefficient  $T(k_{\parallel}, E)$  as a function of the number of layers forming the central  $\text{Ga}_{1-x}\text{Al}_x\text{As}$  barrier for various energies of the incoming electron. The incoming electron is either derived from the GaAs  $L$  point (solid line), or from the GaAs  $\Gamma$  point (dashed line). The alloy composition is  $x = 0.1$ . Energy is measured with respect to the GaAs  $\Gamma$ -point conduction band minimum and  $k_{\perp} = 0$ . Layers are measured in units of  $a/\sqrt{3}$ , where  $a$  is the GaAs lattice constant.

and for an energy  $E = 0.59 \text{ eV} > E_L^{\text{Ga}_{1-x}\text{Al}_x\text{As}}$ , in which case the transport is propagating.

We discuss first the case of incoming electrons derived from the GaAs  $L$ -point valley. In the tunneling regime of transport ( $E < E_L^{\text{Ga}_{1-x}\text{Al}_x\text{As}}$ ), transmission occurs mostly via the coupling to *evanescent* states ( $k_L^{\parallel}$  complex) derived from the  $L$  point of  $\text{Ga}_{1-x}\text{Al}_x\text{As}$ . As seen in Fig. 3, the evanescent character of the wave function in  $\text{Ga}_{1-x}\text{Al}_x\text{As}$  is reflected in the fact that the transmission coefficient  $T(k_{\parallel}, E)$  is an exponentially decaying function of the  $\text{Ga}_{1-x}\text{Al}_x\text{As}$  barrier thickness. These results are similar to those obtained from the thick-barrier WKB approximation.<sup>17,18</sup> In the propagating regime of transport ( $E > E_L^{\text{Ga}_{1-x}\text{Al}_x\text{As}}$ ), transmission occurs mostly via the coupling to *propagating* states ( $k_L^{\parallel}$  real) near the conduction band  $L$  point of  $\text{Ga}_{1-x}\text{Al}_x\text{As}$ . For energies of the  $L$ -point incoming electron greater than  $E_L^{\text{Ga}_{1-x}\text{Al}_x\text{As}}$ , the transmission coefficient is a periodic function of the  $\text{Ga}_{1-x}\text{Al}_x\text{As}$  barrier thickness. The period is determined by the wave vector  $q_L^{\parallel} = k_L^0 - k_L^{\parallel}$ , where  $k_L^0$  is the  $L$ -point Brillouin zone edge. The transmission coefficient is unity when the thickness of the  $\text{Ga}_{1-x}\text{Al}_x\text{As}$  barrier contains an integral number of half-wavelengths (deter-

mined by  $q_L^{\parallel}$ ) in the barrier region. Since the wave vector  $q_L^{\parallel}$  increases with the energy of the incoming  $L$ -point Bloch state, the period of the transmission amplitude decreases with the energy of the incident  $L$ -point electron. The off-resonance transmission amplitudes increase with increasing incident energy. The general qualitative behavior of the transport is similar to that exhibited by plane wave states incident on a rectangular quantum-mechanical barrier. Similar regimes of transport have also been reported for incoming states near the GaAs  $\Gamma$  point for  $\text{GaAs-GaAs}_{1-x}\text{P}_x\text{-GaAs}$  strained (100)DHS<sup>4</sup> and for  $\text{GaAs-Ga}_{1-x}\text{Al}_x\text{As-GaAs}$ (100)DHS.<sup>19</sup>

Also shown in Fig. 3 is a comparison between the transmission for incoming electrons derived from the GaAs  $\Gamma$  point and from the GaAs  $L$  point at the same energy, namely  $E = 0.59 \text{ eV}$ . At this energy,  $k_L^{\parallel}$  and  $k_L^{\perp}$  are real and, consequently, the Bloch states  $\psi(k_{\parallel}, k_L^{\parallel})$  and  $\psi(k_{\parallel}, k_L^{\perp})$  are propagating. At a given layer thickness, the transmission is greater for states incoming from the GaAs  $\Gamma$  point than for the states derived from the  $L$  point. This is due to the fact that, for a given energy of  $E = 0.59 \text{ eV}$ , the  $\Gamma$ -point states lie at an energy of about  $0.46 \text{ eV}$  above the  $\Gamma$ -point minimum of the alloy,  $E_{\Gamma}^{\text{Ga}_{1-x}\text{Al}_x\text{As}} = 0.135 \text{ eV}$ . On the other hand, the  $L$ -point states lie at an energy of only  $0.03 \text{ eV}$  above the  $L$ -point valley of the alloy  $E_L^{\text{Ga}_{1-x}\text{Al}_x\text{As}} = 0.565 \text{ eV}$ . As seen in the figure, it seems possible to tune the thickness of the  $\text{Ga}_{1-x}\text{Al}_x\text{As}$  barrier in such a way as to reduce the transmission for the incoming states derived from the GaAs  $L$  point while the transmission for the  $\Gamma$  point remains close to unity.

Figure 4 shows the transmission coefficient  $T(k_{\parallel}, E)$  as a function of alloy composition for two different  $\text{Ga}_{1-x}\text{Al}_x\text{As}$  barrier thicknesses. The incoming Bloch state is either derived from the GaAs  $L$  point ( $k_{\perp} = k_L^{\perp}$ ), or from the GaAs  $\Gamma$  point ( $k_{\perp} = k_{\Gamma}^{\perp}$ ). The incoming Bloch state has  $k_{\parallel} = 0$ . The energy of the incoming state is  $E = 0.501 \text{ eV}$  above the GaAs  $\Gamma$ -point conduction band minimum. As mentioned above, the  $\Gamma$ -point and  $L$ -point energy edges,  $E_{\Gamma}^{\text{Ga}_{1-x}\text{Al}_x\text{As}}$  and  $E_L^{\text{Ga}_{1-x}\text{Al}_x\text{As}}$ , scale linearly with the alloy composition for  $x < 0.3$ . The composition  $x$  is therefore directly related to the  $\Gamma$ -point and  $L$ -point barrier heights at the interface. For the range of alloy compositions studied, the  $\Gamma$ -point and the  $L$ -point energies of  $\text{Ga}_{1-x}\text{Al}_x\text{As}$  vary in the range  $0 \text{ eV} < E_{\Gamma}^{\text{Ga}_{1-x}\text{Al}_x\text{As}} < 0.405 \text{ eV}$  and  $0.50 \text{ eV} < E_L^{\text{Ga}_{1-x}\text{Al}_x\text{As}} < 0.70 \text{ eV}$ , above the GaAs  $\Gamma$ -point conduction band minimum. For a fixed energy of  $E = 0.501 \text{ eV}$ , the transport is propagating for Bloch states incoming from the  $\Gamma$  point although it is mostly tunneling for Bloch states incoming from the  $L$  point in the composition range  $x < 0.3$ . This is due to the fact that, in this composition range, we have  $E_{\Gamma}^{\text{Ga}_{1-x}\text{Al}_x\text{As}} < E < E_L^{\text{Ga}_{1-x}\text{Al}_x\text{As}}$  so that  $k_{\Gamma}^{\parallel}$  is real whereas  $k_L^{\parallel}$  is mostly complex.

We first discuss the case of incoming electrons derived from the GaAs  $L$ -point valley. As the Al concentration increases, the  $L$ -point energy edge in  $\text{Ga}_{1-x}\text{Al}_x\text{As}$ ,  $E_L^{\text{Ga}_{1-x}\text{Al}_x\text{As}}$ , increases and so does the magnitude of  $\text{Im}(k_L^{\parallel})$ . Therefore, the  $L$ -point derived states have smaller decay lengths and tunnel less efficiently across the

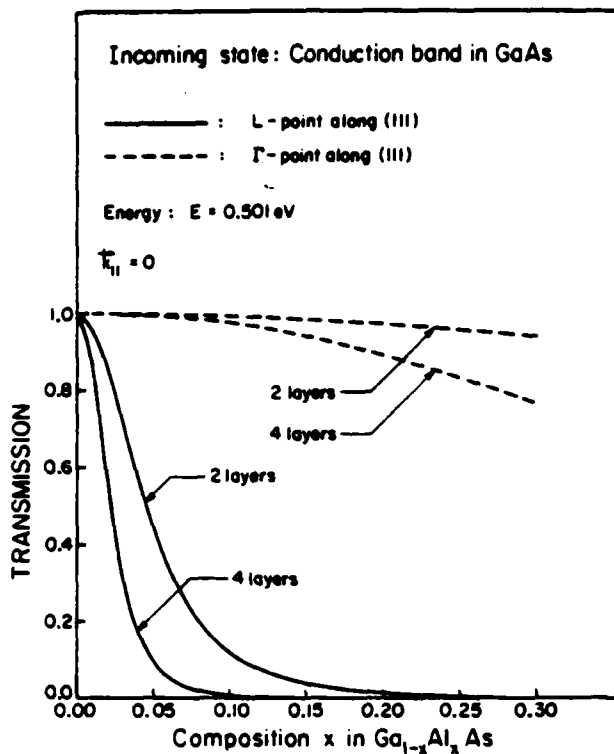


FIG. 4. Transmission coefficient  $T(k_1, E)$  as a function of alloy composition for two different  $\text{Ga}_{1-x}\text{Al}_x\text{As}$  barrier thicknesses. The incoming electron is either derived from the GaAs  $L$  point (solid line), or from the GaAs  $\Gamma$  point (dashed line). The energy of the incoming state is  $E = 0.501$  eV above the GaAs  $\Gamma$ -point conduction band minimum and  $k_1 = 0$ . Layers are measured in units of  $a/\sqrt{3}$ , where  $a$  is the GaAs lattice constant.

barrier. This, in turn, implies an increased reflection probability for the  $L$ -point derived states. At a given alloy composition  $x$ , the transmission is greater for the states incoming from the GaAs  $\Gamma$  point than for the states derived from the  $L$  point. This is due to the fact that the  $\Gamma$ -point states are transmitted in the propagating regime ( $E > E_{\Gamma}^{\text{Ga}_{1-x}\text{Al}_x\text{As}}$ ), whereas the  $L$ -point states are transmitted in the tunneling regime ( $E < E_L^{\text{Ga}_{1-x}\text{Al}_x\text{As}}$ ).

Since the mixing between  $L$ -point and  $\Gamma$ -point states appears to be small, there seems to exist two distinctive energy barriers for  $L$ -point and  $\Gamma$ -point electrons. In light of the results presented above, it seems possible to create a situation (by either selecting the energy, the barrier thickness, or the alloy composition) such that both the  $\Gamma$ -point and the  $L$ -point states were propagating in GaAs but only the  $\Gamma$ -point states would be propagating in  $\text{Ga}_{1-x}\text{Al}_x\text{As}$ , the  $L$ -point states being evanescent in the barrier. Such a situation may have applications in GaAs high speed low power devices to provide a way of reflecting back the low velocity  $L$ -point component of the current while allowing the high velocity  $\Gamma$ -point component to be transmitted.

#### IV. SUMMARY AND CONCLUSION

We have calculated the transport coefficients of  $L$ -point  $\Gamma$ -point electrons through GaAs- $\text{Ga}_{1-x}\text{Al}_x\text{As}$ -GaAs(111) double heterojunctions within a ten-band tight-binding formalism. The model takes into account band effects through

the use of complex- $k$  band structures and transfer matrix methods reasonably well. Within this theoretical framework,  $k_x$ -resolved transport coefficients can be calculated. This, in turn, allows for a better understanding of the transmission coefficients of electrons derived from different extrema of the conduction band in GaAs. Calculation of transport coefficients associated with various conduction band valleys were carried out as a function of (1) energy of the incoming electron, (2) thickness of the central  $\text{Ga}_{1-x}\text{Al}_x\text{As}$  barrier, and (3) alloy composition  $x$  in the central  $\text{Ga}_{1-x}\text{Al}_x\text{As}$  barrier.

States originating from the same extremum of the conduction band appear to couple strongly to each other, whereas states derived from different extrema are found to couple weakly. For energies of the incoming states near a given GaAs conduction band extremum ( $L$  or  $\Gamma$ ), transmission through the  $\text{Ga}_{1-x}\text{Al}_x\text{As}$  barrier occurs mostly via the coupling to states (evanescent or propagating) that connect to the alloy conduction band at the same extremum ( $L$  or  $\Gamma$ ). Transmission through the  $\text{Ga}_{1-x}\text{Al}_x\text{As}$  barrier is either tunneling or propagating depending on the nature of the Bloch states available for strong coupling in the alloy. Since the mixing between  $L$ -point and  $\Gamma$ -point states appears to be small, there seems to exist two distinctive energy barriers for  $L$ -point and  $\Gamma$ -point electrons. This observation may lead to interesting effects in GaAs high speed low power electronic devices whereby the low velocity  $L$ -point component of the current could be blocked (i.e., small transmission below the  $L$ -point barrier) while the high velocity  $\Gamma$ -point component could be transmitted (i.e., large transmission above the  $\Gamma$ -point barrier).

#### ACKNOWLEDGMENTS

One of us (CM) has been supported by the NSERC of Canada and by the Fonds FCAC pour l'aide et le soutien à la recherche of Québec.

- <sup>1</sup>Work supported in part by the Army Research Office under Contract No. DAAG29-80-C-0103.
- <sup>2</sup>G. C. Osbourn and D. L. Smith, *Phys. Rev. B* **19**, 2124 (1979).
- <sup>3</sup>G. C. Osbourn and D. L. Smith, *J. Vac. Sci. Technol.* **16**, 1529 (1979).
- <sup>4</sup>G. C. Osbourn, *J. Vac. Sci. Technol.* **17**, 1104 (1980).
- <sup>5</sup>G. C. Osbourn, *J. Vac. Sci. Technol.* **19**, 592 (1981).
- <sup>6</sup>Y. C. Chang and J. N. Schulman, *Phys. Rev. B* **25**, 3975 (1982).
- <sup>7</sup>J. N. Schulman and Y. C. Chang, *Phys. Rev. B* (to be published).
- <sup>8</sup>D. H. Lee and J. D. Joannopoulos, *Phys. Rev. B* **23**, 4988, 4997 (1981).
- <sup>9</sup>J. Pollmann and S. Pantelides, *Phys. Rev. B* **18**, 5524 (1978).
- <sup>10</sup>D. H. Lee and J. D. Joannopoulos, *J. Vac. Sci. Technol.* **19**, 355 (1981).
- <sup>11</sup>Y. C. Chang and J. N. Schulman, *J. Vac. Sci. Technol.* **21**, 540 (1982).
- <sup>12</sup>P. Vogl, H. P. Hjalmarson, and J. D. Dow, *J. Phys. Chem. Sol.* (in press).
- <sup>13</sup>J. N. Schulman and Y. C. Chang, *Phys. Rev. B* **24**, 4445 (1981).
- <sup>14</sup>H. C. Casey and M. B. Panish, *Heterostructure Lasers* (Academic, New York, 1978), Part A, Chap. 4.
- <sup>15</sup>R. Dingle, W. Weigmann, and C. Henry, *Phys. Rev. Lett.* **33**, 827 (1974).
- <sup>16</sup>S. M. Sze, *Physics of Semiconductor Devices*, 2nd ed. (Wiley-Interscience, New York, 1981), p. 850.
- <sup>17</sup>L. I. Schiff, *Quantum Mechanics*, 3rd ed. (McGraw-Hill, New York, 1968), pp. 102-104.
- <sup>18</sup>W. A. Harrison, *Phys. Rev.* **123**, 85 (1961).
- <sup>19</sup>C. B. Duke, *Tunneling Phenomena in Solids* (Plenum, New York, 1969), p. 31.
- <sup>20</sup>C. Mailhot, T. C. McGill, and J. N. Schulman, *J. Vac. Sci. Technol. B* **1**, 439 (1983).

# A DLTS study of deep levels in *n*-type CdTe

R. T. Collins, T. F. Kuech<sup>1)</sup>, and T. C. McGill

California Institute of Technology, Pasadena, California 91125

(Received 13 November 1981; accepted 11 February 1982)

We report the results of a DLTS study on the majority carrier deep level structure of three samples of *n*-type CdTe and the effects on the deep level structure of indium doped CdTe due to H<sub>2</sub> annealing. H<sub>2</sub> annealing did not qualitatively change the deep level structure of the annealed sample. It did cause the shallow level concentration to decrease with a proportional decrease in the deep level concentrations as a result of indium out-diffusion and compensation by native defects. Levels present in all of the materials studied have been characterized and attributed to either native defects or innate chemical impurities. Other levels present in indium doped material require above band gap illumination of the sample before they are observed. A possible model proposes that these levels arise from defect complexes.

PACS numbers: 71.25.Tn, 71.55.Ht, 72.20.Jv, 81.40.Ef

## I. INTRODUCTION

The presence of crystal defects has long complicated our understanding of II-VI semiconductors. These defects are a result of the wide phase stability regions of II-VI compounds, and they often dominate the electrical characteristics of the material. The defect structure of CdTe, a II-IV semiconductor which exhibits large deviations from stoichiometry, is recently of great interest because of the use of CdTe in infrared devices. Annealing CdTe at elevated temperatures under fixed partial pressures of its constituent elements, Cd and Te, can modify the material's defect structure.<sup>1,2</sup> Annealing CdTe at a high temperature in an H<sub>2</sub> ambient prior to its use as a substrate for epitaxial growth has been shown to alter the electrical properties of the CdTe in the near surface region through the introduction of crystal defects.<sup>3</sup> Despite the importance of crystal defects in CdTe, they are poorly characterized and understood at present.<sup>4</sup>

We present here a deep level transient spectroscopy (DLTS) study of deep levels in both indium doped and undoped CdTe. The effects on the deep level structure of indium doped CdTe due to H<sub>2</sub> annealing are also presented.

## II. EXPERIMENTAL PROCEDURES

Physical and electrical measurements made on three different single crystals of *n*-type CdTe are reported here. Material IN1, indium doped CdTe obtained from Eagle Picher Ind., was initially on the Cd excess side of the phase stability region. Its indium concentration was  $\sim 10^{18}$  cm<sup>-3</sup>. Materials UN1 and IN2, undoped CdTe from Eagle Picher Ind. and indium doped CdTe from the II-VI Corporation, respectively, were annealed in Cd vapor at 750 °C for between 6 and 12 h to raise their carrier concentrations. The concentration of indium in IN2 was several orders of magnitude less than in IN1.

Electrical measurements were performed on Au Schottky barrier devices. Two methods of sample preparation were used in fabricating devices on IN1. In both methods clean surfaces of CdTe were prepared by cleaving rods of bulk CdTe in air. One set of samples was immediately placed into an ion pumped vacuum system ( $< 10^{-6}$  Torr) where 160-

$\mu\text{m}$ -diam Au dots were evaporated onto the cleaved CdTe surfaces. A second set of samples was annealed at 350–370 °C for 1 h in Pd purified H<sub>2</sub> ambient before Au dots were deposited onto the annealed, cleaved sample surfaces. Au Schottky devices were also made on air cleaved surfaces of UN1 and IN2. No H<sub>2</sub> annealing treatment was used in these samples.

Capacitance voltage (*C-V*) profiling of the CdTe samples was carried out at room temperature using a Model 71A Boonton capacitance meter. DLTS spectra were taken on a fast capacitance bridge using a double boxcar integrator as described by Lang.<sup>5</sup>

Secondary ion mass spectroscopy (SIMS) was used to depth profile the indium concentrations at H<sub>2</sub> annealed and unannealed surfaces of IN1.<sup>6</sup>

## III. RESULTS

The results of DLTS and capacitance measurements made on the various CdTe structures are summarized below and in Figs. 1, 2, and 3. Since there is negligible minority carrier injection in a Schottky barrier device only majority carrier traps were observed. The shallow level concentrations ( $N_D - N_A$ ) were determined from measurements of reverse bias capacitance characteristics.

We begin our discussion with the results on the two crystals from Eagle Picher Ind. The shallow level concentrations of samples from IN1 (CdTe originally doped with  $N_{in} \sim 10^{18}$  cm<sup>-3</sup>) were  $7 \times 10^{17}$  cm<sup>-3</sup> for unannealed surfaces and  $3 \times 10^{15} - 5 \times 10^{16}$  cm<sup>-3</sup> for H<sub>2</sub> annealed surfaces. SIMS measurements showed a minor surface buildup of indium followed by a 2–3  $\mu\text{m}$  layer depleted of indium by a factor of two at the H<sub>2</sub> annealed surface. DLTS spectra for unannealed and H<sub>2</sub> annealed surfaces of IN1 did not differ markedly as a result of the two methods of sample preparation. These DLTS measurements probed a region extending 1–2  $\mu\text{m}$  below the surface. Typical DLTS spectra are given in Fig. 1(a) and (c). In the temperature range from 80 to 400 K three main electron traps (*E* 1, *E* 2, and *E* 3) were evident. A shoulder was visible on the low temperature side of *E* 2 (*E* 2a). Some of the samples also exhibited a level (*E* 1a)

which occurred at a lower temperature than  $E 1$ . The activation energies of levels  $E 1$  and  $E 2$ , determined from Arrhenius plots shown in Fig. 3, were  $0.34 \pm 0.06$  and  $0.77 \pm .05$  eV, respectively, relative to the conduction band. The concentrations of levels  $E 1$  and  $E 2$  tracked the shallow level concentration at approximately 3% and 8% of the shallow level concentration in all of the samples made from IN1. Level  $E 3$  was not studied in detail because, even for rate windows corresponding to long time constants, rapid changes occurred in the Schottky barrier device characteristics at the temperatures where  $E 3$  was observed.<sup>1</sup>

The DLTS spectrum for IN1 was modified by above band gap illumination (HeNe laser) as shown in Fig. 1(b). A spectrum was taken with the sample in the dark as the sample was cooled to 100 K (dashed curve). After exposure to above band gap light, a DLTS spectrum was taken with the sample in the dark as the sample temperature increased (solid curve). Level  $E 1a$  increased in amplitude, a new level ( $E 1b$ ) appeared, and a background which is visible in the difference spectrum (dotted curve) appeared under  $E 1$  ( $E 1c$ ). The device capacitance at 100 K also increased by 5%–15% as a result of illumination. Changes in the device capacitance and DLTS spectrum persisted for at least an hour after the light source was removed, independent of the biasing voltage maintained, provided the sample temperature remained  $\sim 100$  K. After warming to room temperature and waiting  $\sim 15$  min, these light associated effects were not evident in subsequent dark measurements. Activation energies for levels  $E 1a$  and  $E 1b$  were estimated as suggested by Lang to be 0.24 and 0.30 eV.<sup>8</sup> The spectra in Fig. 1 are for  $H_2$  annealed

IN1. The same effect was observed in unannealed IN1 although the amplitudes of  $E 1a$  and  $E 1b$  relative to  $E 1c$  were smaller.

We also examined the unintentionally doped crystal from Eagle Picher Ind. Samples from UN1 had shallow level concentrations of approximately  $2 \times 10^{15} \text{cm}^{-3}$ . Five majority carrier levels are observed, ( $E 2, E 4, E 5, E 6,$  and  $E 7$ ) in a typical DLTS spectrum for UN1 [Fig. 2(a)].  $E 2a$  was also seen in most samples, and a peak corresponding to level  $E 3$  observed in IN1 was present in a number of UN1 samples. The concentration of  $E 2$  was  $\sim 5\%$  of the shallow level concentration. The Arrhenius plot for  $E 2$  in Fig. 3 includes points taken from UN1.  $E 6$  was not observed until the device being studied was mechanically stressed. Subsequent heating to 400 K removed  $E 6$ . No optical effects similar to those found in IN1 were observed.

To investigate how much these results depend on the source of the crystals, we have also studied a crystal doped with indium from II-VI Corporation. The shallow level concentration of samples taken from IN2 were approximately  $2 \times 10^{17} \text{cm}^{-3}$ . This is larger than the reported indium concentration, possibly because of the presence of other impurities or the introduction of native defects during the Cd vapor anneals. A typical DLTS spectrum for IN2 is shown in Fig. 2(b). Three main levels ( $E 2, E 8,$  and  $E 9$ ) can be resolved. In most spectra  $E 2a$  and  $E 3$  are also visible. Illumination at low temperatures did cause a capacitance change and an increase in the low temperature background of a subsequent dark DLTS scan, but no new peaks could be resolved from this background.

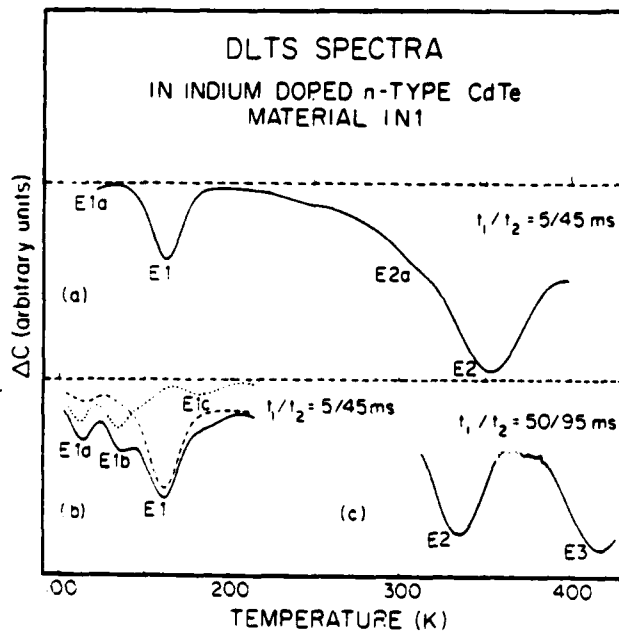


FIG. 1. DLTS spectra of electron traps in indium doped  $n$ -type CdTe (material IN1). The positions of the boxcar windows are given by  $t_1$  and  $t_2$ . (a) A typical spectrum in IN1. (b) Optical effect in IN1. The dashed scan was made before illumination; solid scan after illumination at 100 K. The dotted curve is the difference. (c) Spectrum in IN1 using a small rate window to show  $E 3$ .

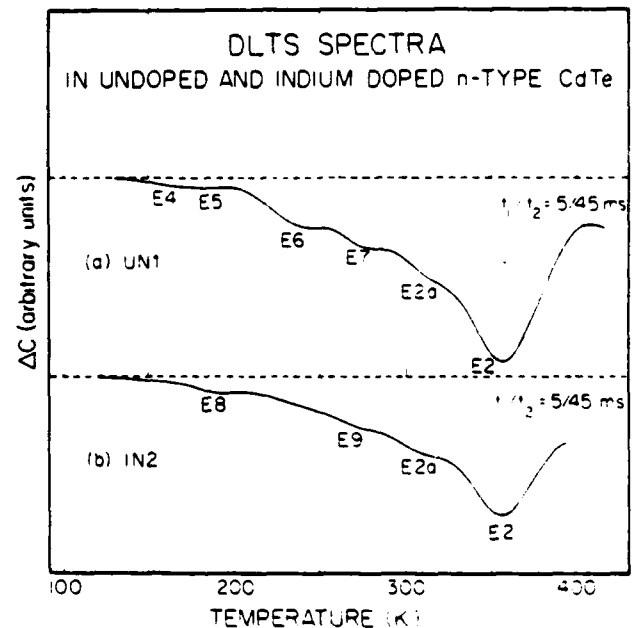


FIG. 2. DLTS spectra of electron traps in undoped and indium doped  $n$ -type CdTe (materials UN1 and IN2, respectively). The positions of the boxcar windows are given by  $t_1$  and  $t_2$ . (a) A typical spectrum in UN1. (b) A typical spectrum in IN2.

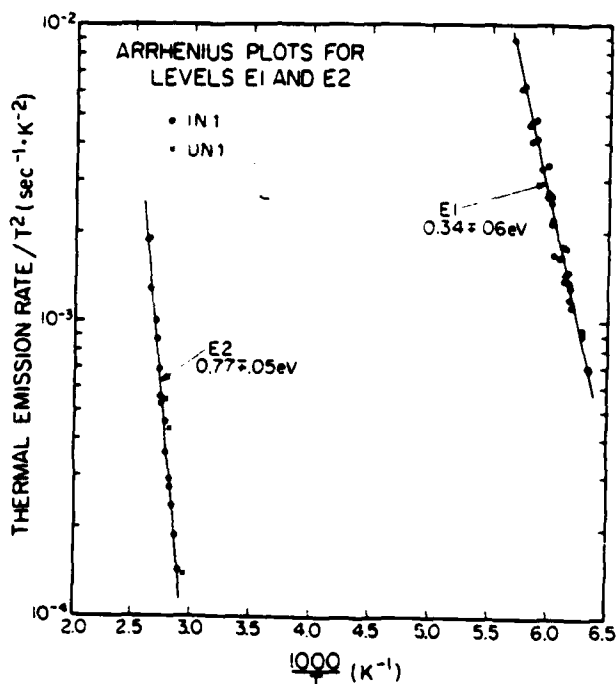


FIG. 3. Arrhenius plots for electron traps  $E1$  and  $E2$  present  $n$ -type CdTe.

#### IV. DISCUSSION AND CONCLUSIONS

The predominant effect of  $H_2$  annealing IN1 was the drop in shallow level concentration. The estimated deep level concentrations also fell proportionately, suggesting that the deep and shallow levels are in some way related. An understanding of the effects of  $H_2$  annealing on the shallow levels may lead to a better understanding of the origin and character of the deep levels. The drop in carrier concentration during anneal can be attributed to two main sources, loss of indium through indium evaporation, or the introduction of compensating defects. Such native crystal defects can also lead to the loss of electrically active indium through the formation of indium telluride precipitates. The decrease in indium concentration at annealed surfaces, as measured by SIMS, is not sufficient to account for the observed drop in shallow donor concentration, suggesting that the introduction of native crystal defects is the dominating process.

DLTS spectra for all three samples are strikingly similar near  $E2$  and  $E2a$ , also, from Fig. 3, we see that the emission rate as a function of temperature is the same for level  $E2$  in materials IN1 and UN1. From this we conclude  $E2$  arises from a source present in all of these samples. We suggest that  $E2$  and  $E2a$  are associated with impurities or native defects which are either commonly found in CdTe, or easily introduced during the Cd vapor anneals performed on the samples. Although the data are less conclusive,  $E3$  appears to be present in all of our samples indicating that it has an origin similar to that of  $E2$ .  $E8$  and  $E9$  in IN2 are probably the same as some of the levels in UN1 ( $E4$ – $E7$ ). But, all of these levels are buried too deeply in the background to make conclusive measurements on them.

Levels  $E1$ ,  $E1a$ ,  $E1b$ , and  $E1c$  are probably indium related. They would be expected to appear in IN2 with concen-

trations several orders of magnitude less than in IN1. If they did have concentrations which were within the limits of the sensitivity of the DLTS, they were probably buried in the background of the other peaks present in IN2. Electron emission from  $E1b$ ,  $E1c$  and to a certain extent  $E1a$  only occurs after above band gap illumination. The predominant effect of this illumination is the creation of electron-hole pairs in the depletion region. Since electrons can be introduced electrically, the appearance of these levels in the spectrum can be attributed to the presence of holes in the depletion region. This suggests that there are associated hole traps in the depletion region which must bind holes before these electron traps can be observed. Increased device capacitance following illumination supports this interpretation. Similar conclusions have been drawn from observations of DLTS spectra in InP.<sup>9</sup> Persistent photoconductivity and photocapacitance have been previously observed in CdTe, but this is the first study correlating them with changes in DLTS spectra.<sup>7,10</sup>

Identifying the centers responsible for levels  $E1a$ ,  $E1b$ , and background  $E1c$  is not possible without further study. We can, however, propose a model. Because all of these levels are affected by illumination, it seems likely that the centers responsible for each of these levels are of a similar nature. One possibility is that each center results from a different configuration of a defect complex.

Comparing these results with those previously reported, we find several observations of levels in  $n$ -type CdTe approximately 0.6 eV (0.55–0.70 eV) from the conduction band have been made.<sup>4</sup> These could correspond to levels presented in this study, but the variety of samples studied and techniques used do not allow a definite conclusion to be drawn. When comparing the energies presented here to those from other studies, it must be remembered that these are activation energies and have not been corrected for electric field effects or thermally activated capture cross sections.

Huber *et al.*<sup>11</sup> have made DLTS measurements on  $n$ -type, indium doped CdTe films grown on BaF<sub>2</sub> and PbTe. Of the six levels they observe between 100 and 300 K, which they attribute to native defects and native defect complexes; none correspond to  $E2$  presented here. Levels  $E1$ – $E4$  in their study are at energies near 0.34 eV and may correspond to  $E1$ ,  $E1a$ , or  $E1b$ , but one must be careful in comparing materials grown so differently.

#### ACKNOWLEDGMENTS

We wish to acknowledge Marti Mäenpää for his help with these experiments, Dr. J. O. McCaldin for valuable discussions, and Rockwell International for providing some of the samples. This work was supported in part by the Army Research Office under Contract No. DAAG29-80-C-0103. One of us (TFK) wishes to acknowledge the Office of Naval Research (Contract No. N00014-76-C-1068) for support during this work.

\*Present address: IBM T. J. Watson Research Center, P. O. Box 218, Yorktown Heights, New York 10598.

<sup>1</sup>C. E. Barnes and K. Zanio, *J. Appl. Phys.* **46**, 3959 (1975).

<sup>2</sup>D. de Nobel, *Philips Res. Rep.* **14**, 361 (1959).

<sup>3</sup>T. F. Kuech and J. O. McCaldin, *J. Appl. Phys.* **53**, 3121 (1982).

<sup>4</sup>K. Zanio, in *Semiconductors and Semimetals*, edited by R. K. Willardson and A. C. Beer (Academic, New York, 1978), Vol. 13.

<sup>5</sup>D. V. Lang, *J. Appl. Phys.* **48**, 3023 (1974).

<sup>6</sup>Charles Evans Assoc., 1670 South Amphlett Boulevard, Suite 120, San Mateo, CA 94402.

<sup>7</sup>M. R. Lorenz, B. Segall, and H. H. Woodbury, *Phys. Rev.* **134**, A751 (1964).

<sup>8</sup>D. V. Lang, in *Topics in Applied Physics*, edited by P. Braunlich (Springer-Verlag, Berlin, 1979), Vol. 37.

<sup>9</sup>A. Sibille and A. Mircea, *Phys. Rev. Lett.* **47**, 142 (1981).

<sup>10</sup>G. W. Iseler, J. A. Kafalas, and A. J. Strauss, *Solid State Commun.* **10**, 619 (1972).

<sup>11</sup>Von W. Huber, H. Sitter, and A. Lopez-Otero, *Vak. Tech.* **29**, 35 (1980).

# Electronic properties of deep levels in $p$ -type CdTe

R. T. Collins and T. C. McGill

California Institute of Technology, Pasadena, California 91125

(Received 1 March 1983; accepted 25 May 1983)

DLTS and associated electrical measurements were made on unintentionally doped CdTe crystals obtained from several vendors, on Cu-doped CdTe, and on Te-annealed CdTe. All of the crystals were  $p$ -type. Four majority carrier deep levels were observed in the temperature range from 100–300 K with activation energies relative to the valence band of 0.2, 0.41, 0.45, and 0.65 eV. Two of these levels were specific to certain crystals while the other two were seen in every sample and are attributed to common impurities or native defects. Fluctuations in the concentrations of levels across samples and as a result of modest sample heating (400 K) were also observed.

PACS numbers: 72.80.Ey, 72.20.Jv, 71.55.Fr

## I. INTRODUCTION

The electronic properties of II–VI compound semiconductors are not well understood. The situation is complicated by the presence of native defects and defect complexes, in addition to impurities incorporated into the crystals during growth. CdTe is a II–VI semiconductor which is of recent interest because it serves as a substrate for the growth of the lattice-matched ternary  $\text{Hg}_{1-x}\text{Cd}_x\text{Te}$ . It has also been proposed for use as a nuclear detector and in solar cells. In all of these applications an understanding of the deep-level properties of the material is important to successfully fabricating devices from CdTe. There have been a number of studies of deep levels in CdTe.<sup>1</sup> The results of early measurements are hard to compare because of the variety of techniques and samples used. Recently, more sensitive and reproducible deep-level transient spectroscopy (DLTS) measurements have been made on  $n$ -type CdTe, but the CdTe typically used for the above applications is unintentionally doped, as-grown material which is generally  $p$ -type.<sup>2–4</sup> Very little information about deep levels in these crystals exists.

This paper presents the results of a study of the majority carrier deep levels in  $p$ -type CdTe using the technique of DLTS. The experimental method will be described, and the properties of each sample studied will be discussed. Results of the measurements will be presented providing a comparison of as-grown CdTe crystals obtained from various sources. Information on the deep levels in CdTe doped with Cu and CdTe which had been annealed in Te vapor will also be given. Finally, possible explanations for the observations that were made and conclusions based on these observations will be suggested.

## II. EXPERIMENTAL

DLTS and  $C$ - $V$  measurements were made on six different crystals of  $p$ -type CdTe. All of the crystals were examined in an as-grown condition. One was also annealed in Te vapor prior to the measurements. The history and properties of each of these materials is given in Table I. Shallow level concentrations ( $N_A - N_D$ ) taken from reverse bias capacitance measurements are also given in Table I. Five of the six crystals were unintentionally doped. It is not known if the

observed shallow level concentrations in these crystals, which are quite high, were due to residual impurities or to stoichiometry. The latter is suspected. Crystal E was made from material which was taken from crystal B and annealed at 800 °C for  $\approx 2$  h in a sealed, evacuated quartz ampule containing elemental Te. Crystal F was CdTe doped with Cu at a level of  $10^{16} \text{ cm}^{-3}$ .

The measurements described here were performed on Schottky barrier devices fabricated on samples taken from the crystals. Both Au and Cd barriers were used. Au and Cd Schottky barriers were prepared in two different ways. In the first method, 160  $\mu\text{m}$  diameter dots were evaporated onto air-cleaved {110} surfaces in an ion pumped vacuum system at  $10^{-6}$  Torr. Ni or a Cu/Au alloy was evaporated onto the rear face of the sample following an etch in  $\text{K}_2\text{CrO}_7$  and  $\text{H}_2\text{SO}_4$  solution to provide the ohmic contact.<sup>5</sup>

In the second method of preparation, Au or Cd was evaporated onto polished {111} sample surfaces which had been etched for 5 min in a 0.5% Br-Methanol solution. These dots were 500  $\mu\text{m}$  in diameter. Again, evaporated Ni or Cu/Au alloy provided the Ohmic contact.

Reverse bias capacitance characteristics for samples prepared as described above were recorded at room temperature using a model 71A Boonton capacitance meter with a 15 mV, 1 MHz test signal. DLTS spectra were taken on the

TABLE I. Shallow level concentrations and histories of each of the CdTe crystals used in the DLTS measurements.

Crystal	Shallow level concentration	Comments
A	$5-8 \times 10^{15} \text{ cm}^{-3}$	Bridgman growth by II-VI Corp
B	$6 \times 10^{16} \text{ cm}^{-3}$	Traveling heater method by Radiation Monitor
C	$2-3 \times 10^{16} \text{ cm}^{-3}$	Bridgman growth by Rockwell Int
D	$1.5 \times 10^{16} \text{ cm}^{-3}$	Bridgman growth by II-VI Corp
E	$> 2 \times 10^{16} \text{ cm}^{-3}$	Crystal "B" annealed in Te vapor at 800 °C $\approx 2$ h
F	$1.2 \times 10^{16} \text{ cm}^{-3}$	Bridgman growth by II-VI Corp Doped with $10^{16} \text{ cm}^{-3}$ Cu
G	$6 \times 10^{15} \text{ cm}^{-3}$	Bridgman growth by Texas Instruments

same samples using a fast capacitance bridge and double boxcar integrator as described by Lang.<sup>6</sup>

Photoresponse and I-V measurements were also made on the Au and Cd Schottky barriers prepared on the air-cleaved {110} sample surfaces to determine the Schottky barrier heights.

### III. RESULTS

Results of the DLTS measurements on the various crystals are presented below. Minority carrier injection is negligible in Schottky barrier devices if the barrier height is considerably less than the band gap, as is the case for Cd and Au on *p*-type CdTe.<sup>7</sup> For this reason, only majority carrier traps were observable in this study. No differences in the spectra were evident as a result of the method of device preparation or the Schottky barrier used.

As shown in Figs. 1-4, four major deep levels were seen in the crystals in the temperature range from 100-300 K. Deep level H1 was seen in A (Fig. 1) and D (Fig. 2) at concentrations of  $1 \times 10^{14}$  and  $3 \times 10^{13}$  cm<sup>-3</sup>, respectively. This level may have been present in F but at a very low concentration. The low temperature region where H1 occurred was scanned for all the crystals, although it is only shown for A and D. Level H2 was only seen in crystal C (Fig. 2). Its concentration was between  $2 \times 10^{13}$  and  $3 \times 10^{14}$  cm<sup>-3</sup>. Levels H3 and H4 were seen in all of the crystals (Figs. 1-4). Level H3 appeared over approximately a 5 K range of temperatures in the samples studied. This variation was even observed in samples taken from the same crystal. This suggests that H3 may really be due to more than one level, and relative concentration changes in the levels caused the position of H3 to shift. The concentrations of H3 in crystals A through D were  $4 \times 10^{13}$ - $4 \times 10^{14}$ ,  $1 \times 10^{12}$ ,  $3 \times 10^{13}$ - $3 \times 10^{14}$  and  $2 \times 10^{13}$ - $1 \times 10^{14}$  cm<sup>-3</sup>, respectively. In G (Fig. 4) its concentration

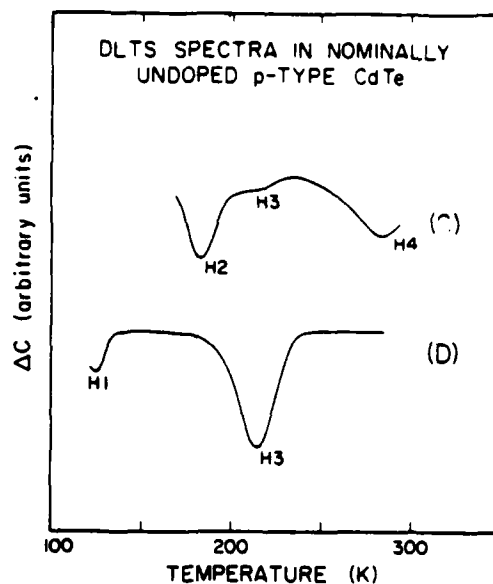


FIG. 2. Characteristic DLTS spectra for hole traps in nominally undoped, *p*-type CdTe crystals C and D. The positions of the boxcar windows during the scans were  $t_1 = 5$  ms and  $t_2 = 45$  ms.

was  $4 \times 10^{12}$  cm<sup>-3</sup>. H3 in E and F will be discussed below. There was a lot of fluctuation in the trap concentrations, as can be seen from the above values. These fluctuations even occurred from device to device on the same sample. In the case of level H4 this effect was more pronounced. At the sensitivity used in the spectrum chosen for D in Fig. 2, the level was not visible, although, in other cases, its concentration matched that of H3. These deep trap concentrations were estimated from the formula  $2\Delta C/C = N_d/N$ , where  $C$  is the capacitance of the diode,  $\Delta C$  is the change in capacitance caused by completely filling the deep level,  $N_d$  is the deep level concentration, and  $N$  is the shallow level concen-

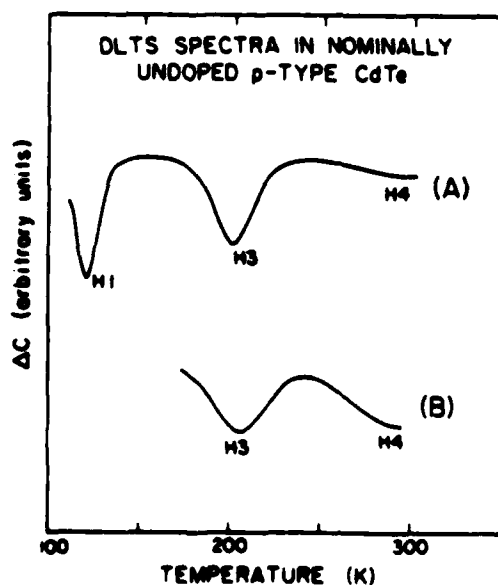


FIG. 1. Characteristic DLTS spectra for hole traps in nominally undoped, *p*-type CdTe crystals A and B. The positions of the boxcar windows during the scans were  $t_1 = 5$  ms and  $t_2 = 45$  ms.

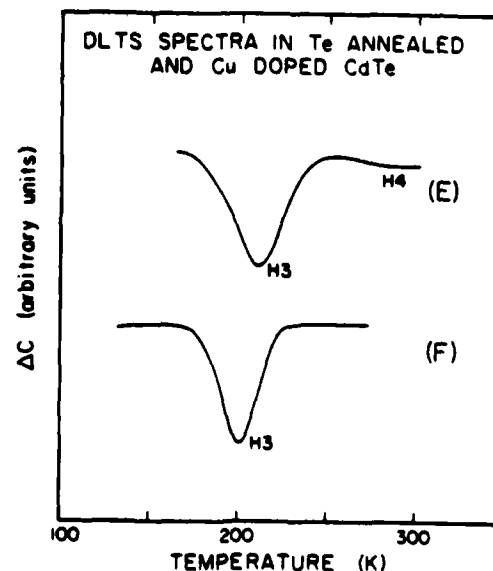


FIG. 3. Characteristic DLTS spectra for Te-annealed (E) and Cu-doped (F) *p*-type CdTe. The positions of the boxcar windows during the scans were  $t_1 = 5$  ms and  $t_2 = 45$  ms.

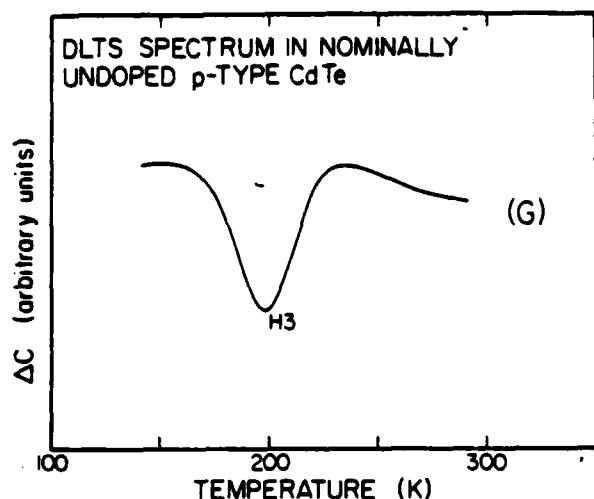


FIG. 4. DLTS spectra for hole traps in nominally undoped, *p*-type CdTe crystal G. The positions of the boxcar windows during the scans were  $t_1 = 5$  ms and  $t_2 = 45$  ms.

tration.<sup>6</sup> Edge region effects are neglected using this method, but, such accuracy is not necessary in light of the large variations in trap concentrations which were mentioned above.

Material E was CdTe which had been taken from crystal B and annealed in Te vapor at 800 °C for about 2 h. The anneal caused the shallow level concentration to increase by two orders of magnitude. As can be seen from Fig. 3, H3 and H4 were still present. H3's concentration was approximately  $5 \times 10^{14} \text{ cm}^{-3}$ . This value is also about two orders of magnitude higher than prior to the anneal.

Crystal F had been doped with Cu at about  $10^{16} \text{ cm}^{-3}$ . This concentration is close to the shallow level concentration obtained from the C-V profile and may indicate that the Cu dopants were not strongly compensated by native defects. The DLTS spectrum for F, as seen in Fig. 3, contains H3 at a concentration of  $4 \times 10^{13} \text{ cm}^{-3}$ , a value similar to that found in the undoped crystals. H4 was also present at a much lower concentration and is not seen in the spectrum shown. Attempts were also made to dope crystals with Cu following procedures outlined by Ref. 8. Again, there were no new levels or significant enhancements of existing levels.

Other trapping states were visible in the above room temperature range of the spectra, but, after the samples were heated to 400 K in the process of taking the data, changes occurred in the DLTS spectra. Levels which were seen above room temperature left completely. Some of the below room temperature levels also suffered concentration increases or decreases of as much as an order of magnitude. The direction of the change was not always the same. For this reason no above room temperature spectra are given. The DLTS spectra shown are for unheated samples immediately after preparation.

Arrhenius plots for levels H1-H4, along with their associated activation energies, are given in Fig. 5. Capture cross sections for the various states were not directly measurable with our system because, for the shortest reduced bias pulse we could apply ( $\approx 20$  ns), all the levels were completely filled with holes. From this we can place a lower bound of

$5 \times 10^{-14} \text{ cm}^2$  on the capture cross section for holes, a value which is in reasonable agreement with that determined from the  $y$  intercepts of the Arrhenius plots. Because of this, the activation energies in Fig. 5 have not been corrected for temperature dependent cross sections. No correction for electric field effects has been applied either. The data used for H3 in Fig. 5 is for a particular device. If other devices are used, the temperature fluctuations mentioned above cause the line to shift, but the slope stays within the error range given.

Au and Cd barrier heights on the {110} air-cleaved surface of the CdTe were found to be approximately 0.6 and 1.0 eV, respectively. The Au value is in agreement with previous measurements.<sup>9</sup> The value for the Cd barrier height is approximately equal to the CdTe band gap minus the Cd barrier height on *n*-type CdTe taken from Ref. 10.

#### IV. CONCLUSIONS

Impurities and native defects are both potential sources of deep levels in CdTe.<sup>1</sup> Although the crystal defects responsible for the deep levels observed in this study cannot be directly identified, it is possible to draw some conclusions about them based on the results of these measurements. Levels H1 and H2 were specific to certain crystals and are, therefore, likely candidates for impurities. Levels H3 and H4, on the other hand, were present in all of the crystals. They could be the result of a common impurity, native defects, or even grosser crystal defects (such as Te precipitates). There have been previous reports of levels approximately 0.3 eV from the valence band that were due to Cu, Au and Ag.<sup>11,12</sup> Identifications were based on associating the levels that were observed with the crystal dopants. Although Au and Ag diffusions have yet to be tried, the present work seems to indicate that the levels we observe are not due to Cu, since the presence of Cu in crystal F did not enhance any of the levels seen and because the attempts at Cu doping did not significantly

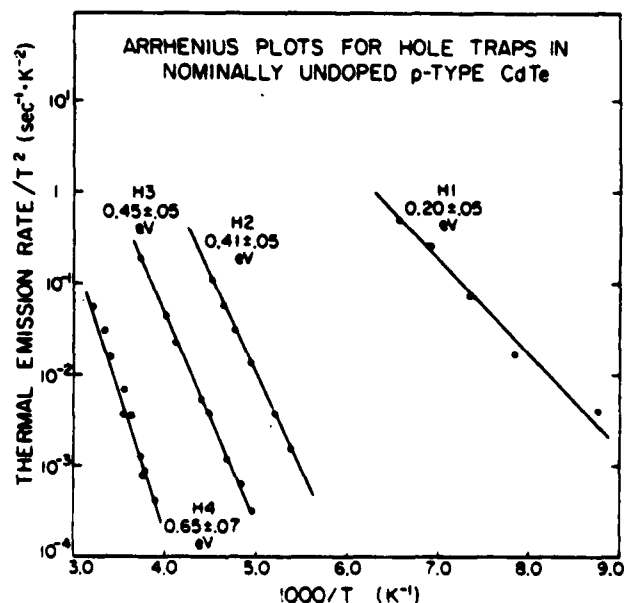


FIG. 5. Arrhenius plots for the four majority carrier deep levels seen in DLTS measurements on *p*-type CdTe.

increase the concentrations of any of the traps. It is possible that there are deep levels associated with the Cu, but that the temperature range of this study did not include Cu-related peaks. This remains to be tested. The fact that H3 and H4 along with  $(N_A - N_D)$  were effected by the Te anneals suggests that native defects are responsible.

Concentrations of deep levels in as-grown crystals were generally  $10^{14} \text{ cm}^{-3}$  or less. Although this is quite low, fluctuations were also seen in the concentrations of traps from device to device on a given sample. Even more disturbing were the changes in peak amplitudes produced by very modest sample heating (400 K). No attempts were made to determine if similar concentration changes occurred for samples heated before device fabrication, but since the same levels were observed for both Au and Cd barriers, it is unlikely that the changes occurred as a result of diffusion of barrier metal into the active region of the CdTe diode.

In summary, we have made DLTS measurements on *p*-type CdTe crystals. Four deep levels were observed (H1-H4) in the temperature range from 100-300 K. Levels H1 and H2 only occurred in a few of the samples leading us to believe they are associated with impurities in the crystals. H3 and H4 are in every crystal and may be related to native defects. Measurements on Cu-doped samples indicate that the levels seen are not due to residual Cu in the CdTe. We also noted variations in the concentrations of the observed levels from

device to device on a given sample and significant changes in trap concentrations as a result of modest sample heating.

#### ACKNOWLEDGMENTS

The authors wish to acknowledge Rockwell International and Texas Instruments for providing the CdTe used in this research. This work was supported in part by the Army Research Office under Contract No. DAAG29-80-C-0103.

<sup>1</sup>K. Zanio, in *Semiconductors and Semimetals*, edited by R. K. Willardson and A. C. Beer (Academic, New York, 1978), Vol. 13.

<sup>2</sup>T. Takebe, J. Sarate, and H. Matsunami, *J. Appl. Phys.* **43**, 5 (1982).

<sup>3</sup>R. T. Collins, T. F. Kuech, and T. C. McGill, *J. Vac. Sci. Technol.* **21**, 191 (1982).

<sup>4</sup>D. Verity, D. Shaw, F. J. Bryant, and C. G. Scott, *J. Phys. C* **15**, 573 (1982).

<sup>5</sup>T. Anthony, A. L. Fahrenbruch, and R. H. Bube, *J. Electron. Mater.* **2**, 89 (1982).

<sup>6</sup>D. V. Lang, *J. Appl. Phys.* **45**, 3023 (1974).

<sup>7</sup>S. M. Sze, *Physics of Semiconductor Devices* (Wiley, New York, 1981), p. 265.

<sup>8</sup>J. P. Chamonal, E. Molva, and J. L. Pautrat, *Solid State Commun.* **43**, 801 (1982).

<sup>9</sup>J. P. Ponpon, M. Saraphy, E. Buttung, and P. Siffert, *Phys. Status Solidi A* **59**, 259 (1980).

<sup>10</sup>T. F. Kuech, *J. Appl. Phys.* **52**, 4874 (1981).

<sup>11</sup>D. de Nobel, *Philips Res. Rep.* **14**, 361 (1959).

<sup>12</sup>M. R. Lorenz and B. Segall, *Phys. Lett.* **7**, 18 (1963).

END

FILMED

3-84

DTIC